THESIS

SURFACE AND SYNOPTIC FEATURES OF LEADING AND PARALLEL STRATIFORM MESOSCALE CONVECTIVE SYSTEMS

Submitted by

Jesse Matthew Steinweg-Woods

Department of Atmospheric Science

In partial fulfillment of the requirements

For the Degree of Master of Science

Colorado State University

Fort Collins, Colorado

Fall 2010

Master's Committee:

Department Head: Richard Johnson

Advisor: Richard Johnson

Steve Rutledge
Jorge Ramirez

ABSTRACT

SURFACE AND SYNOPTIC FEATURES OF LEADING AND PARALLEL STRATIFORM MESOSCALE CONVECTIVE SYSTEMS

This study investigates the surface wind, pressure, and temperature patterns associated with mesoscale convective systems meeting the classification of leading or parallel stratiform. Cases were surveyed over the period of 2002 to 2007 inside the state of Oklahoma. Thirteen leading stratiform cases and ten parallel stratiform cases were identified. The synoptic environment these cases developed in was also investigated and compared to previous studies.

The Oklahoma Mesonetwork is utilized to examine the surface features associated with these cases. Mesoscale contributions were isolated through filtering of these data in order to focus on fine-scale features. Streamlines, surface pressures, potential temperatures, and equivalent potential temperatures were analyzed through this method.

The study concluded that leading and parallel stratiform systems had similar synoptic environments to previous studies, with some minor differences. Leading stratiform systems were more dependent on low-level jet influence than parallel stratiform systems were. Both system types also formed in the warm sector of a frontal system along its boundary, which typically was a warm or stationary front. These systems also tended to be located in the outer edge of the right entrance region of jet streaks.

Leading stratiform systems had a surface pressure pattern very different from trailing stratiform systems. It was found that, in leading stratiform systems, a mesohigh formed behind the main convective region, and a mesolow formed ahead of the stratiform region. Parallel stratiform results were more inconclusive due to a lack of quality cases, but one case showed a surface pressure pattern almost identical to asymmetrical trailing stratiform systems. Maxima and minima of potential and equivalent potential temperatures tended to be located in the same areas, with lower temperatures near mesohighs and higher temperatures near mesolows.

It is possible that a leading inflow jet is causing the surface pressure to decrease ahead of the stratiform region in leading stratiform systems. This needs to be confirmed in future study by investigating the vertical wind profile of these systems and validate the presence of this jet.

Jesse Matthew Steinweg-Woods
Department of Atmospheric Science
Colorado State University
Fort Collins, CO 80523
Fall 2010

ACKNOWLEDGEMENTS

This research was supported by a National Science Foundation grant, ATM-0500061. I thank the National Science Foundation for the funding provided to do this research. I also must thank Dr. Richard Johnson for obtaining the grant funding so that I would have the opportunity to be here.

I would first like to thank the members of my committee, Drs. Steve Rutledge and Jorge Ramirez, for willing to be on my committee and for their helpful comments on this work. I also wish to thank my advisor, Dr. Richard Johnson, for his valuable insight and prudent guidance.

I also need to thank several members of the Johnson research group. Paul Ciesielski was very helpful with GrADS interaction and providing help on coding for my thesis work. Rick Taft was very helpful for any FORTRAN related questions I may have had and for trying to find archived information. Brian McNoldy was an immense help for IDL related questions and for advice on graphics. Eric James was very helpful in providing a framework for the entry stages and answering any questions I may have had. Becky Adams-Selin was also extremely beneficial, helping me modify code, providing a framework of programs with which to utilize my research, giving advice, and explaining how better to use GEMPAK and other programs.

Other people I wish to thank are Dr. Dan Lindsey for help with utilizing AWIPS and for being a great teacher. Jamie Schmidt has been invaluable with scheduling, reminders of deadlines, and answering graduate school related questions. Last, I wish to thank my friends and family for their continued support and encouragement throughout my graduate school experience, even when things got difficult. My mother has also been especially helpful, lending an empathetic ear to a process she has been through herself. I have greatly appreciated everyone's support, and I couldn't have done this without all of your help. Thank you.

TABLE OF CONTENTS

Chapter 1

INTRODUCTION

Leading and parallel stratiform systems, originally categorized by Parker and Johnson (2000), are two of three types of linear Mesoscale Convective Systems. Named based upon the orientation of their stratiform region in relation to the strongest convection of the system, these linear systems are frequently observed in the central plains of the United States during the spring months. The most common type, called trailing stratiform, has already been thoroughly studied. Leading and parallel stratiform systems are more uncommon and have very few studies about them.

Work has already been done on the vertical wind profile and synoptic environment of these systems (Parker and Johnson 2000). There has also been research on the structure of these systems and their internal flow characteristics (Parker and Johnson 2004; Pettet and Johnson 2003; Parker 2007b). Where the research is currently lacking is in regard to the surface features of both leading and parallel stratiform systems. This is probably due to a lack of dense observation networks required for such a study to take place. In order to study the surface aspects of these systems, a high-resolution dataset is required, and the only such dataset currently in existence available for this type of study is based on observations from the Oklahoma Mesonetwork.

Several studies have already been concluded on trailing stratiform systems (Fujita 1955; Pedgley 1962; Loehrer and Johnson 1995; Johnson and Hamilton 1988). These studies have found the locations of mesohighs, wake lows, and surface flow patterns for trailing stratiform systems. It has been shown that a mesohigh is found immediately to the rear of the strongest convection, with a wake low located just behind the stratiform region. It is theorized based on the results of Haertel and Johnson (2000) that a similar pattern of a mesohigh/wake low couplet already observed in trailing stratiform systems could also be observed in parallel and leading stratiform systems as well as long as the systems are moving.

This study aims to ascertain whether leading and parallel stratiform systems have a similar behavior, with pressure couplets straddling the stratiform region regardless of its orientation. It also needs to be determined if this pattern of behavior is common among many different cases or if the pattern varies. Additional work in this study will try to determine if parallel stratiform systems have a similar surface pressure pattern to asymmetrical trailing stratiform systems, where the stratiform region migrates towards the northern end of the system as detailed in Loehrer and Johnson (1995). It also needs to be determined if these systems can have strong pressure gradients capable of severe surface winds in their wake caused by the rearward direction of the pressure gradient force as detailed in studies from Gaffin (1999) and Coleman and Knupp (2009). Last, the study also evaluates the synoptic environment these systems form in to see if these results agree with those found in Parker and Johnson (2000).

Discovering patterns in the surface pressure features can allow more detailed modeling studies that would improve understanding of these systems' evolution. This would allow

better forecasts of system behavior, enabling timelier and more accurate warnings of severe weather, especially flash flooding which these systems are known for causing.

The current literature available on these systems and similar linear Mesoscale Convective Systems is reviewed in Chapter 2. Research on the dynamics and vertical wind profiles of trailing stratiform systems is included, as the research on this type of system is far more prevalent and can be used to find similarities between the three system types. Chapter 3 discusses the methods used to analyze the surface features of these systems along with the synoptic environment. Details of how the cases were chosen, what datasets were used to analyze surface and synoptic features, and how the data were processed through use of a high-pass filter and other mesoanalysis techniques are detailed in this chapter. Chapter 4 discusses the synoptic environment present in these cases and compares the results found to Parker and Johnson (2000) to see what similarities and differences were observed. Chapter 5 shows the results of the surface analysis with regard to several surface features and how these features differ between the two cases. Finally, Chapter 6 analyzes the results presented in Chapter 5 with greater detail and addresses the questions raised in this introductory chapter to make conclusions about the hypotheses proposed. Chapter 6 also presents conceptual models of both system types to help further visualize the evidence presented in Chapter 5.

Chapter 2

LITERATURE REVIEW

2.1 Leading and parallel stratiform MCS structure and previous research

Although research has been done on trailing stratiform systems for decades, research on the classifications of leading and parallel stratiform systems (originally classified by Parker and Johnson 2000, hereafter referred to as PJ 2000) has been very limited. Part of the issue has been the fact that PJ 2000 alluded to; only about 20 percent of linear convective systems are leading stratiform and another 20 percent are parallel stratiform. The remaining 60 percent tend to be trailing stratiform, making this linear system far more common.

As can be seen in Fig. 2.1 below, the label of which kind of Mesoscale Convective System (or MCS) is occurring depends upon how the stratiform region is structured in relation to the strongest area of convection. Parallel stratiform systems have a stratiform region extending typically to the northeast of the main convective region, with the stratiform remaining small in width due to advection ahead of the convective cells. Steering winds are mainly parallel to the development of the convective line. Leading stratiform systems appear to be the exact opposite of typical trailing stratiform systems; the stratiform region leads the convective cells.

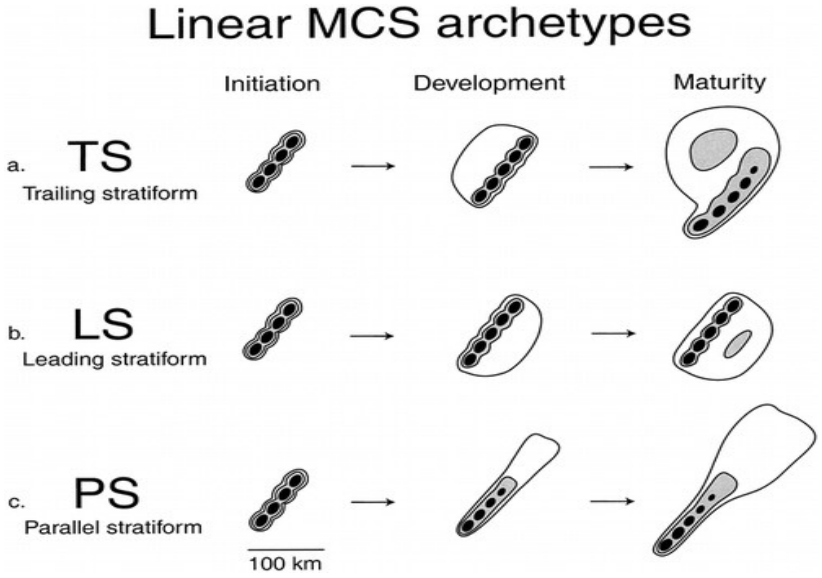

Figure 2.1: Schematic reflectivity drawing of idealized life cycles for three linear MCS archetypes: (a) TS, (b) LS, and (c) PS. Approximate time intervals between phases: for TS 3–4 h; for LS 2–3 h; for PS 2–3 h. Levels of shading roughly correspond to 20, 40, and 50 dBZ. From Parker and Johnson (2000).

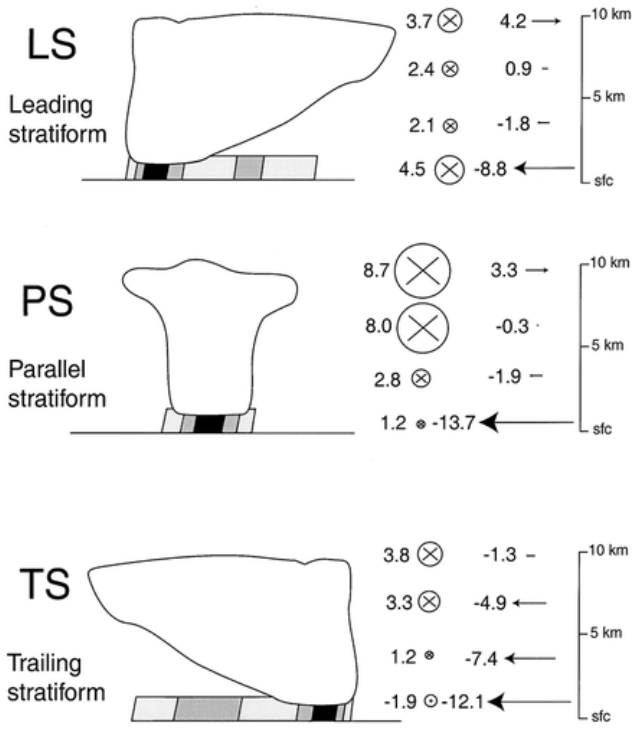

Figure 2.2: Vertical profiles of layer-mean storm-relative pre-MCS winds for linear MCS classes. Wind vectors depicted as line-parallel (X) and line-perpendicular (→) components in m s^{-1}. Layers depicted are 0–1, 2–4, 5–8, and 9–10 km. Typical base scan radar reflectivity patterns (shading) and hypothetical cloud outlines are drawn schematically for reference. MCSs' leading edges are to the right. From Parker and Johnson (2000).

PJ 2000 also compared the difference in wind structure between the three systems. They found that PS systems had significant middle and upper-tropospheric line-parallel storm-relative winds and the greatest wind shear of the three types. LS systems had weak middle and upper-tropospheric rear-to-front storm-relative winds. Winds at the surface of all three systems had strong front-to-rear inflow (see Fig. 2.2). TS systems tended to be the longest-lived of the three, and the other two systems typically evolved into a TS structure. This seems to be the most common structure for linear MCSs.

Although Fig. 2.2 shows LS systems being fed from the front, leading stratiform systems can either be fed from the front or the rear of the system (as discussed in Parker and Johnson 2004, hereafter referred to as PJ 2004). Referred to as front-fed leading stratiform (FFLS) and rear-fed leading stratiform (RFLS), PJ 2004 discuss how their structures differ. FFLS systems have a front-to-rear inflow that ascends in the main updraft region and then is overturned and flows from rear-to-front in the upper troposphere (Fig 2.3). This rear-to-front flow is the source of humidity and hydrometeors for the leading stratiform region in front of the main convective region. RFLS, by contrast, have a rear-to-front flow that ascends into the upper troposphere; this arrangement is a near mirror image of the flow structure in typical TS systems where there is ascending front-to-rear flow (Fig 2.4).

Pettet and Johnson (2003) found that there was in fact a significant difference between RFLS and FFTS systems and that the two weren't simply mirror images of each other. Unlike a FFTS where a rear-inflow jet reverses direction as it approaches the surface, the leading front-to-rear inflow jet in RFLS never changes direction. Convective cells of LS

systems also appear to be more discontinuous in nature compared to TS systems, with more elongation and space between the convective cells in the LS archetype.

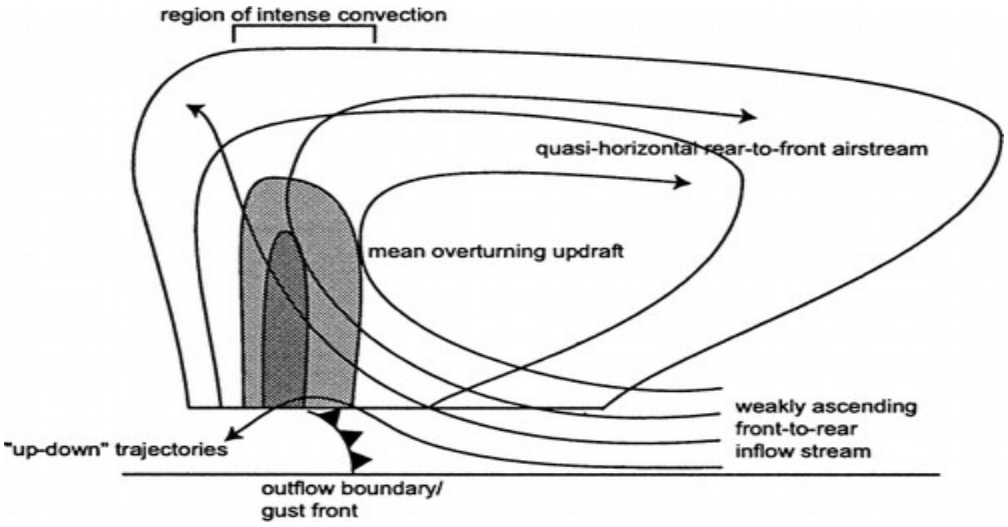

Figure 2.3: Conceptual model, based on compiled radar observations, of a front-fed convective line with leading precipitation, viewed in a vertical cross section oriented perpendicular to the convective line and parallel to its motion. From Parker and Johnson (2004).

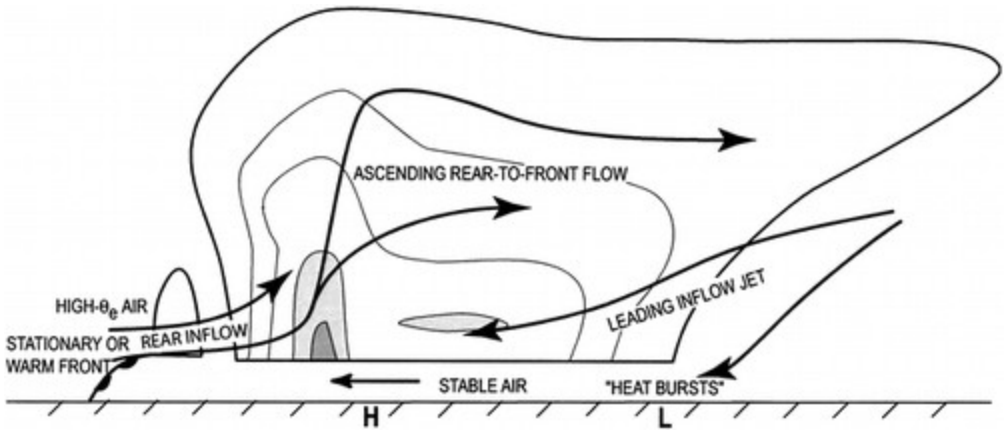

Figure 2.4: Conceptual model of a rear-fed LS MCS above a stable surface layer viewed in a vertical cross section oriented perpendicular to the convective line (i.e., parallel to its motion) during the mature stage of its life cycle. Arrows indicate mean, storm-relative flow. Radar reflectivity is indicated by thin contours. Cloud outline is thicker contour. Areas of enhanced reflectivity are shaded. Surface high and low pressure centers are indicated by H and L, respectively. From Pettet and Johnson (2003).

It would seem that having inflow from the stratiform region in the case of a FFLS system would cause the system to weaken from the evaporative cooling of the rainfall. Storm et al. (2007) addressed this issue and found that a destabilization mechanism

results from the vertical profile of cooling in the leading stratiform region. This allows the cooler air to be advected above the warmer surface air, providing increased instability that allows the convection to be maintained. They also found that LS systems tended to evolve into TS systems due to a local decrease in the low-level line-perpendicular vertical wind shear over time, as well as an increase in the surface cold pool's strength. This caused a jump updraft to form, resulting in the main updraft transitioning to the front line of the system.

Parker and Johnson (2004a) also had a similar finding, demonstrating that lower-tropospheric inflowing air in the simulations ascends, overturns in deep updrafts, and subsequently carries its water content forward from the convective line, where it gives rise to the leading stratiform region. Although it is correct that the middle and upper-tropospheric wind shear contributes significantly to the overturning of the inflow, the leading stratiform region can also provide pressure gradients that help overturn the flow as well, preventing the system from dissipating.

The shear and moisture characteristics necessary to form LS and PS systems can be similar to those required for supercell thunderstorm development. French and Parker (2008) found that very slight differences in wind shear can cause a different system to be formed. PS systems tended to have strong shear oriented parallel to a surface dryline, coupled with dry air in the middle and upper levels. LS systems tended to have moderate wind shear coupled with high instability and strong linear forcing. As can be seen in Fig. 2.5, PS and LS systems tend to require greater values of 0-6 km shear than TS systems do and require a similar amount of shear as do the lower 40% of typical supercells.

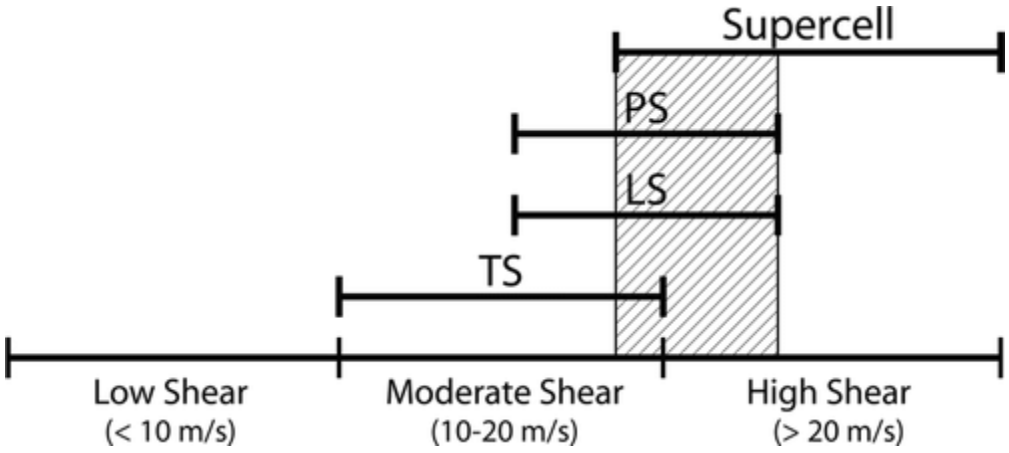

Figure 2.5: Schematic relating the convective mode to a spectrum of 0 to 6-km vertical wind shear values. Approximate shear values (m s^{-1}) are included in addition to the low, moderate, and high shear descriptors. The hatching denotes overlap between the environments for the various modes. This figure is based on the results of past climatological studies, including Parker and Johnson (2000; for LS and PS MCSs), Parker et al. (2001; for LS and PS MCSs), Evans and Doswell (2001; for TS MCSs), and Thompson et al. (2003; for supercells). From French and Parker (2008).

Parker (2007a) conducted a simulation of PS systems and found a restorative mechanism. Because precipitation particles move primarily along their convective lines, PS systems produce most of their lower-level outflow in very close proximity to the surface outflow boundary. This outflow, in turn, causes new convection to form at the boundary's location. As a result, their cold pools strengthen quite rapidly. The side effect of the intensifying outflow, however, is that the system tends to evolve into a TS archetype. The greater outflow causes a diminished line-parallel flow along the system's axis, making the flow more similar to that of a TS system with mainly front-to-rear inflow.

Parker (2007b) then describes how the environment for PS systems is very similar to that of supercell thunderstorms. Initially, supercells can develop, but if the outflows merge then a linear system forms instead. The study finds that PS systems can avoid transitioning into a TS system the longest if the line-parallel shear is large; if this is not

large enough the inflow will develop too much of a front-to-rear orientation and advect the stratiform region to the rear of the main convective lines. Figure 2.6 shows a diagram of a typical PS system, revealing that the inflow is raised in the updraft of the main convective region and is then advected in the line-parallel flow away from the convection. Notice that the pressure gradient forces generated by the updrafts also help steer the hydrometeors towards the "front" of the line.

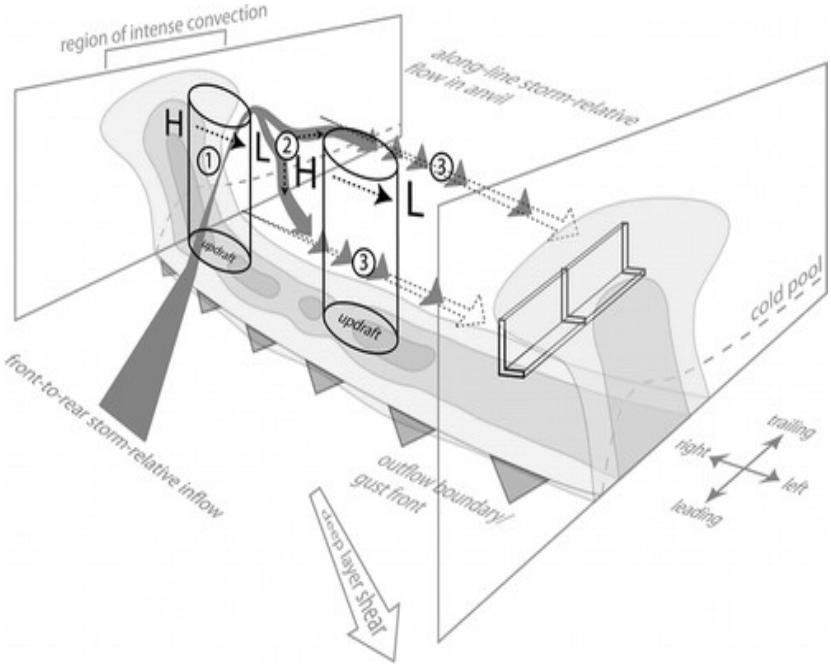

Figure 2.6: Conceptual model of along-line accelerations for a convective line within line-parallel shear, viewed in a schematic three-dimensional rendering in which the orientation of the vertical planes is perpendicular to the convective line and parallel to its motion. Typical parcel trajectories are indicated by the solid gray arrows. Pressure maxima and minima discussed in the text are indicated by "H" and "L" symbols, and pressure gradient accelerations are indicated by dashed black arrows. The solid arrows and pressure features are associated with the storm-scale, dynamic part of the pressure field; the open arrows and pressure features are associated with the mesoscale, buoyant part of the pressure field. The labels 1, 2, and 3 are used for reference in the text. From Parker (2007b).

FFLS systems also have a tendency to evolve into TS systems as well. Running a simulation of three different vertical wind profiles (see Fig. 2.7), Parker and Johnson

(2004b) discovered that middle and upper-tropospheric winds are very important to the updraft structure of the system. As the system matures, the pressure fields associated with the FFLS system tend to decrease vertical wind shear in the leading stratiform region. This is due to a low pressure center directly behind the main convective region. As this low intensifies, the pressure gradient force increases. The decreased wind shear and rearward pressure gradient force causes the updraft to shift towards the rear, advecting stratiform behind the main convective region instead of to the front.

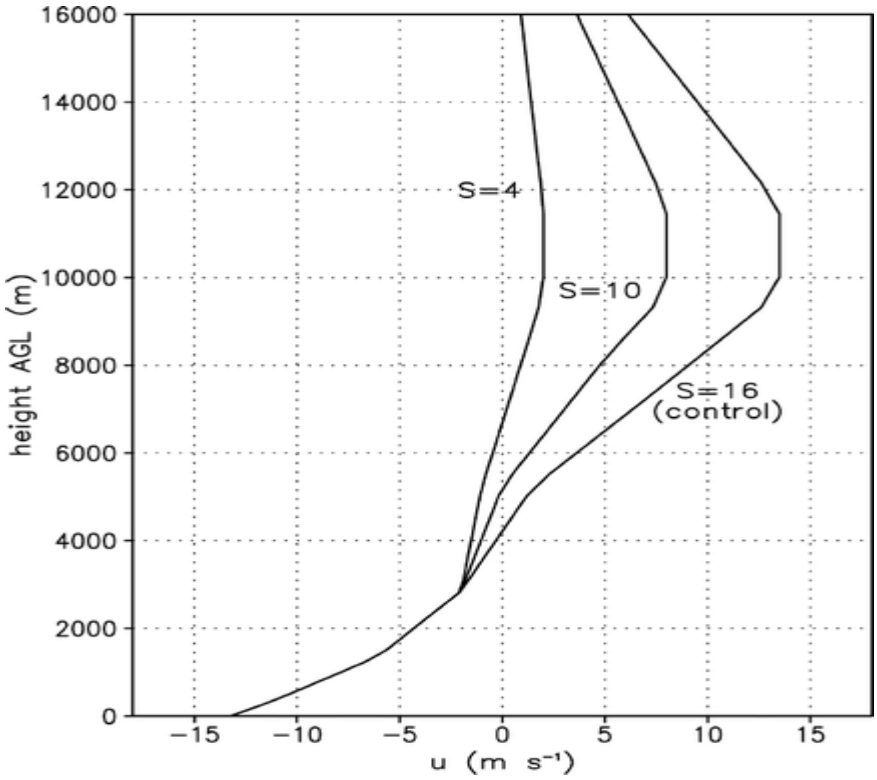

Figure 2.7: Profiles of u wind used by Parker and Johnson (2004b). The mean front-fed LS MCS wind profile is labeled as S=16 (3–10-km vector wind difference ≈ 16 m s^{-1}); S=10 and S=4 are modified wind profiles with decreased wind shear above 3 km AGL (3–10-km vector wind differences ≈10 and 4 m s^{-1}, respectively).

In terms of the severe threat between the two systems, both LS and PS systems can cause significant problems. Gallus et al. (2008) compared the number of severe weather reports that occurred between nine different types of systems. Among these systems, LS

and PS archetypes had a larger threat of tornado and hail reports than TS systems did. PS systems were also among the most likely to cause flash flooding, even more so than TS systems.

The reason behind the increased tornado and hail threat likely has to do with the increased vertical wind shear necessary for LS and PS structure; TS systems don't require as much vertical shear to maintain their structure as the other two types do. PS systems also have a tendency to rebuild themselves, producing rain that can train over one area for a large period of time.

As can be seen in Fig. 2.8, LS and PS systems produced a severe weather report a greater percentage of the time than TS systems did. In fact, LS systems were the most likely type of storm system to produce a severe report among the archetypes studied.

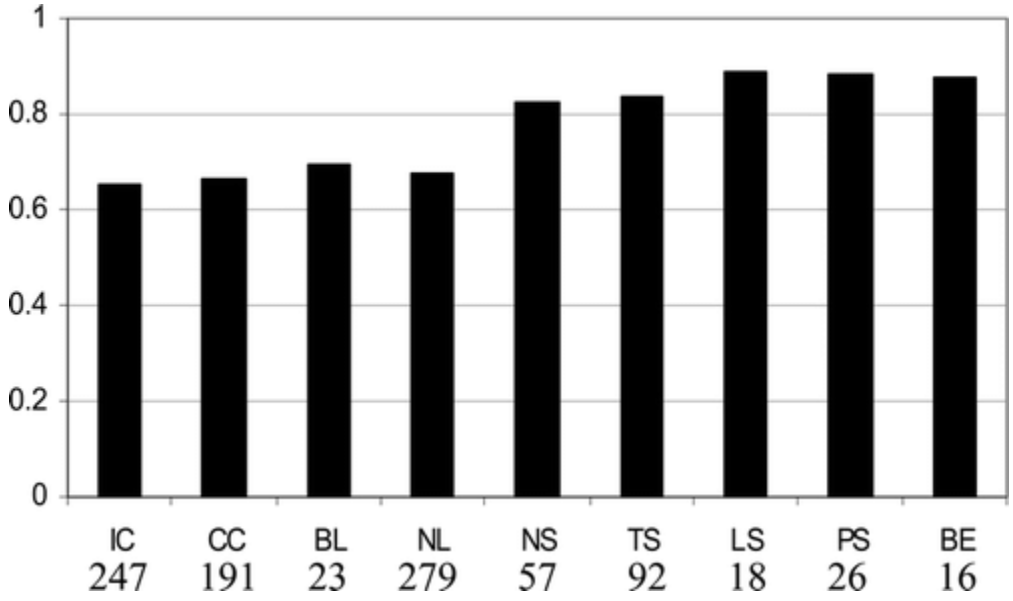

Figure 2.8: Percentage of storms with at least one severe report (not including flooding), organized by morphology with notation. IC are individual cells, CC are clusters of cells, BL are broken squall lines, NL are nonlinear convective systems, NS are squall lines with no stratiform rain, TS are trailing stratiform, LS are leading stratiform, PS are parallel stratiform, and BE are bow echoes. From Gallus et al. (2008).

2.2 Synoptic and wind features of MCSs

Even though the number of studies on LS and PS systems are sorely lacking, Mesoscale Convective Systems have been studied for quite some time. There are many similarities that can be shown between LS/PS systems and the more common generic squall line, so it is helpful to examine what other research has been done on the synoptic and wind structure of MCSs.

Cohen et al. (2007) studied which synoptic and vertical wind profiles were best suited to strong MCSs. They separated MCSs into three different categories: weak (producing less than six severe wind reports, strong (producing six or more wind reports, but with no reports greater than or equal to 26 m s^{-1}), and derecho (actual wind damage reports or winds greater than or equal to 26 m s^{-1}). The best discriminator among these three was an analysis of the vertical wind shear profile and how perpendicular this shear profile was to the convective line; the more perpendicular the shear profile is, the greater the wind threat.

In Fig. 2.9, it can be shown that greater magnitudes of vertical shear, regardless of where the shear vector is considered (with the exception of the 6-10 km shear magnitude), result in greater surface wind intensity. The difference is most profound in the 0-10 km shear magnitude.

Low-level jets (or LLJ) typically occur in the early morning hours. Their influence on MCSs can be profound due to the amount of moisture they advect into the systems. Gale et al. (2002) studied the dissipation of MCSs and found LLJs to have a significant impact.

Out of the 47 cases studied, 90% of their cases were affected by an LLJ at some point in their evolution. They found a slight tendency for MCSs to dissipate after the LLJ weakened, but there was a much better connection to MCS dissipation when the LLJ either ends or no longer affects the MCS. Thus, it is important to monitor the influence of the LLJ on any MCS, as the behavior of the LLJ can be used as a proxy for MCS prediction.

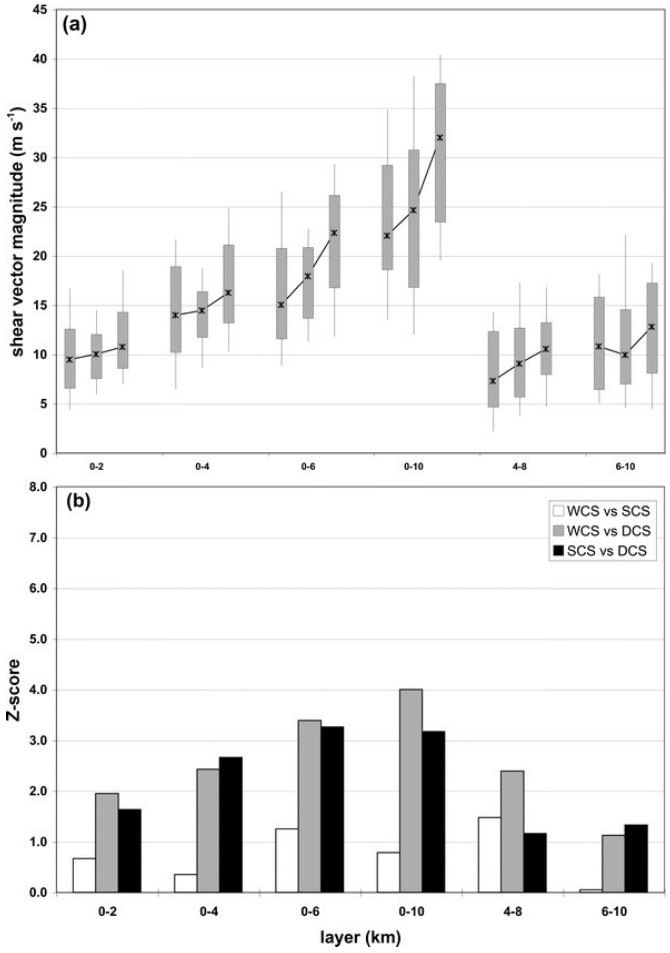

Figure 2.9: (a) Box-and-whiskers plots for the 0–2-, 0–4-, 0–6-, 0–10-, 4–8-, and 6–10-km shears. Each set of three categories indicates the results for the WCSs, SCSs, and DCSs, from left to right. The whiskers stretch to the 10th and 90th percentiles and the boxes enclose the 25th and 75th percentiles. The lines connect the medians (asterisks) for the distributions for each variable. (b) Absolute values of Z scores resulting from the Mann–Whitney test between WCSs and SCSs, SCSs and DCSs, and WCSs and DCSs for the 0–2-, 0–4-, 0–6-, 0–10-, 4–8-, and 6–10-km shears. From Cohen et al. (2007).

As previously discussed, TS systems tend to be a mirror image of RFLS systems, consisting of a rear-to-front downdraft and a front-to-rear updraft. To prove these wind patterns were not simply due to synoptic scale influences, Knievel and Johnson (2002) studied a MCS with trailing stratiform structure and investigated the wind flow of the system. Using a Barnes scheme, which is similar to the filtering method used in this paper (this will be discussed later in Chapter 3), the synoptic wind was filtered out so that only the mesoscale contribution remained. After the filtering was complete, four flows remained: a rear-to-front mesoscale downdraft and a front-to-rear mesoscale updraft that horizontally converged in the middle troposphere, as well as divergent outflows in the lower and upper troposphere. Because the flows remained even after the synoptic influences were removed, the authors concluded these flows must be internal and fundamental to the MCS.

The movement speed of an MCS is also an important prediction tool in severe weather forecasting. Mahoney et al. (2009) discovered the connection between convective momentum transport and the overall movement speed of MCSs. The authors utilized the Weather Research and Forecasting (or WRF) model to simulate these MCSs and analyze their evolution. One of their findings was that the speed of the cold pool and overall speed of the MCS are very similar. As can be seen in Fig. 2.10, MCS speed and average maximum wind speed in the leading portion of the cold pool are closely matched, even throughout the system's existence. Thus, the MCS moves largely at the same speed as the leading edge of its cold pool.

They identified the primary source of the momentum field in the leading edge of the cold pool as being the vertical advection of the perturbation wind. This enhances the cold

pool's strength, enabling a positive feedback mechanism that further accelerates the system. The authors claim that current numerical weather prediction models do not take convective momentum transport into account, resulting in a prediction that is too slow. The models need to be improved in order for more accurate speeds of these systems to be assessed properly.

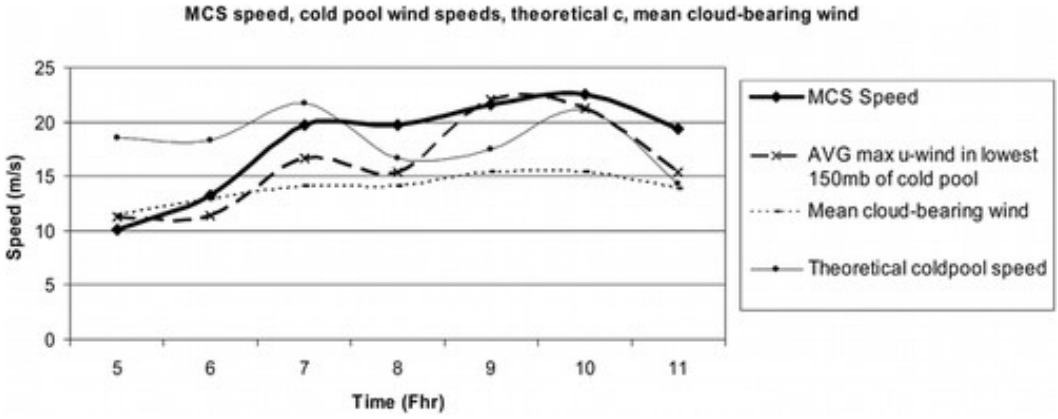

Figure 2.10: Speed of MCS (m s^{-1}, solid), average of gridpoint maximum wind speed in the lowest 3 km of the cold pool (m s^{-1}, large dashed), average mean cloud-bearing wind (from 900 to 200 hPa, m s^{-1}, small dashed), and theoretical cold pool speed (m s^{-1}, thin solid). From Mahoney et al. (2009).

Dial et al. (2010) investigated which synoptic and wind environments are best suited to discrete cells as opposed to linear systems. Although many factors differentiated the two, there were a few that were most pronounced. One of the largest discrepancies between the two is which kind of initiating boundary caused the initial convection. If it was a dryline, 65% of the storm systems would have discrete cells. If the boundary was a cold front, 60% of the storm systems would be linear. The reasoning for this has primarily to do with the mean cloud-layer wind. Near cold fronts, the cloud-layer wind tends to be oriented parallel to the front (somewhat north to south). Drylines tend to have

cloud-layer winds more perpendicular to the front alignment, thus causing convection development to form in a more discrete manner.

A caveat to this rule, however, is presented at the conclusion of the paper. If the zone of development has strong, deep, linear forcing, the growth will rapidly transition into a linear system regardless of the cloud-layer wind vector. Thermodynamic parameters also didn't discriminate between a more likely mode of convection; high values of Convective Available Potential Energy (CAPE) don't necessarily trend towards discrete or linear systems.

Forcing, or lack thereof, can have a significant impact on the evolution of squall lines. Jewett and Wilhelmson (2006) explored the difference in evolution between squall lines with and without a cold front present. With the cold front present, as can be seen in Fig. 2.11, the modeled three-dimensional squall lines produce different vertical structures. The updraft is more intense and narrow in scale when the cold front is present, whereas in the isolated system the updraft is less intense. However, this also results in a great quantity of rainfall in the isolated system.

They also found that, without forcing, the cells would split. This splitting interfered with neighboring cells destructively and diminished their strength. Cells with the cold front present didn't have this problem due to differences in anticyclonic cell intensity and propagation. The increased shear provided by the cold front was considered the primary factor in allowing this to happen. Because of this, cell interaction is deemed more important to storm propagation than the role of frontal ascent or enhanced moisture convergence.

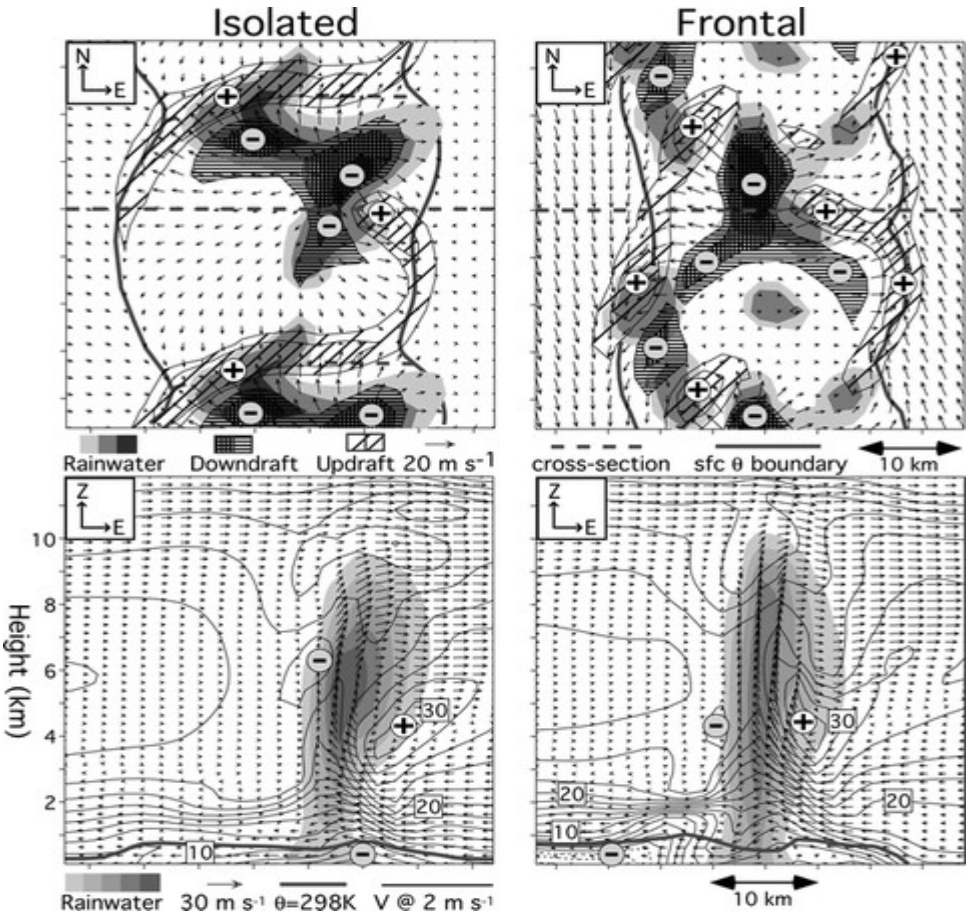

Figure 2.11: Close-up plan view and cross sections at 75 min through (left) isolated and (right) frontal convection: (top) 2.1-km cloud + rainwater (shaded exceeding 0.5, 1.5, and 4 g kg^{-1}), vertical velocity at 125 m AGL (hatched exceeding ±0.5 and 1.5 m s^{-1}), surface perturbation wind vectors, and frontal/gust front boundaries (bold lines). (bottom) Cross sections taken along bold dashed line above. Rainwater (shaded exceeding 0.5, 2, 4, 6, and 8 g kg^{-1}), V (normal velocity contoured every 2 m s^{-1}), in-plane velocity vectors, and 298-K isentrope (bold solid line) for the lowest 12 km are shown. Prominent local maxima and minima are indicated with a + or −. From Jewett and Wilhelmson (2006).

Skamarock et al. (1994) did a modeling experiment entirely absent of large-scale forcing. Even without the forcing present, the resulting MCSs formed from the modeling experiment strongly resembled many observed systems that occurred in forcing. Because of this, the authors conclude large-scale forcing is unnecessary to produce the distinguishing features of MCSs. This further strengthens the argument made by Jewett and Wilhelmson (2006) regarding the importance of cell interaction for the evolution of MCS structure.

The LLJ, as previously discussed, has a very important role when interacting with MCSs. Instead of comparing rates of decay, as Gallus et al. (2002) did, French and Parker (2010) investigated how LLJs can enhance the strength of an existing squall line depending on the LLJ's orientation. Figure 2.12 shows that the addition of a LLJ traveling from front to rear strengthens the system, but a LLJ oriented from rear to front actually weakens it. This study assumes that the squall line is a TS system; the results of the study would likely change if this were to be simulated on a LS or PS system.

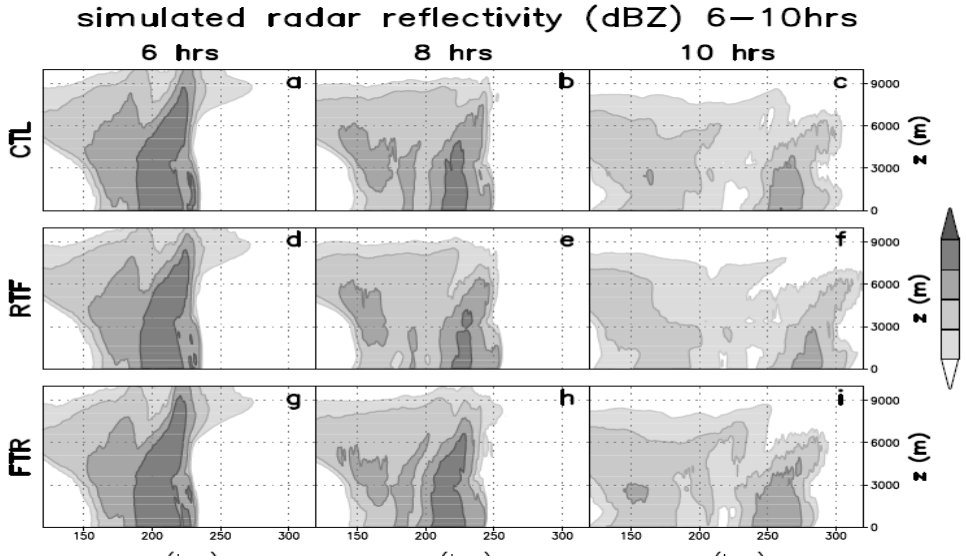

Figure 2.12: Vertical cross sections of simulated radar reflectivity (dBZ, shaded as shown) for the CTL (a,b,c), RTF (d,e,f), and FTR (g,h,i) simulations at (from left to right) t= 6:00, 8:00, and 10:00. From French and Parker (2010).

As previously referenced in Cohen et al. (2007), stronger values of low-level shear in MCSs tend to produce a stronger system. Coniglio et al. (2006) finds that the addition of upper-level shear is also important to the maintenance and growth of a strong MCS as well. To simulate the effect of additional upper-level shear, they modeled three-dimensional simulations of MCSs and added varying levels of upper-level shear to a wind profile with weak to moderate low-level shear. Choosing three different amounts of

shear to add (0, 15, and 30 m s^{-1}) to the 5-10 km section of the vertical wind profile, the model output shows (see Fig. 2.13 below) a definitive increase in overall precipitation levels the greater the amount of shear added.

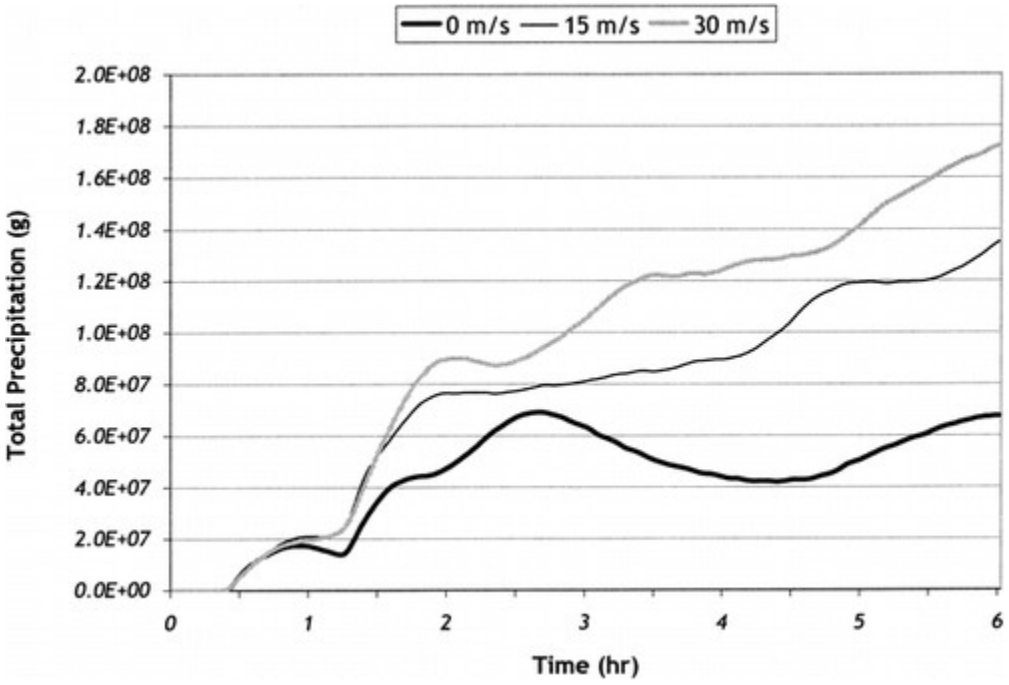

Figure 2.13: Evolution of the domain-integrated rainwater for 3D0, 3D15, and 3D30. From Coniglio et al. (2006).

A later paper by Coniglio et al. (2007) addresses this same issue using a different metric. The authors compared the vertical wind shear profiles from 0-10 km between dissipating and mature MCSs and found that the 0-10 km shear magnitude was greater by 11.7 m s^{-1} on average in mature MCSs compared to dissipating MCSs. This strongly signifies that shear is important to strong and mature MCSs not only in low-levels but at upper-levels as well.

Even though these results seem rather convincing, contrasting articles have found that having too much lower or upper-level shear can actually be a detriment to the MCS's

development. Fankhauser et al. (1992) observed an MCS that formed in strong unidirectional shear. They comment that without a continual supply of front-to-rear flow through the precipitation band on the flanks of the constituent cells, it is unlikely the squall line would have survived as long from the detrimental effects of strong shear aloft. The reason strong upper-level shear can be an issue is that the shear can cause the updraft to tilt towards the front of the system, allowing some of the precipitation to be entrained into the updraft and reduce its buoyancy. If too much precipitation were to be entrained, the entire updraft could be cut off and cause the system to dissipate.

Through a modeling study of MCSs, Szeto and Cho (1994) discovered a major issue with MCS development if the low-level shear were too great. When this happened, they found the propagation speed of the convective line was slower than the middle to upper level winds, and consequently the updraft started to evolve into a downshear tilt. This tilting induced stronger subsidence warming, increasing the stability at the front of the system. The tilting also allowed, as discussed previously, for precipitation to be entrained into the system, reducing the buoyancy of the inflow air.

2.3 MCS structure and dynamics

This section discusses the research addressing the dynamic mechanisms that help to sustain MCSs and some of the specifics regarding the structure and forms MCSs can take. Although this research is on MCSs in general, many of these attributes can also be applied to LS and PS systems as well.

Most squall lines require a cold pool to maintain their strength, acting as a wedge to push air ahead of it up into the storm system. Stoelinga et al. (2003) found that this is not always the case. They did a case study on a 19-20 June 1979 squall line that did significant damage in the central US and modeled it to find what role a CFA (or cold front aloft) played in providing buoyancy for the system's maintenance. Their findings show the CFA was actually the primary cause of buoyancy in the system and that the cold pool was not necessary for the squall line's longevity. It must also be noted, however, that this system had no stratiform region, which may mean this only applies to squall lines without one.

Fovell et al. (2006) explored what occurs when convection initiates ahead of an approaching squall line (in this case at night). In the model simulations the authors used, it was found that convection which formed ahead of the line would eventually be caught up by the squall line itself. When that occurred, if the convection had precipitation before the squall line reached it, the precipitation would interfere with the squall line, causing cold pools of its own to form and cutting off some of the inflow for the squall line, weakening the system. However, this also increases the squall line's propagation speed because the new storms are taking the place of the parent thunderstorms as they flow over the cold pool, thus increasing the overall speed of the system.

Correia and Arritt (2008) analyzed the thermodynamic profiles of several MCSs at various locations inside the systems' structure. The analysis was divided into seven locations among what typically were TS systems: A – wake region, B – stratiform-back edge, C – stratiform gradient, D – stratiform-center, E – transition, F – leading line, and G – environment ahead of the approaching system. Figure 2.14 details the composite

profile of all of the MCSs analyzed. Low-level moisture is prevalent ahead of the system with a drier mid-layer near 750 hPa located between the convective and transition regions. Moisture becomes more elevated towards the stratiform center, with values of relative humidity approaching 100% there. Equivalent potential temperature values also are highest in the environment just ahead of the main convective region, with colder equivalent potential temperature values along the back edge of the stratiform region (a similar analysis of surface θ_e values will be done on this paper's LS and PS cases in Chapter 5).

TS systems tend to evolve into an asymmetrical pattern. Hilgendorf and Johnson (1998) made this conclusion from case studies of WSR-88D data. Initially the system starts out symmetrical, but over time the stratiform region moves towards the northern edge of the system. Two to three hours after this occurs, the strongest convection shifts towards the southern edge of the system, consistent with the asymmetric model of Houze et. al (1990) (Fig. 2.15).

The reason suggested for this shift in organization has to do with (1) the direction and magnitude of the system-relative flows and (2) Coriolis force effects. With respect to (1), along-line flows towards the north are as strong as or stronger than the cross-line flows of the pre-MCS environment. This causes a shift of stratiform to the northern edge and a subsequent shift of convection towards the southern edge of the line afterwards. Regarding (2), Skamarock et al. (1994) showed that the Coriolis force is also an important factor in the development of asymmetry by (a) turning the front-to-rear ascending flow in the convective line toward the north and (b)turning the descending rear-inflow behind the system to the south.

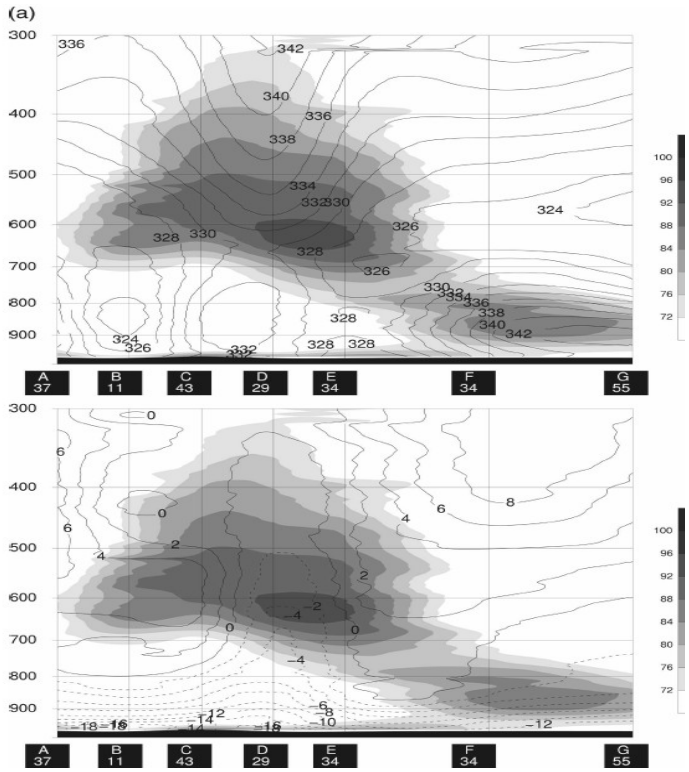

Figure 2.14: Cross section of the composite vertical profiles with regions A (wake; left) to G (environment; right) from above discussion. Relative humidity (shaded greater than 72%), (a) equivalent potential temperature (black contours every 2K), and (b) storm-relative u-wind component in the plane of the cross section (contoured every 2 m s^{-1} from -20 to 10 m s^{-1} with dashed contours indicating negative values). The horizontal scale between the composite soundings is 0.5° each for A through E and 1° each from E to G. The number of dropsondes used in the composite is also shown. From Correia and Arritt (2008).

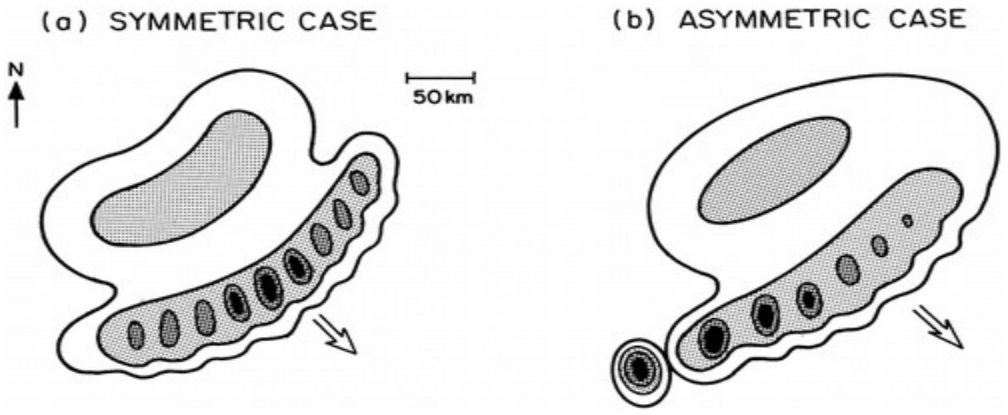

Figure 2.15: Schema depicting (a) symmetric and (b) asymmetric types of leading line-trailing stratiform MCS precipitation organization. Large vector indicates direction of system motion. Levels of shading denote increasing radar reflectivity, with most intense values corresponding to convective-cell cores. Horizontal scale and north arrow are shown. From Houze et al. (1990).

Horizontal negative vorticity plays a major role in MCS dynamics. Rasmussen and Rutledge (1993) observed several squall lines and how negative horizontal vorticity, or the rotation of air along a horizontal axis anti-cyclonically, affected the evolution of the squall lines. A sloping zone of horizontal vorticity is pushed, initially oriented slightly in the vertical, more towards a horizontal orientation. As the system intensifies, the horizontal vorticity strengthens and reaches its most vertical orientation. When the system begins to dissipate, the vorticity weakens and remains in a quasi-horizontal state (see Fig. 2.16). The negative vorticity generated in the storm interior can actually cause a positive feedback mechanism to develop. This is done by the shearing flow associated with the vorticity bringing the anvil cloud rearward over potentially cooler air. This maintains the horizontal buoyancy gradients that can then reinforce the negative vorticity.

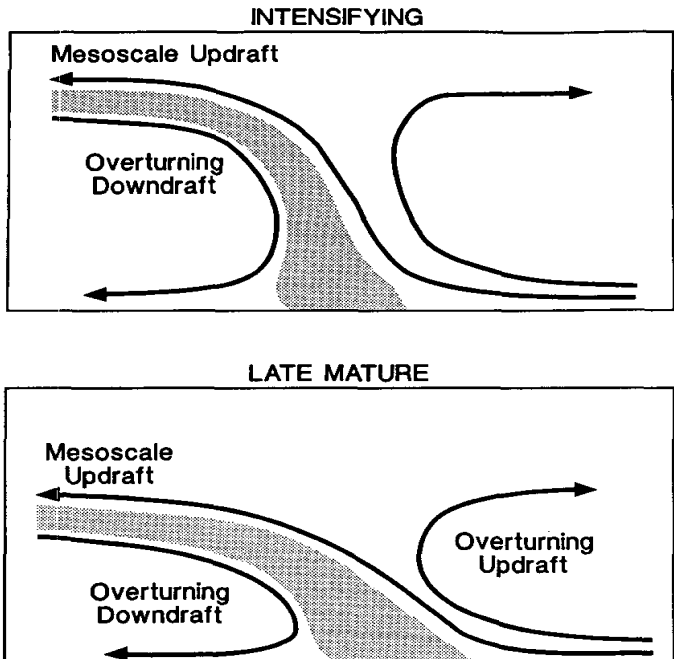

Figure 2.16: Schematic diagram of squall line features adapted from Thorpe et al. (1982). The vorticity zone referred to in the text is shaded. Modifications shown here are the designation of "mesoscale updraft" and the evolution shown: the top schematic is representative of an intensifying squall line and the bottom schematic represents the structure late in the mature stage. From Rasmussen and Rutledge (1993).

2.4 MCS surface pressure features

This section discusses the research that has already been done on mesohighs, wake lows, and other surface pressure features of MCSs. The papers addressed in this section will apply to TS and other similar types of MCSs; LS and PS systems have yet to be addressed in this area in much detail.

The basic structure of surface pressure patterns in MCSs can be seen in Fig. 2.17 below. A mesohigh tends to form at the back edge of the main convective region, with a wake low forming just behind the rear of the stratiform region. There also tends to be a weak pre-squall low that forms ahead of the squall line's approach.

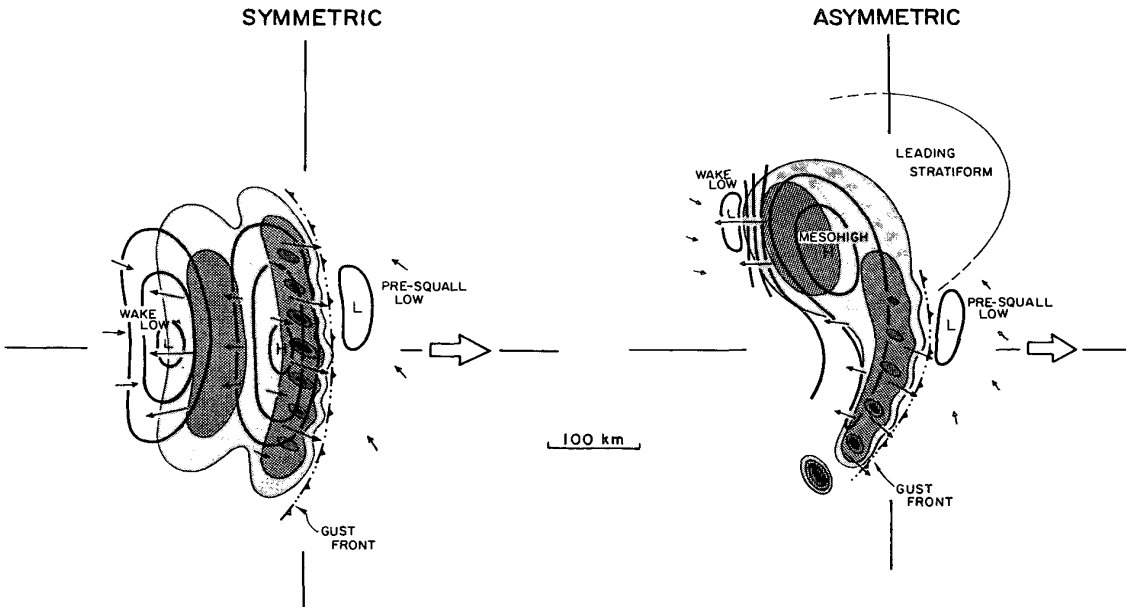

Figure 2.17: Conceptual model of the surface pressure, flow, and precipitation fields associated with the (a) symmetric and (b) asymmetric stages of the MCS life cycle. Radar reflectivity field is adapted from Houze et al. (1990). Levels of shading denote increasing radar reflectivity, with darkest shading corresponding to convective cell cores. Pressure is in 1-mb increments. Small arrows represent the surface flow. Lengths of the arrows are proportional to the wind speed found at their center. The large arrows represent storm motion. From Loehrer and Johnson (1995).

Haertel and Johnson (2000) focused on trying to explain what caused these pressure features. They found both features are formed in part as a linear response to low-level

cooling associated with the stratiform region of precipitation. The mesohigh is due to the cold, dense air just above the surface from evaporative cooling of hydrometeors. This cooling causes the air to sink, increasing the pressure locally at the location of the mesohigh. The wake low can be attributed to subsidence warming in the wake of the system, meaning a less dense lower troposphere.

A possible explanation for the formation of the wake low is the descending rear-inflow jet causing adiabatic warming at the rear of the MCS. Johnson and Hamilton (1988) make this argument and display it via a schematic in Fig. 2.18. A rear-inflow jet descends over the location of the wake low, producing warm, dry air. Even though some evaporative cooling is taking place near the location of the wake low, the adiabatic warming is far stronger due to the precipitation being only light, resulting in a net temperature increase of the air in the vicinity of the wake low. It is postulated the reason for the wake low being located so close to the rear of the stratiform region is due to the contribution of warming in this area. Subsidence warming of the sinking air in the stratiform region is likely contributing to the magnitude of the wake low, thus the pressure is at a minimum where the rear-inflow jet intersects the back edge of the stratiform region.

Fujita had done significant research on the evolution of mesohigh and wake low couplets. The first studies on these couplets were done by Fujita (1955). As detailed by Johnson (2001), Fujita claimed there were five stages in the evolution of the couplet. At first, a small mesohigh develops during the initiation stage. Next, the system further develops and the mesohigh expands in scale. The mature stage causes the mesohigh to decrease in strength and a wake low to develop. As the system dissipates, the wake low

grows and the mesohigh shrinks in intensity. Last, the remnants of the system cause the wake low to fill and the mesohigh to flatten out.

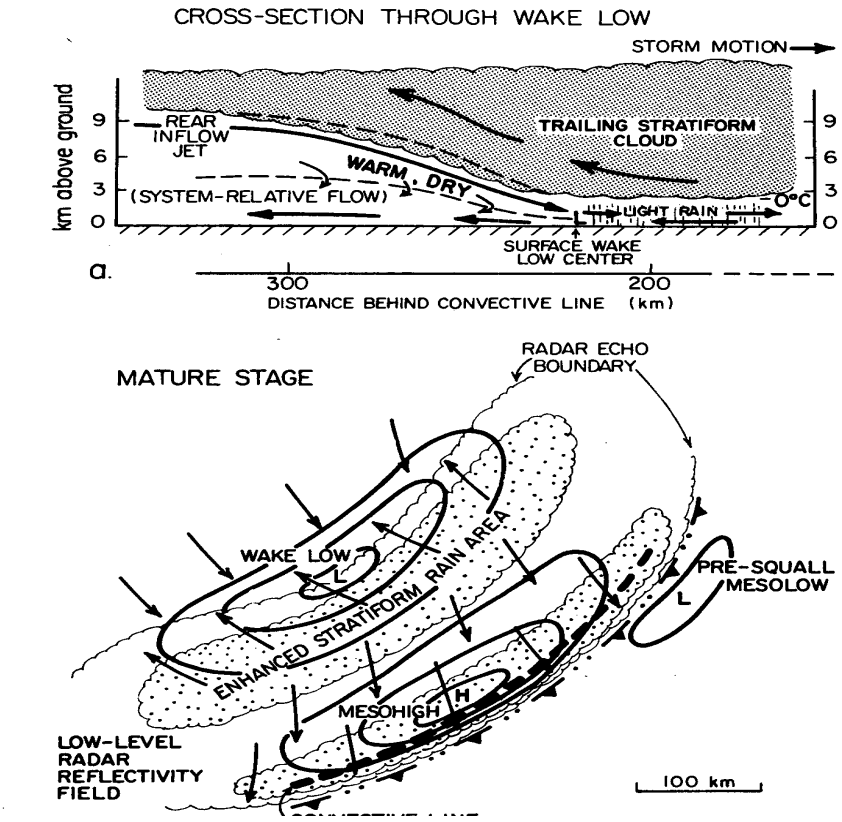

Figure 2.18: Schematic cross section through wake low (a) and surface pressure and wind fields and precipitation distribution during squall line mature stage (b). Winds in (a) are system-relative with the dashed line denoting zero relative wind. Arrows indicate streamlines, not trajectories, with those in (b) representing actual winds. Note that horizontal scales differ in the two schematics. From Johnson and Hamilton (1988).

Inside of these mesohighs and wake lows are transient pressure changes that have relatively short life spans but can contribute to the total pressure field inside of the mesohighs and wake lows. Knievel and Johnson (1998) explored this phenomenon and found many transient highs and lows can occur throughout the life cycle of a typical MCS. The transitory highs only lasted an average of 124 minutes and the transient lows only 91 minutes, so these were difficult to detect. The transients that were detected

seemed to form in a similar cycle to the mesohighs and wake lows they occurred inside of, with highs tending to develop first and lows developing later on in the evolution of the MCS. Transitory highs and lows also matched the same pattern of fluctuation that stratiform and convective precipitation rates had.

The surface-wind flow characteristics caused by this pressure pattern also need to be discerned. Vescio and Johnson (1992) discovered a pattern of wind flow that was consistent not only with a one-dimensional model simulation but also observations. They found westerlies were at a maximum just ahead of the mesolow, easterlies were at a maximum just ahead of the wake low, maximum divergence occurred behind the mesohigh, and maximum convergence occurred to the rear of the wake low (see Fig. 2.19). Model results confirm the locations of these maximum areas of surface flow are due to the eastward propagation of both pressure systems. As the wave moves eastward, the air parcels are moving eastward at a slower rate, or to the west relative to the wave. Eastward moving parcels eventually decelerate as they head towards the mesohigh and reverse direction. The same can be stated about the east winds just ahead of the wake low.

Sometimes the pressure gradient force between the mesohigh and wake low can be so intense, strong easterly surface winds can occur behind the trailing stratiform region and cause significant damage. Two such cases were explored by Gaffin (1999). The winds in both cases exceeded 50 knots, but these strong wind events weren't forecasted properly. The author recommends looking for signs that a wake low is approaching. Two methods can be used: either look for sudden pressure drops of greater than 4 hPa in one hour, or look for sudden temperature increases and dewpoint decreases. Wake lows are often

associated with heat bursts, which can cause temperature rises of 5-10°C and dewpoint falls of 10-15°C.

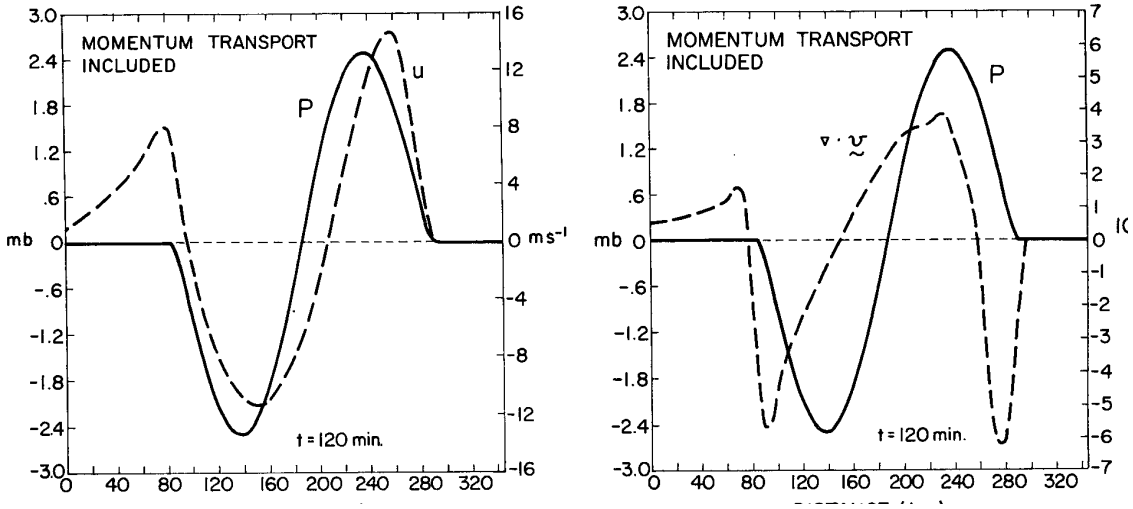

Figure 2.19: Predicted (a) wind distribution (m s^{-1}) and (b) divergence (10^{-4} s^{-1}) at 120 min for 2.5-mb pressure wave with effects of convective-line momentum transport at model-layer top included. From Vescio and Johnson (1992).

Not all wake lows cause such severe winds, but many do. Coleman and Knupp (2009) studied what causes the difference between the two outcomes. After several case studies, three primary factors were considered important: a large pressure gradient, slow intrinsic speed of propagation, and an ambient wind in the same direction as the pressure gradient (headwinds with U<0). As can be seen in Fig. 2.20 below, in order to minimize the pressure gradient necessary for a 25 m s^{-1} wind, the background wind U needs to be as negative as possible, and c – U needs to be as small as possible. For example, a pressure differential of only 2 hPa is required as long as the c – U difference is less than 11 m s^{-1}.

This is due to a requirement of having the eastward component of the wind maximized as much as possible. If there were strong southerly flow at the surface, the easterly component of the wind is not weakened, allowing the easterly surface wind speed to be

maximized. A slow moving storm system (since MCSs tend to head east in the US midlatitudes) would also reduce any eastward momentum, which could weaken the strength of a strong easterly wind.

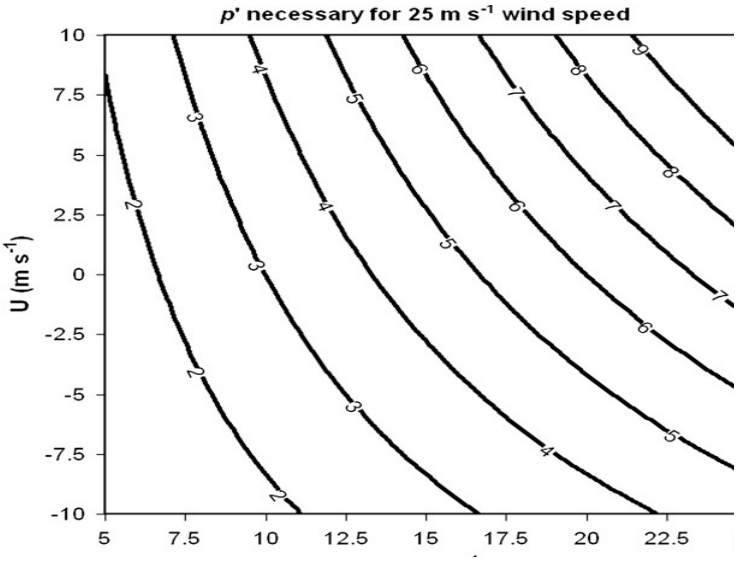

Figure 2.20: The amplitude p' (hPa) required in an idealized trough required to produce winds of 25 m s^{-1} (50 kt, defined as severe) as it varies with the intrinsic speed c – U (m s^{-1}) of the trough and the background wind U (m s^{-1}). Here, U > 0 implies a tailwind, and U < 0 implies a headwind relative to the propagating trough. From Coleman and Knupp (2009).

2.5 MCS relationship to floods

Flash flooding is very problematic, as it causes more deaths on average than any other type of natural disaster based on the National Weather Service's *Storm Data*. Besides hurricanes and high-precipitation supercells, MCSs are particularly prone to causing flash flooding. Because of this, studying their precipitation characteristics and the physical processes behind their precipitation production remains a pressing issue.

Schumacher and Johnson (2005) discovered which types of storm systems caused large amounts of precipitation. Of the 116 events they reviewed, 65% of the extreme rain

producing events were MCSs. Two common archetypes of MCSs were discovered to be the most common of the extreme rain events: trailing line/adjoining stratiform systems (TL/AS) and back-building/quasi-stationary (BB) systems. As seen in Fig. 2.21 below, TL/AS systems look very similar in structure to TS systems with one key difference: the convection is typically oriented east-west instead of north-south. BB systems seem to be somewhat similar to PS systems in structure, except they move far more slowly and tend to have greater levels of new cell formation at the rear of the system than PS systems typically have.

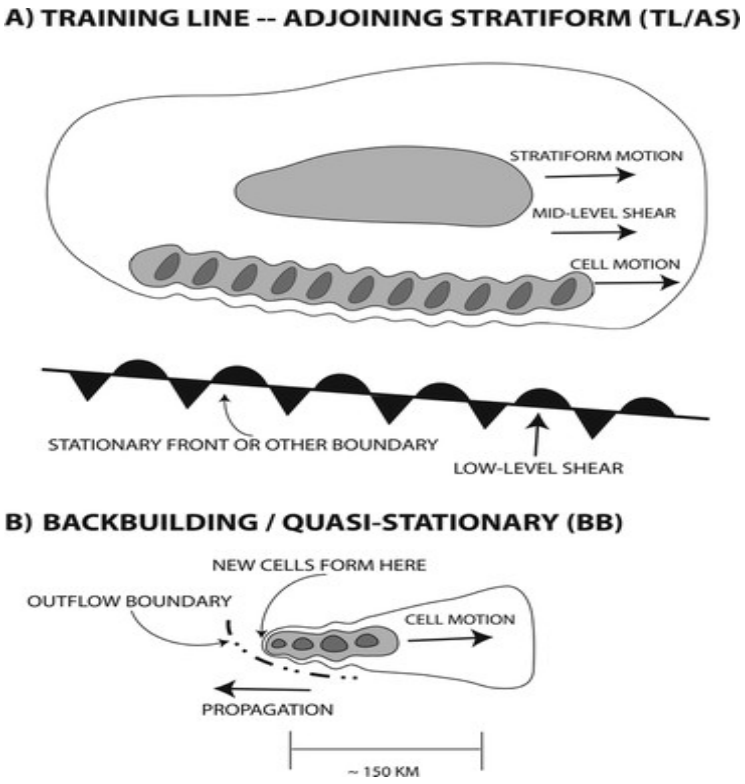

Figure 2.21: Schematic diagram of the radar-observed features of the (a) TL/AS and (b) BB patterns of extreme-rain-producing MCSs. Contours (and shading) represent approximate radar reflectivity values of 20, 40, and 50 dBZ. In (a), the low-level and midlevel shear arrows refer to the shear in the surface-to-925-hPa and 925–500-hPa layers, respectively. The dash–dot line in (b) represents an outflow boundary; such boundaries were observed in many of the BB MCS cases. The length scale at the bottom is approximate and can vary substantially, especially for BB systems, depending on the number of mature convective cells present at a given time. From Schumacher and Johnson (2005).

2.6 Summary

The literature review shows that, while TS systems have been studied in great detail, LS and PS systems need to be studied more rigorously to see if the same surface features and structure apply to these systems as well. The existing studies of LS and PS systems have already indicated the vertical wind structure and synoptic characteristics these systems form in (Parker and Johnson 2000). However, knowledge of the surface parameters of these systems is still lacking.

It has been well documented since Fujita (1955) that squall lines typically have a leading mesolow, a mesohigh in the convective region, and a wake low behind the stratiform region. However, this has only been found to be true for TS systems. This has yet to be documented in LS and PS systems. It needs to be determined if wake lows are associated with the stratiform precipitation region of such systems. Pettet and Johnson (2003) had observed two LS systems and found that in one of the systems, the mesolow actually stayed ahead of the stratiform region instead of following it. This behavior needs to be further examined via the surface pressure fields of other LS systems, which this paper will attempt to solve.

Haertel and Johnson (2000) highlight the problem of not knowing with great certainty as to what exact mechanism causes the formation of the intense wake low. With additional case studies to observe in this paper, perhaps the mechanism can become more transparent. It is possible that the mechanism of wake low production may be different depending upon the system structure.

Several wake lows have also caused severe surface winds (Gaffin 1999). It needs to be discovered if LS and PS systems can have wake lows of similar strength and interior

wind directions that support strong easterly winds. If so, it needs to be determined whether similar forecasting techniques used for TS systems, such as observing rapid pressure drops or temperature rises to identify approaching wake lows, can also be applied to LS and PS systems.

Chapter 3

METHODOLOGY AND DATA ACQUISITION

3.1 Leading and parallel stratiform case definition

It was originally necessary to define which cases were going to be used in this study. In order to do this, archived radar mosaics were studied from the National Center for Atmospheric Research Mesoscale and Microscale Meteorology Division (MMM) archive (available at http://www.mmm.ucar.edu/imagearchive). Using the definition of LS and PS systems from Parker and Johnson (2000), each day was analyzed over the Southern Great Plains region from April to June for the years 2002-2007 to find cases that matched the reflectivity definition from Fig. 2.1.

The reason the months of April to June were chosen is because these months tend to be the peak of MCS activity, especially in the Great Plains. The months of March and July were tried, but unfortunately no cases were found during these months. The years of 2002-2007 were chosen due to the limitations of the WSI NOWrad reflectivity data located at the same site (http://www.mmm.ucar.edu/imagearchive/wsi). These reflectivity data are easily loaded into the General Meteorological Package (GEMPAK) for studying the patterns of reflectivity and surface feature transitions and is of 15-minute resolution.

The cases also had to occur inside of the state of Oklahoma so that the mesoscale features could be analyzed properly with the high-resolution Oklahoma Mesonet, which

consists of 120 stations with 5-minute resolution data. Cases also had to occur in the main state region, as cases occurring in the panhandle had to be discarded due to the lack of resolution in this region. Once cases had been determined meeting the radar reflectivity patterns defined previously, each case was given a score from 1 to 10, with 10 being the closest possible match to the archetype. Only cases scoring a seven or higher were used in the study in order to obtain cases of high fidelity to the specific system category. Higher scores were given for such parameters as duration, horizontal length of the system, the size of the stratiform region, and clearly defined separations between convective and stratiform regions. This procedure is admittedly subjective and relies heavily on individual interpretation of the reflectivity image, but it is the most efficient way to find cases.

After the cases had been identified, each case then was plotted onto a latitude/longitude grid box inside GEMPAK. At each 15-minute radar image, a box of latitude and longitude coordinates was defined surrounding the entire LS or PS system. This is necessary for a time-space transformation of the data which will be discussed in more detail later in this chapter.

Finally, the speed and direction of each case at each 15-minute interval had to be determined. The method chosen for this task was to download the appropriate radar images from the National Climate Data Center Hierarchical Data Storage System (http://has.ncdc.noaa.gov). These radar images were then loaded into the Advanced Weather Interactive Processing System, or AWIPS. This program has a heading-speed tool that can be used to determine the approximate speed and heading of the storm system's movement.

3.2 Mesonet data analysis and editing

The Oklahoma Mesonet, as can be seen in its current state in Fig. 3.1, was used due to its high-resolution and quality controlled dataset. In this study, measurements from the 1.5 m air temperature (°C), station pressure (hPa), average five-minute 10 meter wind speed (m s^{-1}) and direction (degrees), and relative humidity (%) were used.

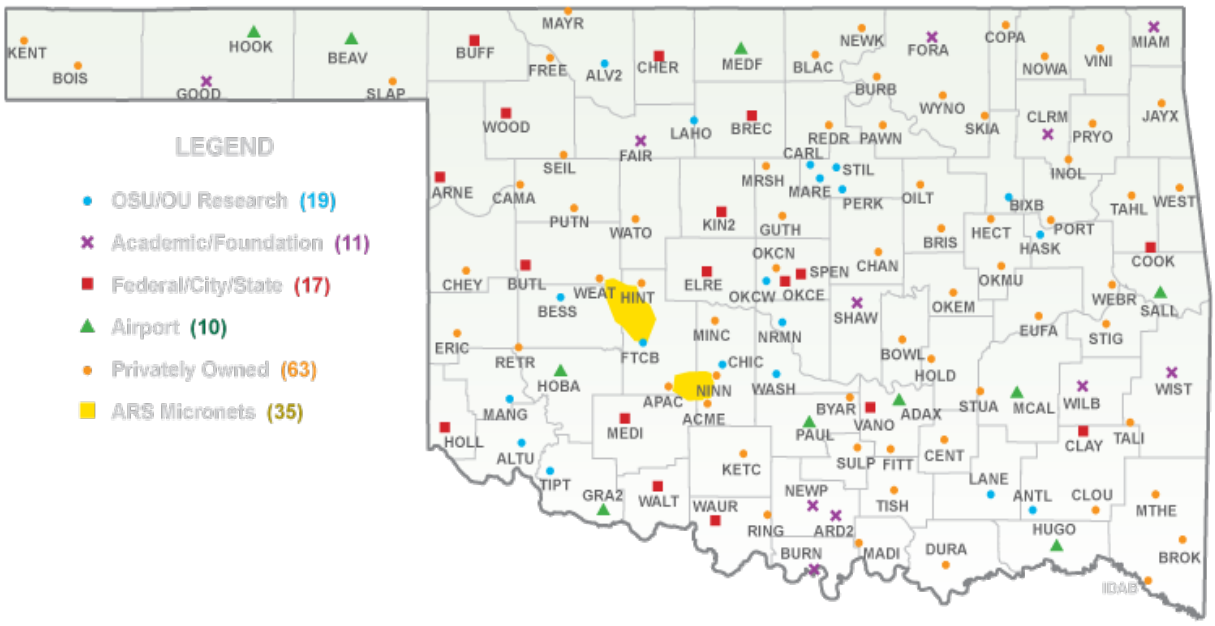

Figure 3.1: A current view of all Mesonet stations as of 2010. Due to the lack of resolution in the panhandle region (only six stations), cases passing through this region of Oklahoma could not be used.

Once all the data had been downloaded for the cases in question, the data had to be filtered in order to identify only the mesoscale components of the system and eliminate other scales of motion. The method is very similar to the one used by Adams-Selin and Johnson (2010) since it can be applied just as well to LS and PS systems as it can to bow echoes. The data filtration methods used in this study include correcting all stations to a constant height, filtering out the diurnal pressure signal, a time-space transformation, a

multiquadric interpolation scheme, and finally applying a Lanczos high-pass Fourier filter.

The station heights were all corrected as if they were on a flat plane, with an average height of 356.5 meters. This height was then used to adjust the pressure readings accordingly using a virtual temperature correction. This was necessary to remove any variance that simple elevation differences could cause in the pressure readings.

The pressure fluctuations from diurnal tides also needed to be removed from the final results. To do this, an average pressure was calculated at each specific station for a specific time of day on a monthly basis (e.g., the average data for all days from station ADAX at 11:05 am during the month of May). An average pressure was also calculated for each station on a monthly basis (e.g., the average at ADAX for the month of May). This monthly average was then subtracted from the time average to give a diurnal variance at that specific time. Johnson and Hamilton (1988) used a similar procedure.

A time-space transformation was also necessary (see Fujita 1955) because of the radar images being at a resolution of 15 minutes but the Mesonet data being at a resolution of 5 minutes. Due to this time difference, the system was assumed to be in a steady state every 15 minutes. The transformation would move all data forward or backward by a five minute time step based upon the speed of the system determined previously from AWIPS. However, it is only appropriate to move the location of the data in close proximity to the system, so only data falling inside the latitude/longitude boxes were moved in this manner.

A multiquadric interpolation scheme was also used to more objectively analyze small-scale features. Nuss and Titley (1994) used this same scheme in their paper and found it

to be the best for small features. The smoothing and multiquadric parameters are the same values as Adams-Selin and Johnson (2010) used: 0, 5, and 1.5.

The most important feature for data quality improvement was a Lanczos high-pass Fourier filter, as used in Duchon (1979). The filter removes any data from features of time length longer than two times a single pendulum day, or for the state of Oklahoma, a period of 82.4 hours. Figure 3.2 includes an example of this filter for a 61-point width response function with a wavelength cutoff of 100.

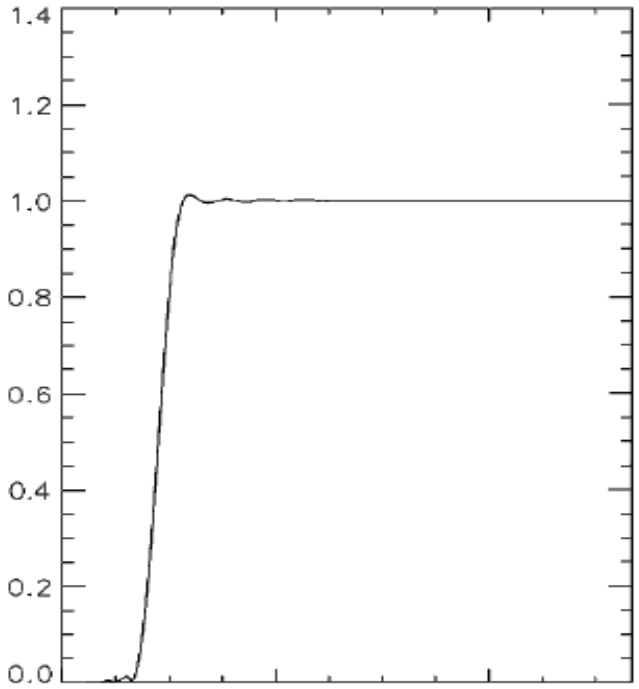

Figure 3.2: Response function for a 61-point width high-pass Lanczos filter with a cutoff wavelength of 100. Vertical axis is the response function value; horizontal axis is the wavelength for a 500-point length time series. From Adams-Selin and Johnson (2010).

The filter is used in this manner to separate the mesoscale features from the synoptic features. Since this study focuses specifically on the fine-scale features of LS and PS systems, such as mesohighs and wake lows, the synoptic data need to be removed from the analysis.

After the data have been filtered, they are read into GEMPAK for plotting. Each 15-minute time step of every case is plotted on a radar reflectivity overlaid with surface pressure contours, streamlines, potential temperature contours, and equivalent potential temperature contours. These plots will be analyzed in Chapter 5.

3.3 Synoptic data analysis

As a comparison to papers such as Parker and Johnson (2000), the synoptic-scale profiles were also examined. For the synoptic-scale information, archived RUC-252 (or Rapid Update Cycle model utilizing grid pattern 252, the details of which can be found at: http://www.nco.ncep.noaa.gov/pmb/docs/on388/tableb.html#GRID252) 0 hour data was utilized (available at http://nomads.ncdc.noaa.gov/data). The 0 hour data is a numerical forecast of current conditions.

In order to identify features such as fronts, pressure centers, trough/ridge patterns, and low-level jet (or LLJ) influence, plots of geopotential height at 1000, 850, 500, and 250 hPa were prepared using the program GrADS (Grid Analysis and Display System). The 1000 hPa plots helped indicate surface pressure features and frontal systems. The 850 hPa plots helped to indicate any LLJ influence by using a similar criterion to Parker and Johnson (2000). Specifically, if the winds at 850 hPa had a southerly component, then they were considered to be part of a LLJ; no minimum wind speed was required. The 500 and 250 hPa plots were used to determine where jet streaks and troughs/ridges were located in relation to the system. The synoptic conditions will be analyzed in Chapter 4.

Chapter 4

SYNOPTIC FEATURES OF LEADING AND PARALLEL STRATIFORM SYSTEMS

As mentioned in Chapter 3, the synoptic features of these systems were analyzed to see how they compared to the results in Parker and Johnson (2000). This will help improve the knowledge regarding what types of conditions these systems tend to form in. Information such as this is beneficial to increasing the forecasting skill of these unique but important systems.

The method of analysis for these systems is to utilize a case study for each type in detail. Each case system investigated was observed to have very similar synoptic features with the overall archetype average. The RUC data are analyzed at a time very close to the beginning of the system's existence. To confirm the location of features such as cold fronts or jet streaks, the RUC plots are compared to archived maps from the Storm Prediction Center (available at http://www.spc.noaa.gov/obswx/maps/) at the closest 12 hour interval available.

4.1 Leading stratiform features

Case 2, which occurred from 2045-0130 UTC on May 24-25 2002, developed into a strong LS system, reaching maturity by 2330 UTC. It originated in the southwest corner of Oklahoma near the Texas border. As seen in Fig. 4.1, a surface low is centered over

central New Mexico with a frontal system extending from eastern New Mexico up through Texas and Oklahoma. The SPC archive map confirms this front is a warm front, with lower temperatures on the western side of the front and higher temperatures behind the front.

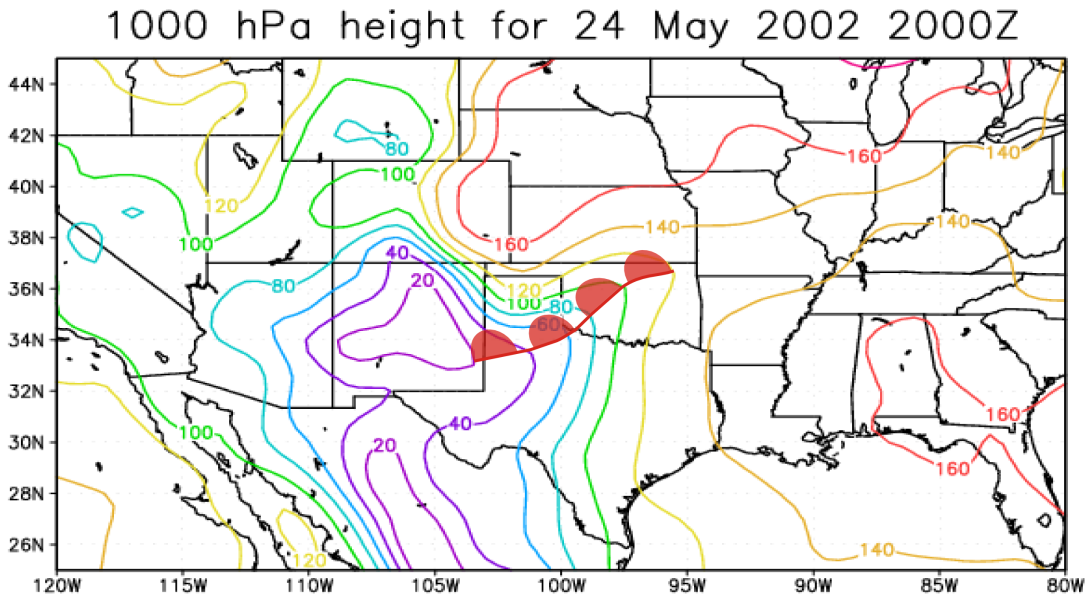

Figure 4.1: Contours of geopotential height in meters at 1000 hPa at 2000 UTC 24 May 2002. The warm front's location is also shown.

Figure 4.2 reveals the general wind structure at 850 hPa. The most important feature here is the moderate southwest flow moving into Oklahoma defined by the relative tightness of the height gradient. Because of this mostly southerly component, it can be assumed that a LLJ is influencing this case. The strength of this southerly flow is confirmed via the SPC archive map reading of 25 knots over southern Oklahoma at 0000 UTC, May 25 2002.

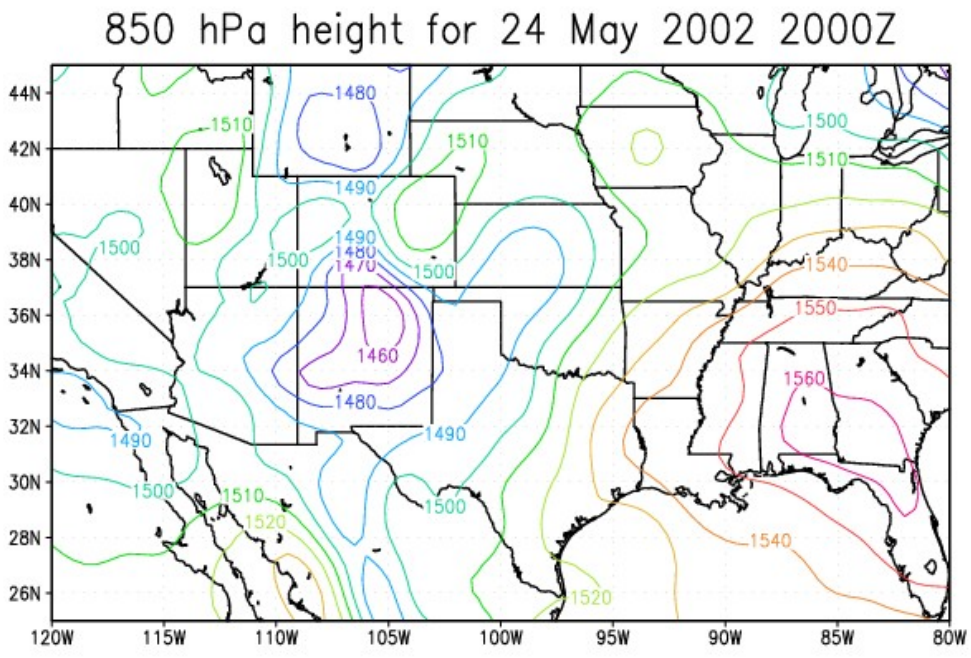

Figure 4.2: Same as Fig. 4.1 except at 850 hPa on 2000 UTC 24 May 2002.

The trough/ridge pattern at 400 hPa is revealed in Fig. 4.3. (500 hPa data were unavailable for this case). A moderate strength trough exists just to the northwest of the system's location, although winds are weaker over southwestern Oklahoma than in northwest Kansas. The trough axis extends through eastern Colorado, and the ridge axis through eastern Iowa.

Lastly, the jet stream is analyzed to identify its location in relation to the system. Shown in Fig. 4.4, case 2 is outside of the jet streak's core, but is located in the outer edge of the jet streak's right entrance region. There is a slight southwest flow, meaning wind direction veered with height from south at the surface to near 240 degrees at 250 hPa, indicating warm advection.

The majority of observed LS cases had very similar features to this case. Most occurred in the warm sector of a frontal boundary with southern flow ahead of the system. There was a low pressure system at the surface with an average location near northeast New Mexico. At 500 hPa, there tended to be an approaching trough of moderate depth with an axis through western Oklahoma. A LLJ was also involved with almost all LS cases, signifying a strong dependence on LLJs for LS development.

The location of LS systems in the right entrance region of a jet streak also concurred with PJ 2000's findings. The most intense portion of the jet streaks tended to be located far to the north in Iowa, but these systems were always located inside the right entrance region if additional isotachs less than 75 knots are included.

These results agree with PJ 2000 when it comes to the direction of upper-level winds as well. These cases had a westerly component to the upper level winds on average, which is important for advecting hydrometeors in advance of the main convective region. This allows the stratiform to lead the system.

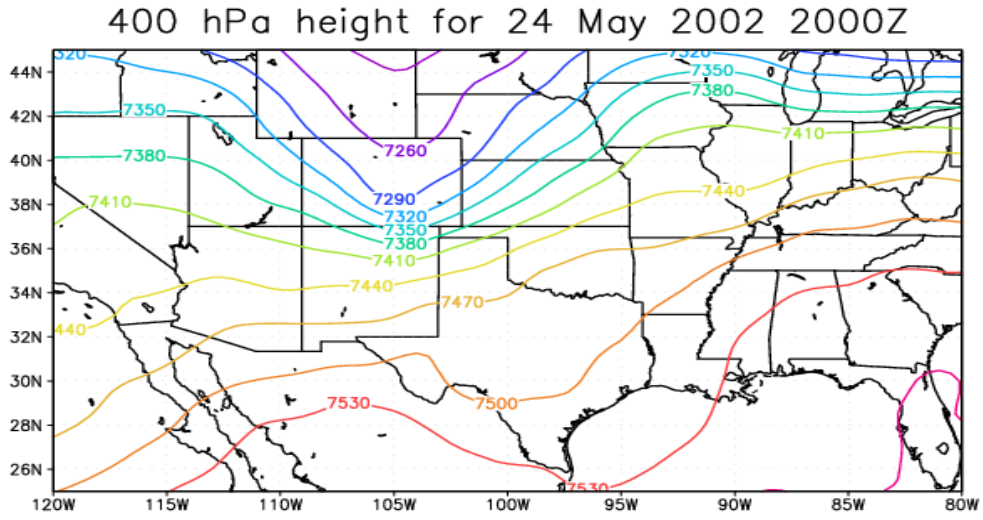

Figure 4.3: Same as Fig. 4.1 except at 400 hPa on 2000 UTC 24 May 2002.

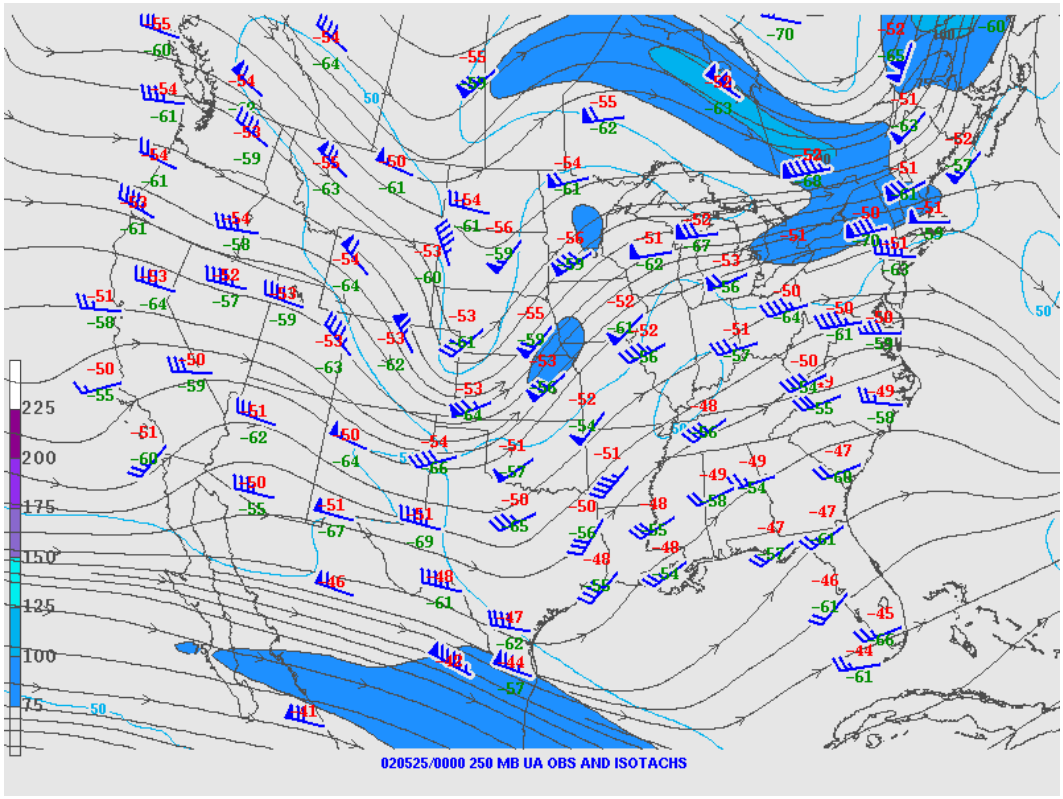

Figure 4.4: Wind observations and isotachs at 250 hPa on 0000 UTC 25 May 2002. The jet streak's location is indicated with the blue shading shown, representing a wind speed of between 75 and 100 knots From the Storm Prediction Center.

4.2 Parallel stratiform features

Case 14 occurred from 0000-0500 UTC on April 21 2004 and reached its maturity by 0130 UTC. This case began in the northeastern corner of the state, with the attached stratiform on the Kansas/Missouri border. As seen in Fig. 4.5, there is an area of low pressure just west of the Oklahoma panhandle. There is also an occluded frontal boundary running from southwest to northeast just behind where the system is located (as confirmed via the SPC).

The next level at 850 hPa shows a lack of strong southerly flow as was seen in the LS case, instead there is weak, mostly westerly flow. As Fig. 4.6 shows, the contouring is not

as tightly packed in northeast Oklahoma as it was for the previous LS case example, and the wind flow is predominantly westerly. Thus, there is no southerly LLJ influence for this case.

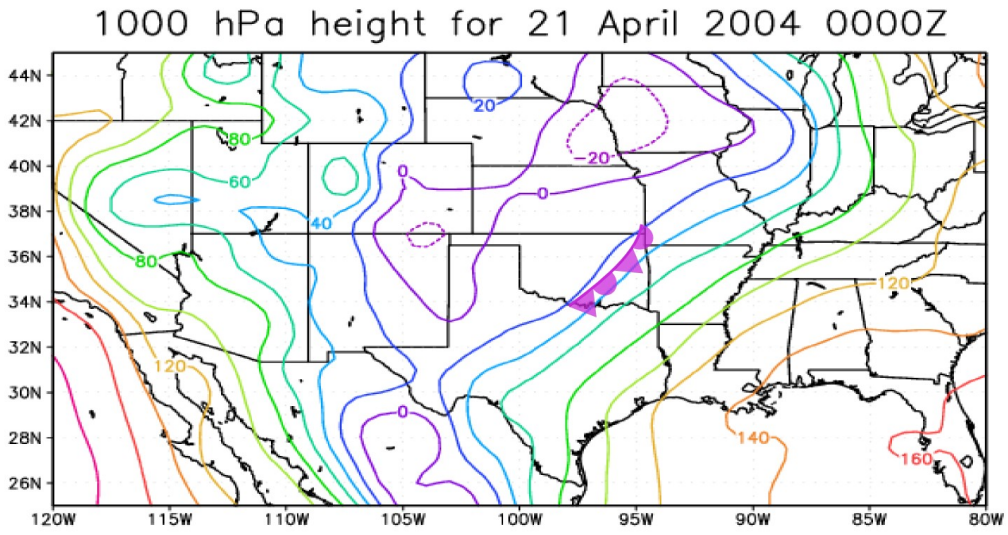

Figure 4.5: Same as Fig 4.1 except at 0000 UTC 21 April 2004. The occluded portion of the front's location is also shown.

At 500 hPa as shown in Fig. 4.7, the flow is mostly zonal. There is a weak trough to the north, with its axis through the Iowa/Nebraska border, but the trough is not influencing the system in Oklahoma. The gradient between height contours is weaker than observed at 400 hPa in the previous LS case, with weaker flow existing over Oklahoma.

At 250 hPa, the trough is deeper now at the jet stream level. As seen in Fig. 4.8, there is still weak flow in northeastern Oklahoma. The SPC archive shows a jet streak centered near the Missouri/Nebraska border, but the system is occurring in the outer edge of the right entrance region.

The PS systems analyzed for this study had more inconsistent averages as it related to the location and strength of the trough. Many troughs were located in western Oklahoma, but others had no troughs at all or very strong troughs. Although case 14 differed from many cases in terms of its trough location, this case met the overall average profile the best in terms of the other parameters being investigated, such as the lack of LLJ influence and surface pressure location.

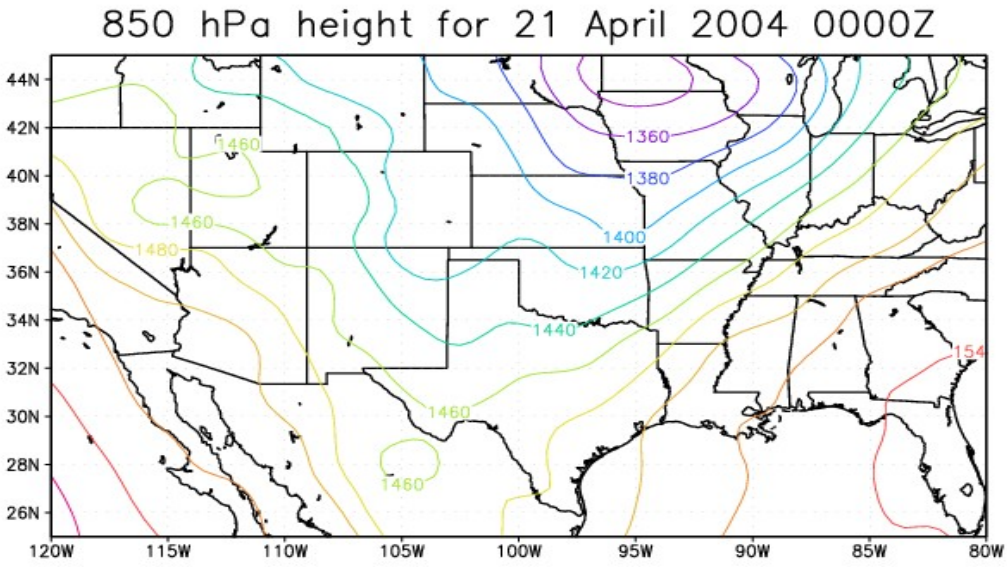

Figure 4.6: Same as Fig. 4.2 except at 0000 UTC 21 April 2004.

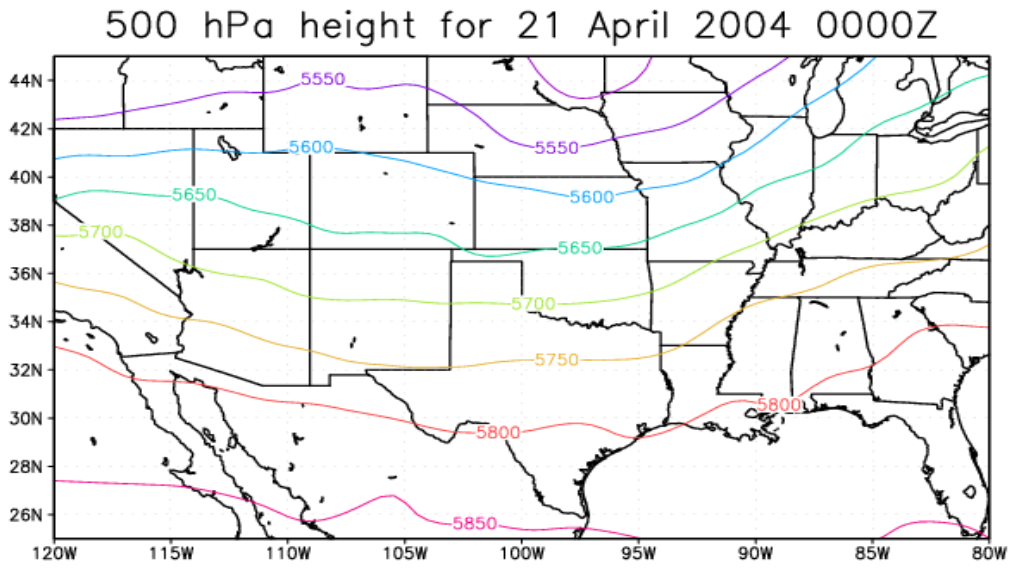

Figure 4.7: Same as Fig. 4.3 except at a height of 500 hPa and a time of 0000 UTC 21 April 2004.

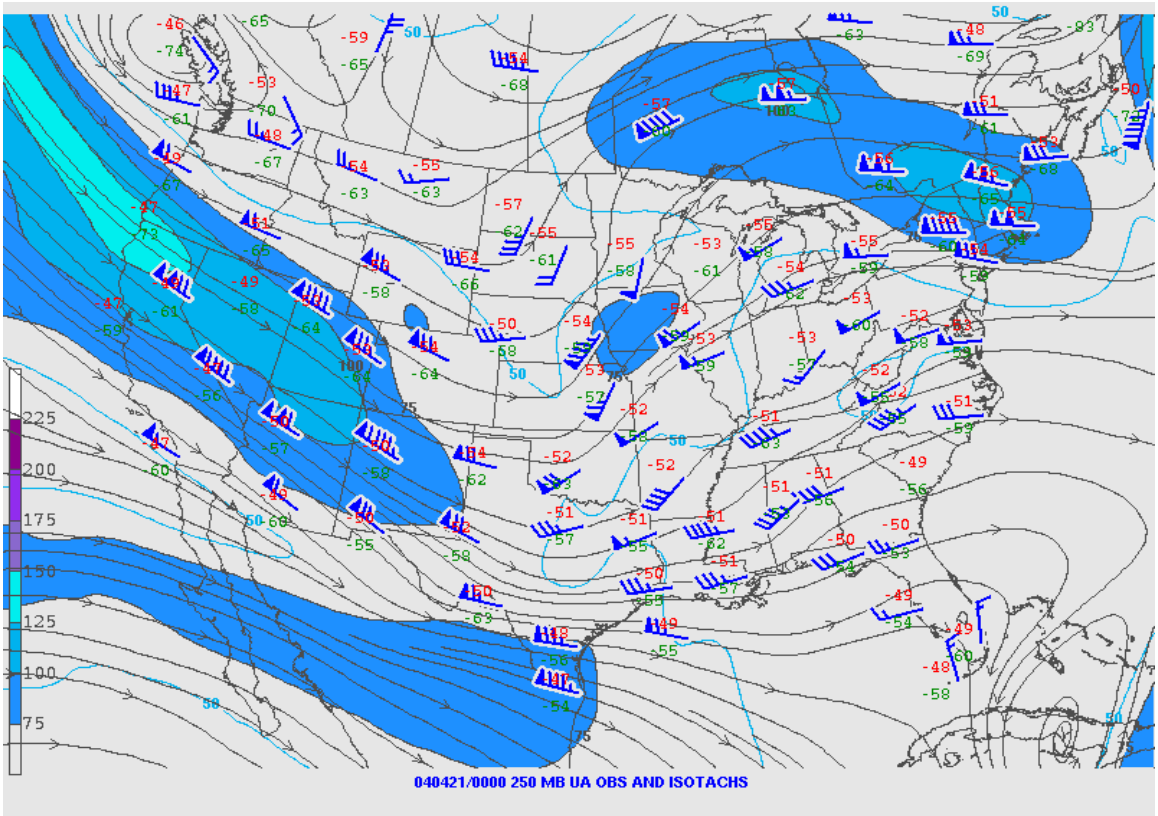

Figure 4.8: Same as Fig. 4.4 except at a time of 0000 UTC 21 April 2004. The jet streak's location is indicated with the blue shading shown, representing a wind speed between 75 and 100 knots. From the Storm Prediction Center.

PS systems also seemed to be much less dependent on LLJs than LS systems. Of the nine cases that had available RUC data, only three had any LLJ influence. Why this is the case remains uncertain. This differs from PJ 2000's finding that all system types, regardless of stratiform orientation, tended to have a LLJ influence 61% of the time.

Surface low pressure systems also tended to be a little weaker on average for PS systems than for LS systems, sometimes with cases having no significant surface low pressure at all. Their location also had a less consistent pattern than LS systems did, varying in range from near the Texas/Mexico border to Iowa. The overall average location, however, was fairly similar to LS systems, being in southwest Kansas.

Even with these differences, PS systems were still very dependent on frontal boundaries for initiation, as LS systems were. Typically, PS systems formed in the warm sector ahead of an advancing frontal system. This is also confirmed by the findings discussed by PJ 2000.

Regarding environmental differences, more case studies are needed to make a final conclusion as to whether the environmental flow leads to distinct differences in MCS organization. The LS cases observed in this study all had upper-level flow that would be similar to the flow necessary for PS systems found by PJ 2000. The only significant difference in the synoptic environments was the lack of LLJ influence on most PS systems and the strong necessity for them in LS systems. Because of their unique precipitation structure, perhaps LS systems need more continually unstable air to maintain their structure than PS systems do. Specifically, as discussed in Chapter 2, unlike PS systems, LS systems (at least front-fed ones) have inflow traveling through the

stratiform region, which decreases the buoyancy of the air. The LLJ may help increase the overall buoyancy of the air, allowing the system to maintain itself.

Chapter 5

SURFACE FEATURES OF LEADING AND PARALLEL STRATIFORM SYSTEMS

Using the analyzed MESONET data, this chapter will focus on the surface features of LS and PS systems. Four different data types will be examined: streamline fields to identify areas of confluence/diffluence, potential temperature contours to find the locations of the cold and warm anomalies, equivalent potential temperature contours to locate areas of high moisture content and positive buoyancy, and most importantly the pressure contours to observe the patterns of mesohigh and mesolow evolution in both types of systems.

Of the 11 LS cases and 10 PS cases analyzed in this manner, two case studies will be analyzed in more detail that exemplify the overall average behavior with the most visible surface features from each category. Any cases of note that are very different from this overall trend will be noted.

5.1 Leading stratiform systems

The first leading stratiform case to be examined in detail is case 4, which occurred on April 16, 2003 in LS form between the hours of 0000-0400 UTC. This case was unusual in that the stratiform region completely separated from the main convective region (MCR

as it will be referred to from now on), but its surface features fit the overall average profile found for LS systems.

As the storm began, it was located on the western border of Oklahoma, so not all of its features could be ascertained yet. Surface confluence was located along the convection axis feeding in from the southeast at 0000 UTC. After 45 minutes, the system was almost entirely inside the state of Oklahoma, with confluence occurring from the southwest and southeast right along the convection axis (not shown). After this, the MCR would begin to weaken; by 0145 UTC the axis of confluence had shifted slightly ahead of the MCR into the transition zone between the stratiform and convection regions (as shown below in Fig. 5.1).

By 0215 UTC, two axes of confluence existed; one was located just ahead of the strongest portion of the stratiform region, which was beginning to surge ahead of the MCR by this point (Fig. 5.2). The second axis was still located along the MCR, but the confluence zone ahead of the stratiform region was more compact. The confluence ahead of the stratiform axis was primarily from the southeast and east.

At 0315 UTC (Fig. 5.3), the stratiform region has almost entirely decoupled from the MCR. One large area of diffluence is occurring inside the heaviest reflectivity portions of the stratiform regions. Confluence is still occurring just ahead of the MCR, and a second strong confluence axis exists just ahead of the stratiform edge with southerly flow being dominant ahead of the line.

By the end of the system being in LS form, at 0400 UTC, the stratiform is completely decoupled from the MCR (not shown). Strong confluence has resumed right along the MCR axis. Strong diffluence now exists across the entire stratiform axis, with strong

confluence still existing along the eastern edge of the stratiform region coming from the south and heading northeast.

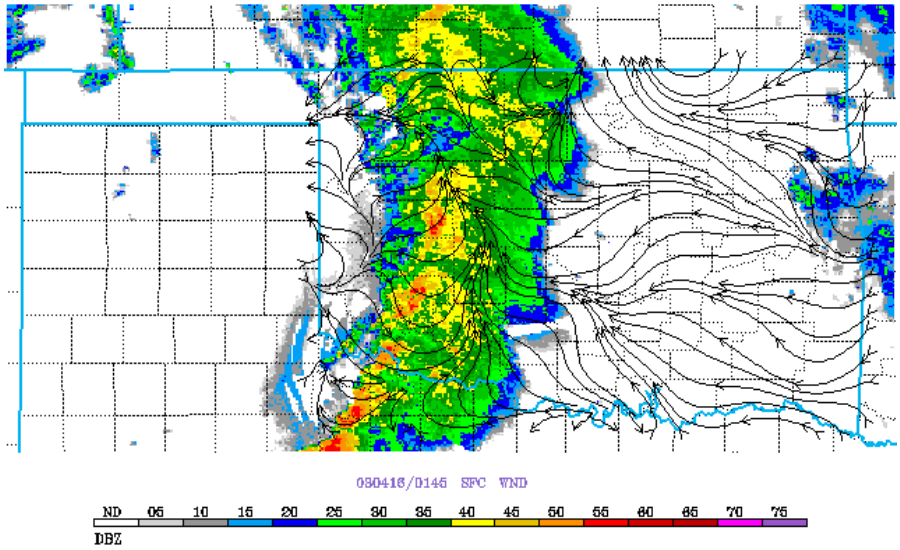

Figure 5.1: Filtered streamlines overlaid onto WSI NOWrad radar mosaic at 0145 UTC 16 April 2003.

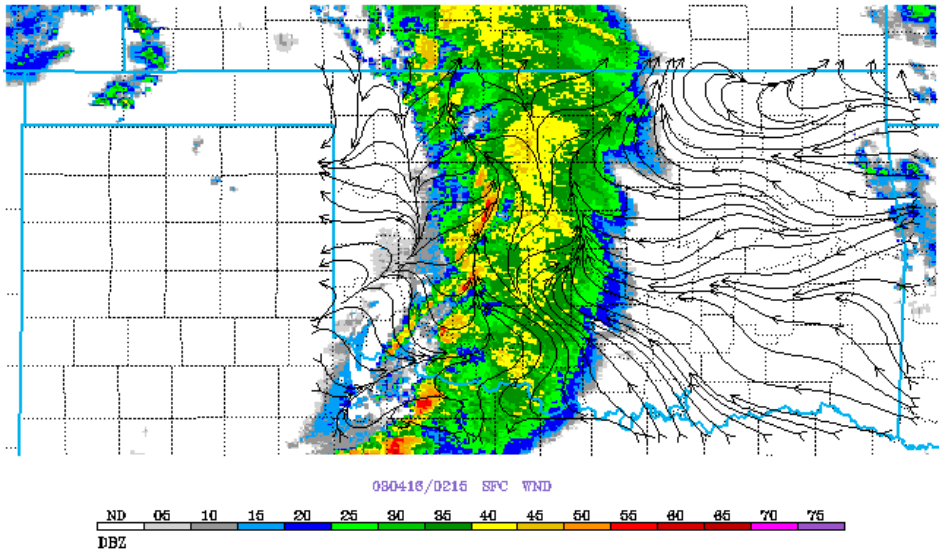

Figure 5.2: Same as Fig. 5.1 except at 0215 UTC 16 April 2003.

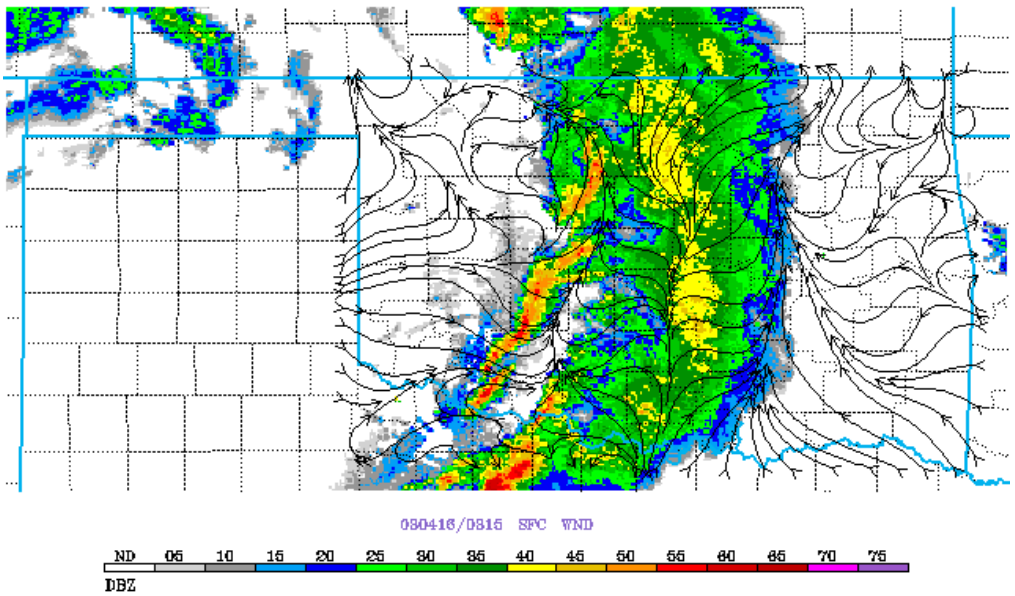

Figure 5.3: Same as Fig. 5.1 except at 0315 UTC 16 April 2003.

It seems that as the stratiform region became further decoupled from the MCR, diffluence increased steadily in the stratiform region. This is likely due to evaporative cooling that significantly increased the negative buoyancy of the air in the stratiform area, causing the amount of diffluence at the surface to increase steadily. Confluence existed strongly ahead of the stratiform region due to southerly flow ahead of the system.

Next, the θ pattern will be presented. At 0045 UTC (Fig. 5.4), a surface temperature differential exists from the front of the system towards the rear, with the warmest temperatures at the eastern side of the system. A warm anomaly (high-pass filtered θ values) exists just ahead of the MCR (to the east) and in the stratiform region, with a cold anomaly in the wake (to the west) of the system.

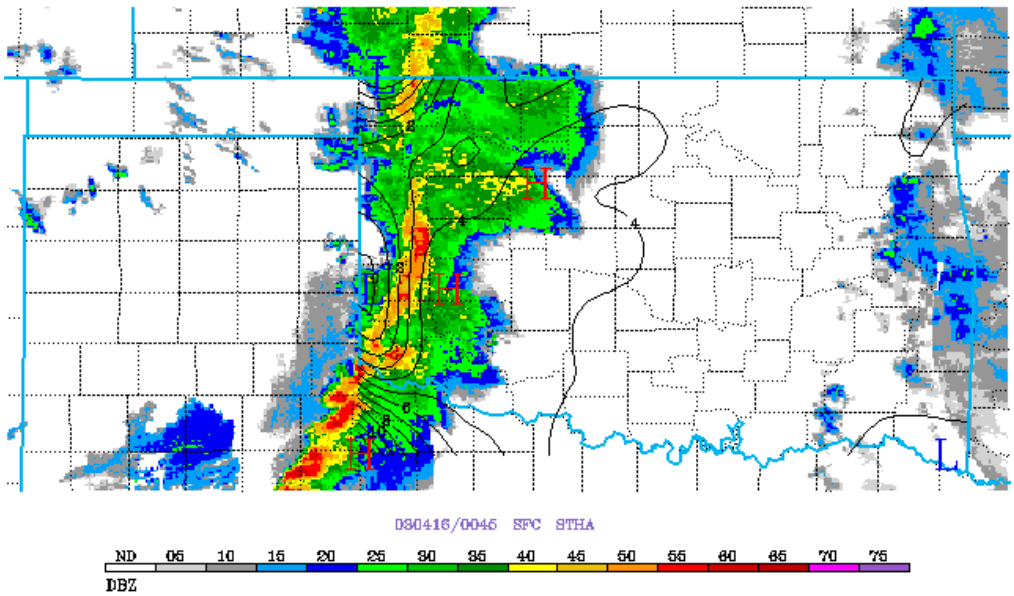

Figure 5.4: Contours of potential temperature after being filtered in ºC at 0045 UTC 16 April 2003. Areas of high potential temperature are marked with an H and areas of low potential temperature are marked with an L.

At 0145 UTC, the temperature differential has become more spread out and has reduced slightly (Fig. 5.5). Warmer readings still exist in the stratiform region, but now the stratiform region has grown with this temperature existing along the entire front edge. Temperatures decrease towards the west with a cool anomaly in the wake of the convective line. While the area of warmer air is broad, the area of colder air is much smaller, similar to what was observed at 0045 UTC.

As the evolution progresses, the differential becomes very weak. By 0300 UTC (Fig. 5.6), warmer temperatures remain prevalent in advance of the stratiform region as it continues to spread. The now small and disorganized MCR has slightly warmer potential temperatures, with a weaker cool anomaly area of larger size than previous wake regions located behind the MCR.

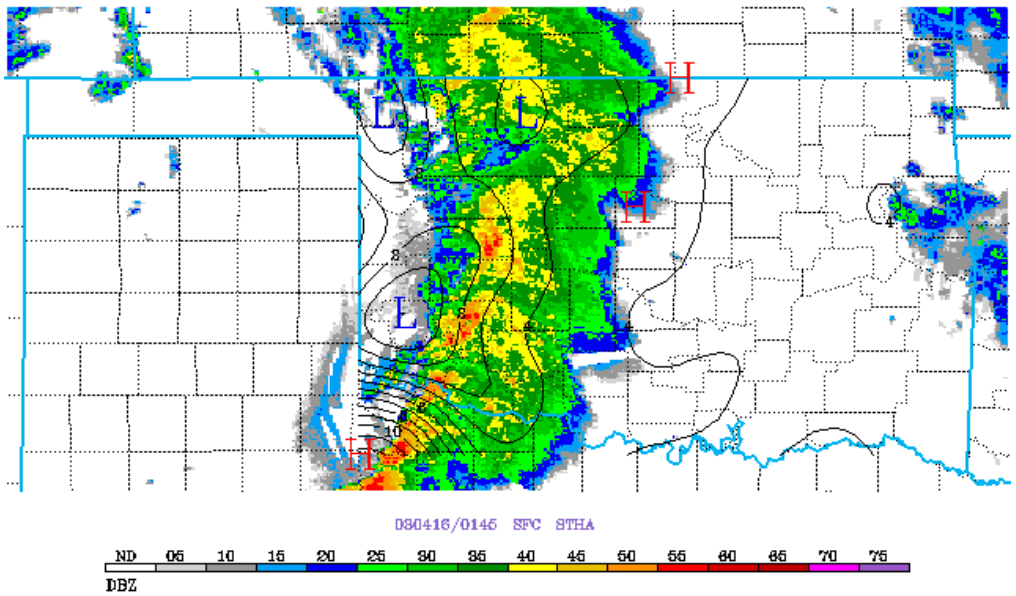

Figure 5.5: Same as Fig. 5.4 except at 0145 UTC 16 April 2003.

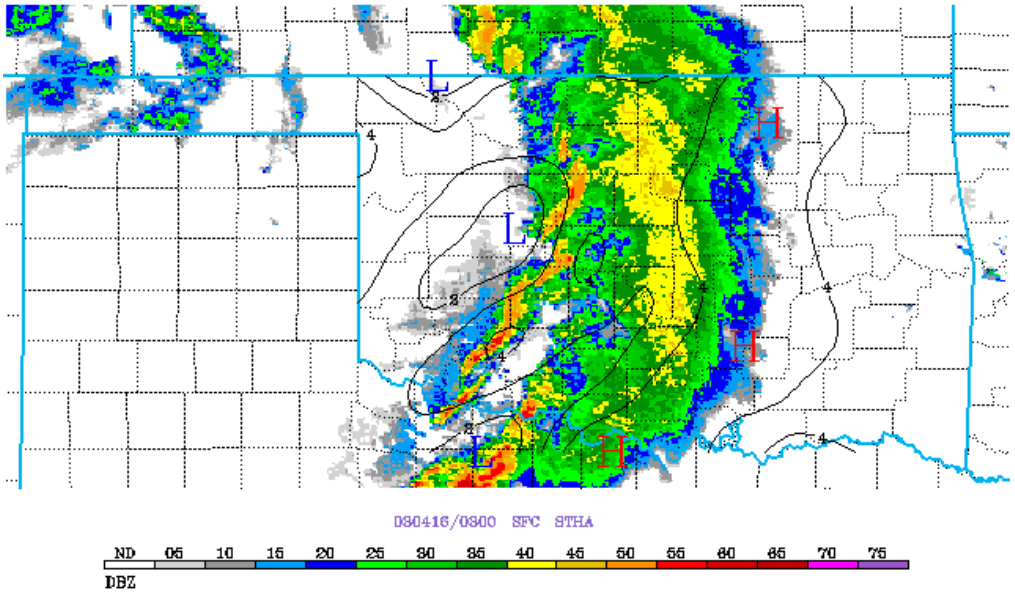

Figure 5.6: Same as Fig. 5.4 except at 0300 UTC 16 April 2003.

The largest differential of potential temperature existed earlier in the system's development, with the largest differential occurring when the MCR was at its most intense. The differentials then weakened as the stratiform region grew and started to separate from the MCR. Warmer temperatures were consistently in the stratiform region, with colder temperatures primarily existing just behind the MCR in its wake.

Next, the surface observations of equivalent potential temperatures will be discussed. Although these measurements can't be used to state whether the air is unstable due to a lack of measurements at other heights, they can be used as an indicator of updraft strength. This is not unprecedented, as the same determination was made by Smith et. al (2000). This study stated that surface equivalent potential temperature measurements could be used to estimate potential maximum updraft speeds. As convective cells move through areas of higher surface θ_e values, the strength of their updraft intensifies. Thus, when equivalent potential temperature values are discussed in this current study, high values will be referring to areas with a positive contribution to buoyancy and lower values will be referring to areas with a negative contribution to buoyancy.

At 0045 UTC (Fig. 5.7) there is a strong differential with a similar pattern to the θ contours. The most positively buoyant air exists on the MCR's eastern border. The temperatures drop towards the west, with the most negatively buoyant air existing in the wake of the system.

As the stratiform region begins to grow in size, the differential decreases and also shifts slightly outward. At 0145 UTC (Fig. 5.8), the lowest values are still located in the wake of the system. The highest values, however, occur very close to the MCR or in the transition region, with a stronger decrease of temperature than before towards the eastern

edge of the system. Towards the east of the maximum temperature, the temperature decreases. Although the potential temperature showed this area to have the warmest temperatures, the air in this region is dry and lacking positive buoyancy.

At 0330 UTC (Fig. 5.9) a similar pattern to the previous time steps is evident. Low θ_e exists near the MCR that has weakened significantly but is currently redeveloping. Moderate θ_e values are prevalent along the front edge of the stratiform region, with temperatures hitting a maximum in the transition area between the now separate stratiform and convective regions. In this area, there is little to no precipitation, but θ_e temperatures reach a maximum towards the north and southwest.

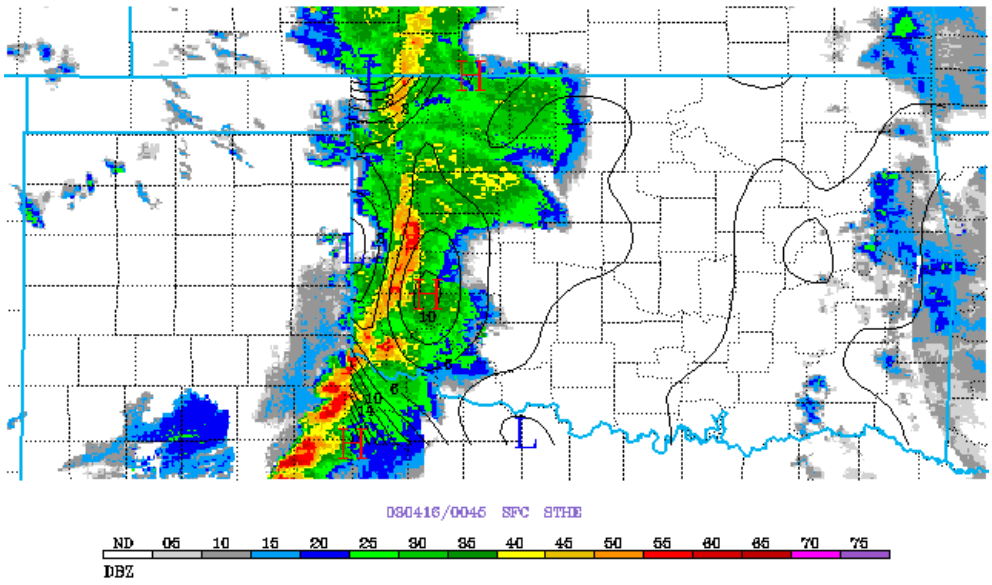

Figure 5.7: Contours of equivalent potential temperature after being filtered in 2°C intervals at 0045 UTC 16 April 2003. Areas of high equivalent potential temperature are marked with an H and areas of low equivalent potential temperature are marked with an L.

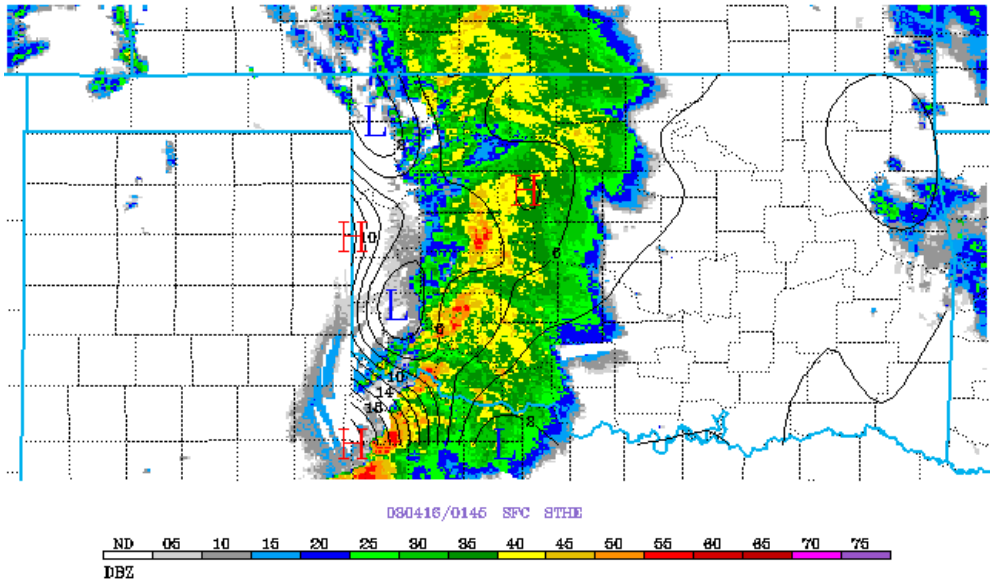

Figure 5.8: Same as Fig. 5.7 except at 0145 UTC 16 April 2003.

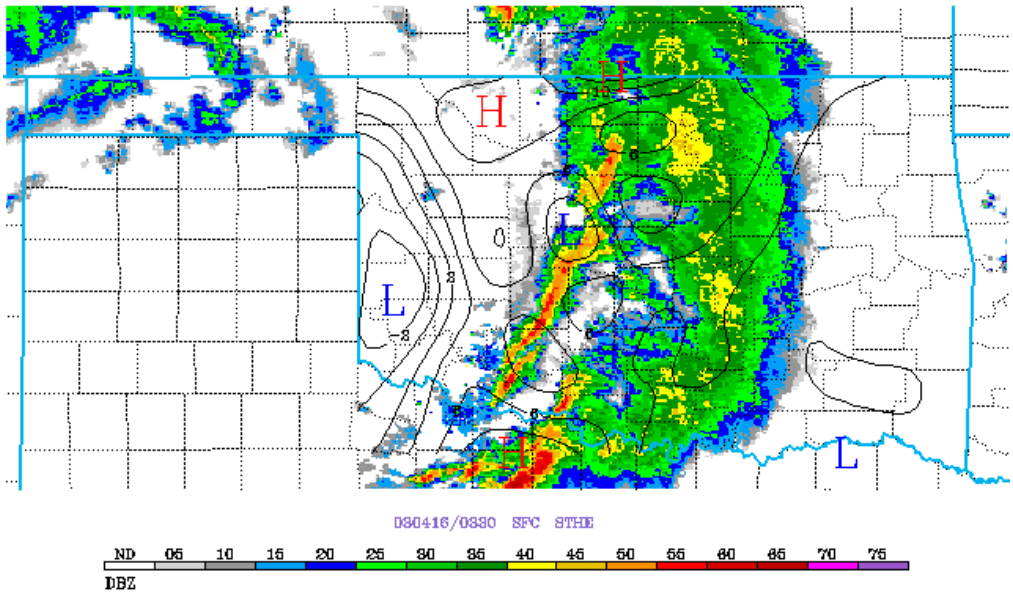

Figure 5.9: Same as Fig. 5.7 except at 0330 UTC 16 April 2003.

This pattern remains consistent throughout this case's lifespan, with the areas of greatest positive buoyancy occurring in the transition zone between the MCR and the stratiform region. The θ_e maximum weakens over time, however, as downdrafts from isolated convective cells transport low θ_e values that weaken the magnitude of these maximum values.

The most negatively buoyant areas occur in the system's wake and at the outer, leading edge of the stratiform region. This result indicates that the air providing the most buoyancy for the system is being fed in just ahead of the system's updraft core, allowing the system to maintain its structure.

Last, the pressure features of this case will be examined to see what pattern the mesohigh and wake low have in terms of their evolution. The best example of a pattern typified by LS systems in this study is an example shown in Fig. 5.10. At 0030 UTC, there is a significant pressure differential (in fact the strongest observed of all cases) from northwest to southeast with a magnitude of 5.5 hPa. A mesolow is located in the stratiform region near its front edge. Towards the rear of the system, a mesohigh is located just behind the MCR to the northwest.

By 0130 UTC, the differential has decreased slightly (Fig. 5.11). The mesohigh is still fairly strong and is located just behind the MCR. The strongest area of low pressure has now moved slightly more eastward to just ahead of the approaching stratiform region. The differential is still directed from northwest to southeast.

At 0330 UTC (Fig. 5.12), the mesohigh and mesolow are no longer as pronounced. The largest change has occurred in the stratiform region, where two areas of high pressure exist. These areas overlap well with the surface diffluence discussed earlier in the

chapter. There is a somewhat broad area of high pressure also existing behind the small convective regions. The mesolow is still located along the southern edge of the system just to the east of the stratiform region.

Although areas of high pressure varied a little more than usual in this case due to how large the stratiform region was, this case showed an overall pattern of the region of highest pressure being located just to the rear of the MCR and the area of lowest pressure located either on the eastern edge or just ahead of the stratiform region. There was a differential of pressure from roughly northwest to southeast across the system. This differs with the confluence, potential temperature, and equivalent potential temperature patterns investigated, which generally saw this pattern occur most strongly from due west to due east.

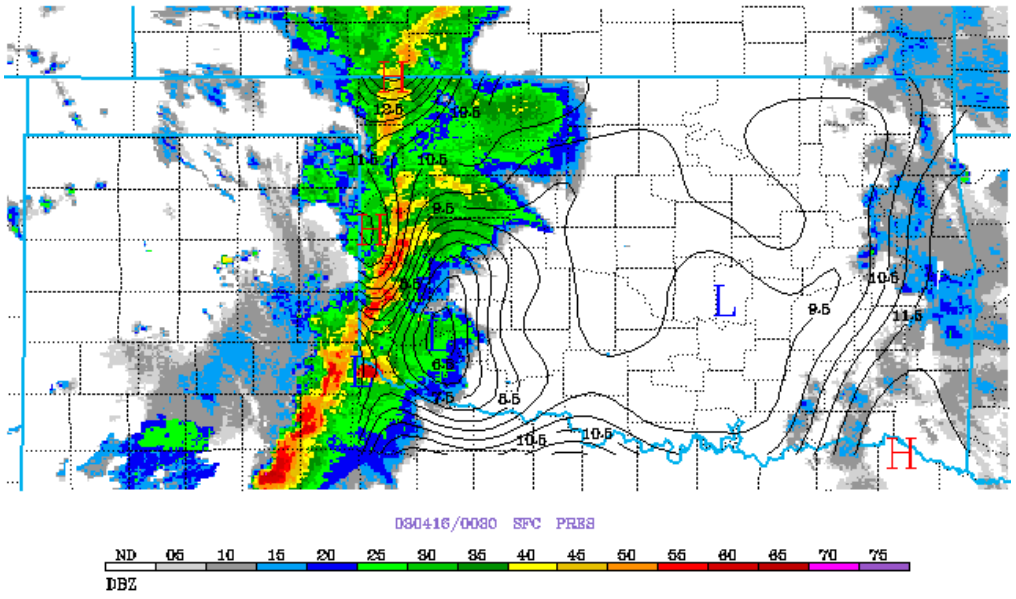

Figure 5.10: Contours of surface pressure after being filtered in units of 0.5 hPa at 0030 UTC 16 April 2003. Areas of high pressure are marked with an H and areas of low pressure are marked with an L.

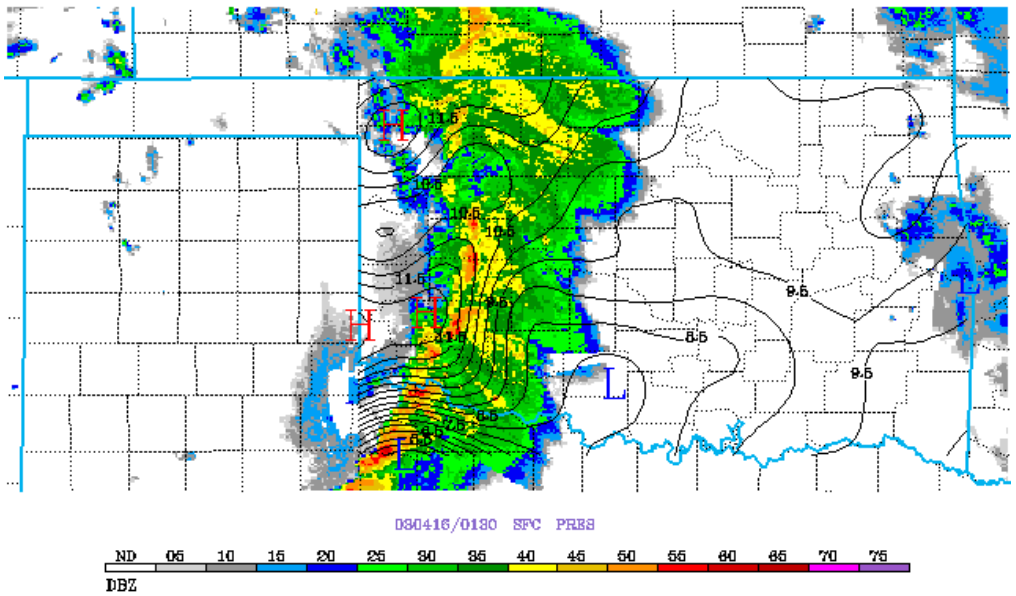

Figure 5.11: Same as Fig. 5.10 except at 0130 UTC 16 April 2003.

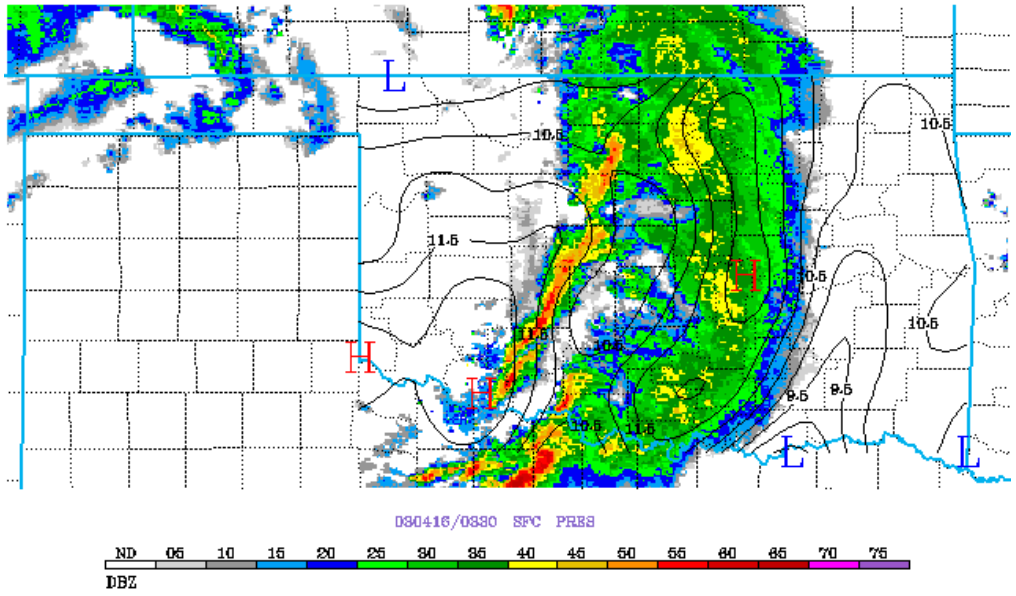

Figure 5.12: Same as Fig 5.10 except at 0330 UTC 16 April 2003.

The second case investigated is case 6. Although the stratiform region in this case was not very large, this case seemed to meet the archetype better than any other case based solely on its radar images. This case started forming at 2045 UTC on April 21 2004 and eventually had its northern end split off.

This case first started meeting the visual requirements for an LS system at 2200 UTC. As shown in Fig. 5.13, this system had two areas of confluence. One was apparent along the MCR, with a second leading towards a northern disconnected cell also exhibiting LS behavior. Similar to case 4, this case also has easterly surface winds at the northern end of the system, which is a pattern case 4 exhibited throughout its lifecycle.

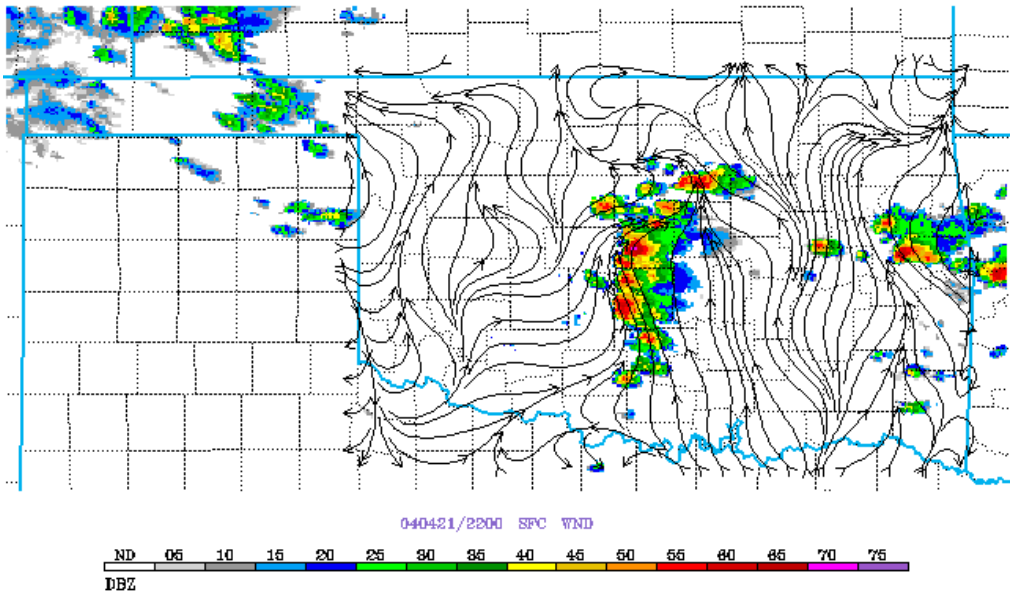

Figure 5.13: Same as Fig. 5.1 except at 2200 UTC 21 April 2004.

At 2300 UTC (Fig. 5.14), which was close to the system's peak maturity, there were still two main areas of confluence. One was along the MCR but heading toward the

northeast corner of the system then sweeping back west. Another area occurred in the northwest region of the system with southerly flow.

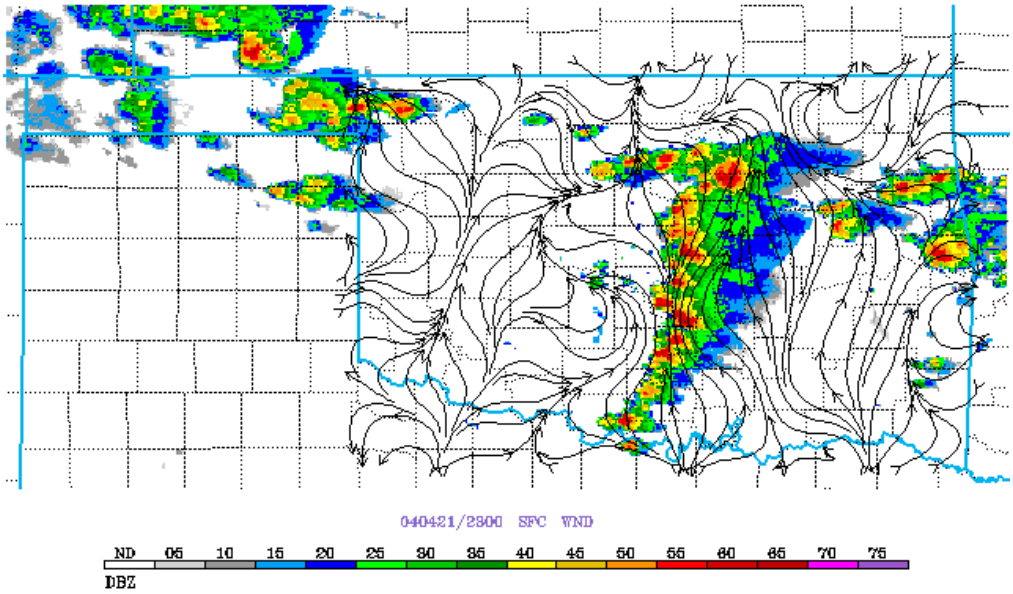

Figure 5.14: Same as Fig. 5.1 except at 2300 UTC 21 April 2004.

Just before the system split into two sections, at 0000 UTC, there was now a strong area of diffluence in addition to a strong area of confluence. As shown in Fig. 5.15, diffluence existed in the center section, just south of the asymmetry now present. Confluence is occurring in the central part of the northern section of the system with winds flowing from southwest to northeast. The easterly flow previously seen in the northern section is now absent.

Case 6 had more discrete cells along a line together than case 4, where they were all completely connected. This distinction is reminiscent of cellular vs. slabular lines convective lines studied by James et. al (2005). This system also had confluence along its

MCR with additional confluence occurring in the northern, asymmetrical section of the system. There was also consistent southerly flow ahead of the stratiform region, similar to case 4.

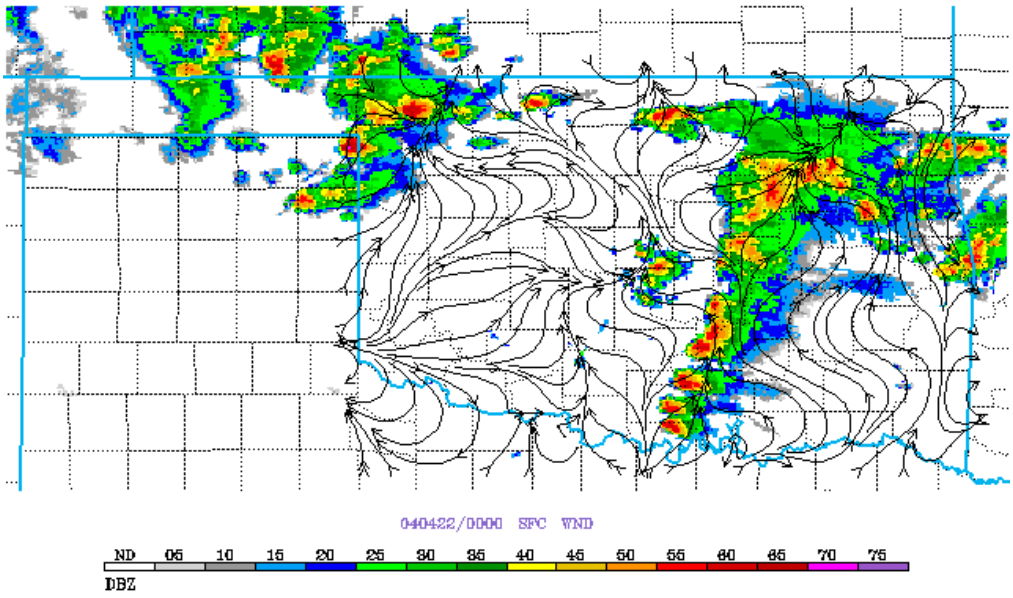

Figure 5.15: Same as Fig 5.1 except at 0000 UTC 22 April 2004.

The θ pattern also had similarities to case 4 in case 6. At 2230 UTC (Fig. 5.16), the coldest air was in the center of the MCR. The warmest air occurred out ahead of the system along the eastern edge of the stratiform region. This temperature differential is nearly east to west but had a slight southern component to it as well.

By 2330 UTC (Fig. 5.17), the differential has decreased. The temperature differential is still mostly west to east, with the lowest temperature existing in the rear center of the system along the western edge of the MCR. The highest temperature is on the outer edge

of the stratiform region. A secondary area of cold air is also present ahead of the system with a cell that has formed to the east.

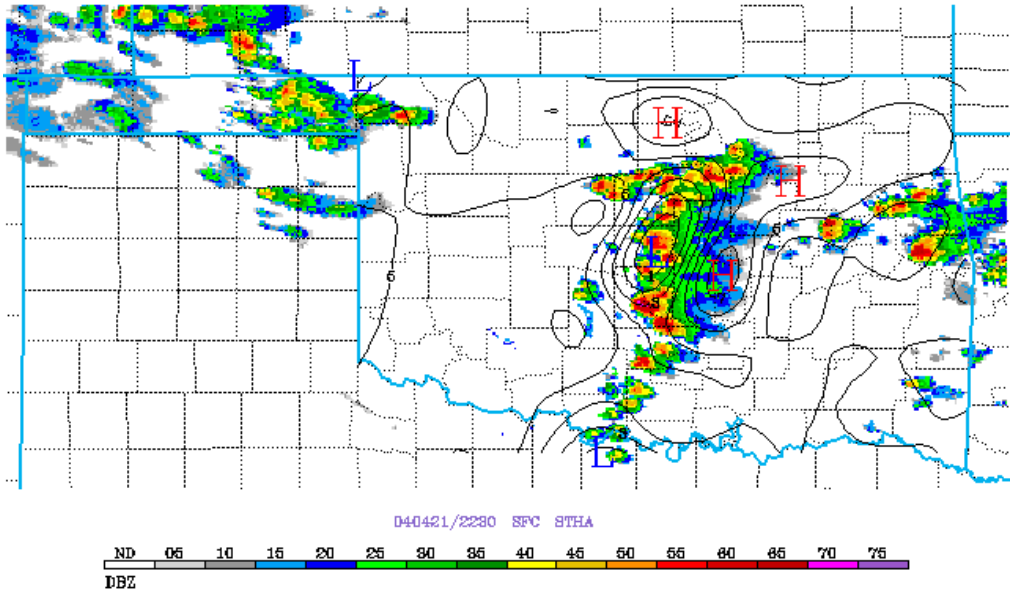

Figure 5.16: Same as Fig 5.4 except at 2230 UTC 21 April 2004.

At 0030 UTC, the stratiform region shifted almost entirely to the northern asymmetrical section of the system. The differential weakened and is also much broader than before. A large area encompassing the region bordering the southern section of the MCR and the disorganized convection in the northern area have the lowest temperatures (Fig. 5.18). The warmest area exists to the east in a clear area of no precipitation, which is along the eastern border of the stratiform region.

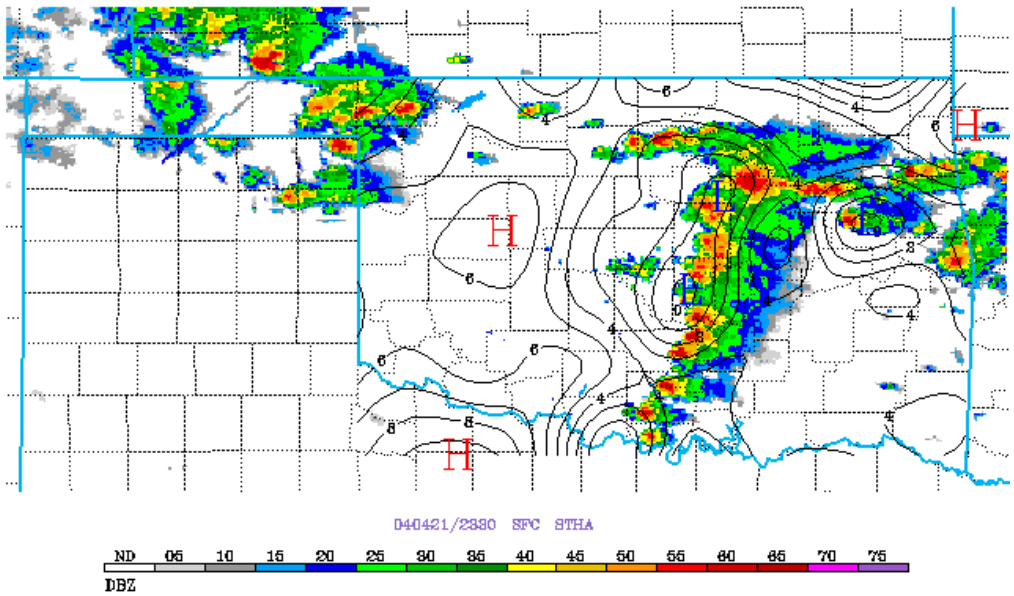

Figure 5.17: Same as Fig. 5.4 except at 2330 UTC 21 April 2004.

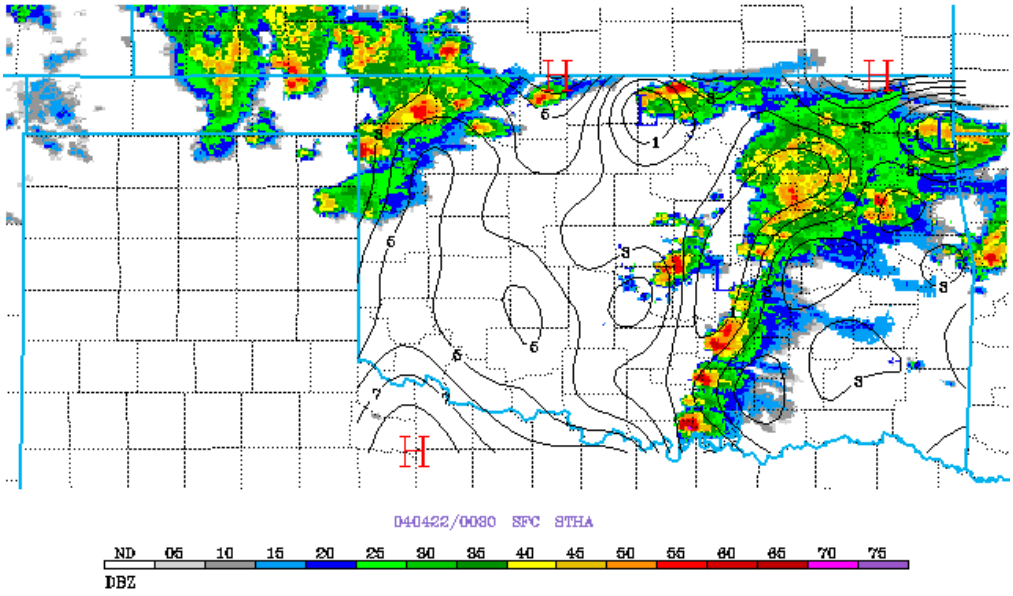

Figure 5.18: Same as Figure 5.4 except at 0030 UTC 22 April 2004.

Similar to case 4, the region of warmest air existed in or just ahead of the stratiform region, and the coldest air occurred in or just behind the MCR. The differential of temperatures was also mostly west to east. The differential of temperatures also weakened as the system progressed, with the largest differential occurring during its greatest level of maturity and weakening later on. As the system aged, the regions of warm and cold air spread out.

The equivalent potential temperature also followed the pattern established from case 4. The largest differential occurred at the system's peak strength at 2230 UTC, as shown in Fig. 5.19. A region of low-θ_e air existed in the center of the MCR. Just ahead of the stratiform region, in the northeast section of the system, an area of high-θ_e air was observed. A large, mostly west to east differential also existed in this case.

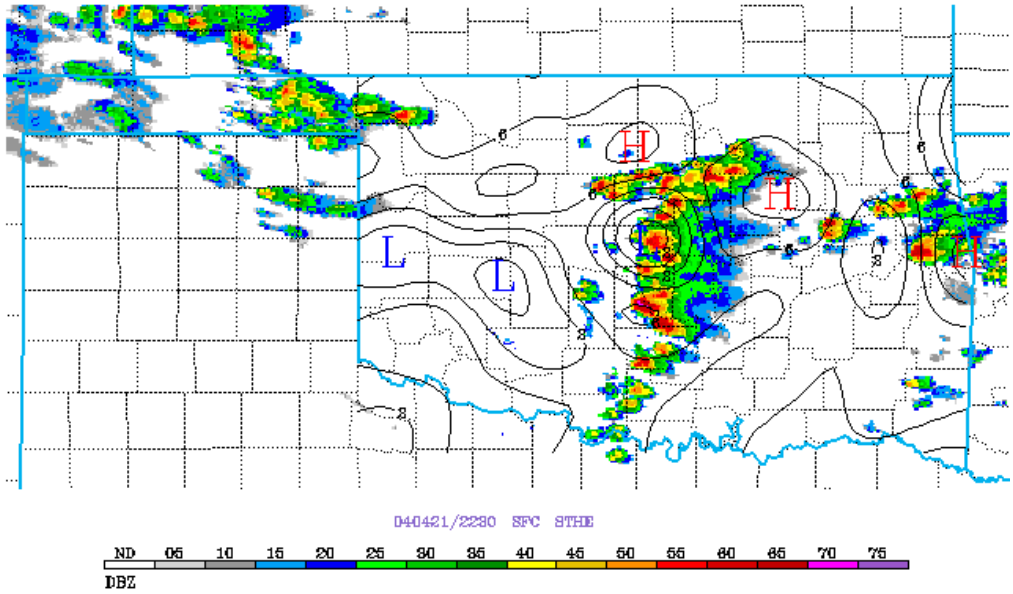

Figure 5.19: Same as Fig. 5.7 except at 2230 UTC 21 April 2004.

This pattern remains consistent an hour later at 2330 UTC, with negatively buoyant air on the western border of the MCR just behind the system (Fig. 5.20). An area of positively buoyant air is again situated on the eastern border of the stratiform region. There is also a region of positively buoyant air along the northern border of the stratiform region extending eastward in the northern section of the system.

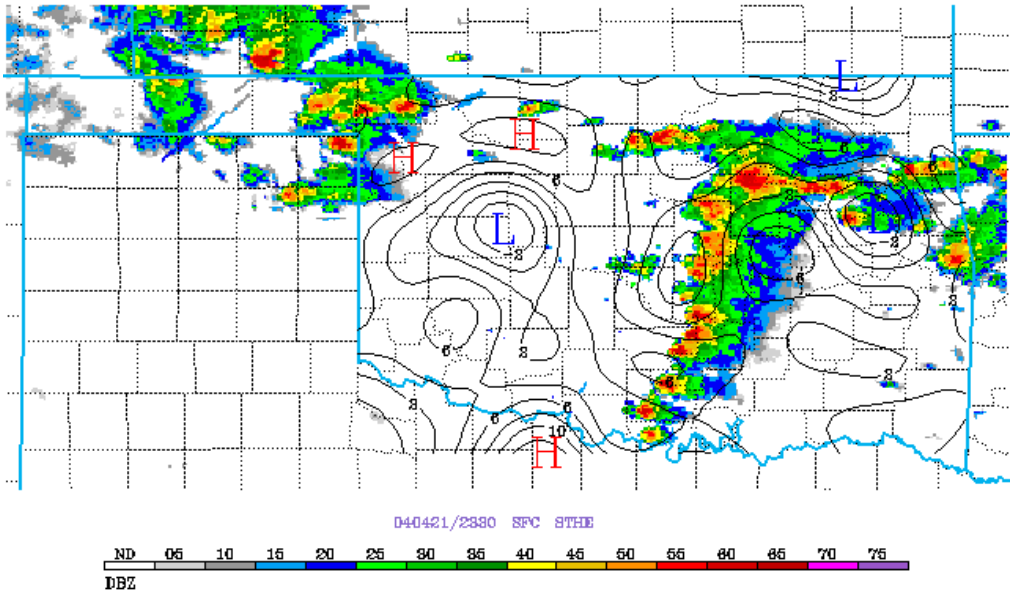

Figure: 5.20: Same as Fig. 5.7 except at 2330 UTC 21 April 2004.

Figure 5.21 shows the separation of the northern and southern halves. In both halves, there is an area of low-θ_e air just to the rear of the MCR. The areas of highest θ_e are both along the eastern section of the stratiform region, where the precipitation is lightest. This west-to-east pattern held consistently at all stages of the system's development. Both cases 4 and 6 exhibited the lowest θ_e air in the MCR, and the highest θ_e air outside of the MCR in either the transition zone or eastern edge of the stratiform region.

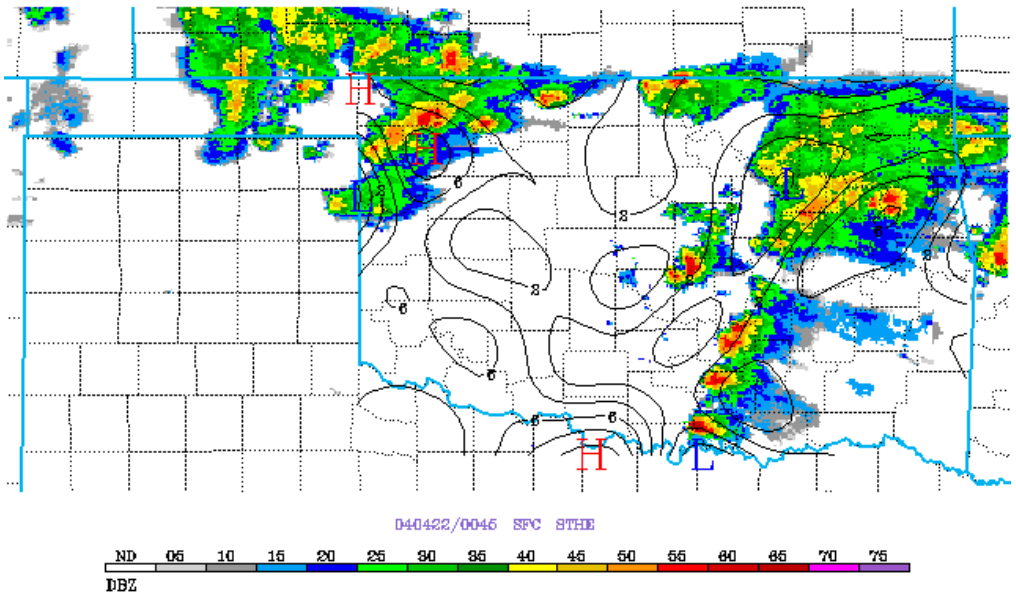

Figure 5.21: Same as Fig. 5.7 except at 0045 UTC 22 April 2004.

Finally, the pressure pattern of the mesohigh and mesolow were in relatively the same positions as case 4. At the system's peak in Fig. 5.22, the pressure differential is not as strong as case 4, but still exists nonetheless. A mesohigh exists on the western edge of the MCR, having a pressure 1.5 hPa higher than a mesolow along the eastern edge of the system.

By 2330 UTC (Fig. 5.23), an isolated cell has moved to the northwest and has met up with the system. The mesohigh still exists at the rear of the system. The mesolow has shifted north to the eastern edge of the stratiform there. This is to be expected, as by this time the strength of the system has shifted to the northern half, meaning the area of lowest pressure shifts with it.

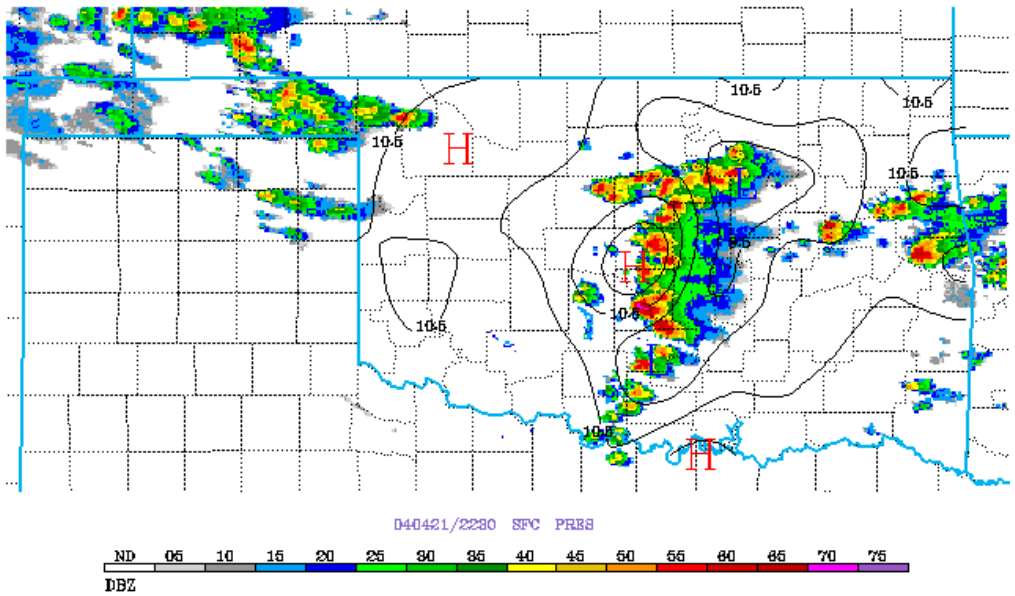

Figure 5.22: Same as Fig. 5.10 except at 2230 UTC 21 April 2004.

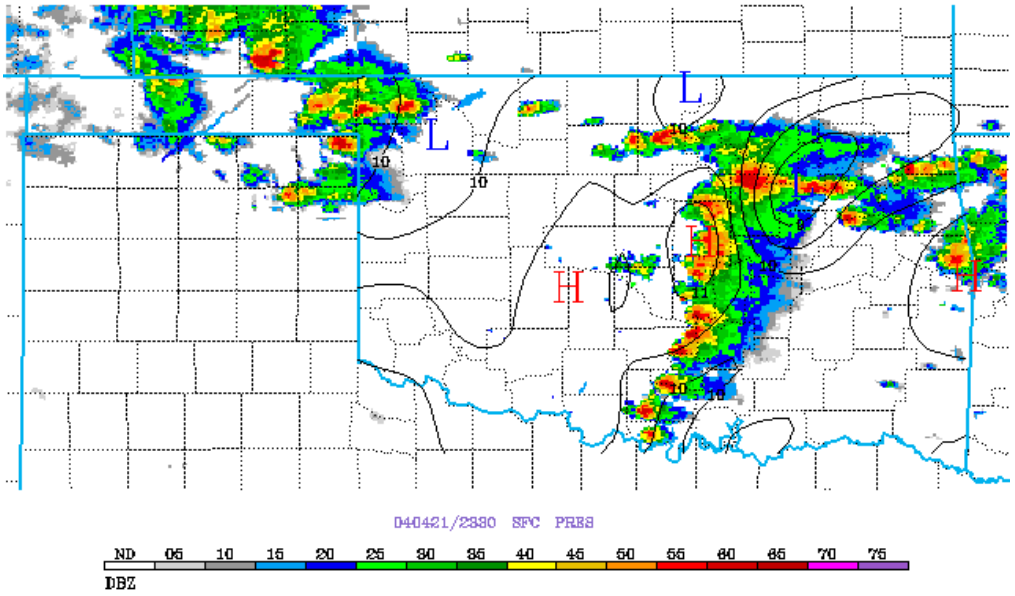

Figure 5.23: Same as Fig. 5.10 except at 2330 UTC 21 April 2004.

As the two halves of the system separated by 0100 UTC, the northern half exhibited a strong pressure differential. As seen in Fig. 5.24, even though the convection is somewhat disorganized, a strong mesohigh exists at the western edge of the MCR. The stratiform that has been advected to the east has created a strong west-to-east differential, with a mesolow occurring along the outer edge of the stratiform region.

Both systems 4 and 6 saw a general pressure differential from west to east. Case 4 saw one typically towards the south, while case 6 saw one typically towards the north. While there is a slight difference between the two cases, the most important similarity is the same; both cases have a mesolow that leads the stratiform region. Both cases also had a mesohigh located just to the rear of the MCR.

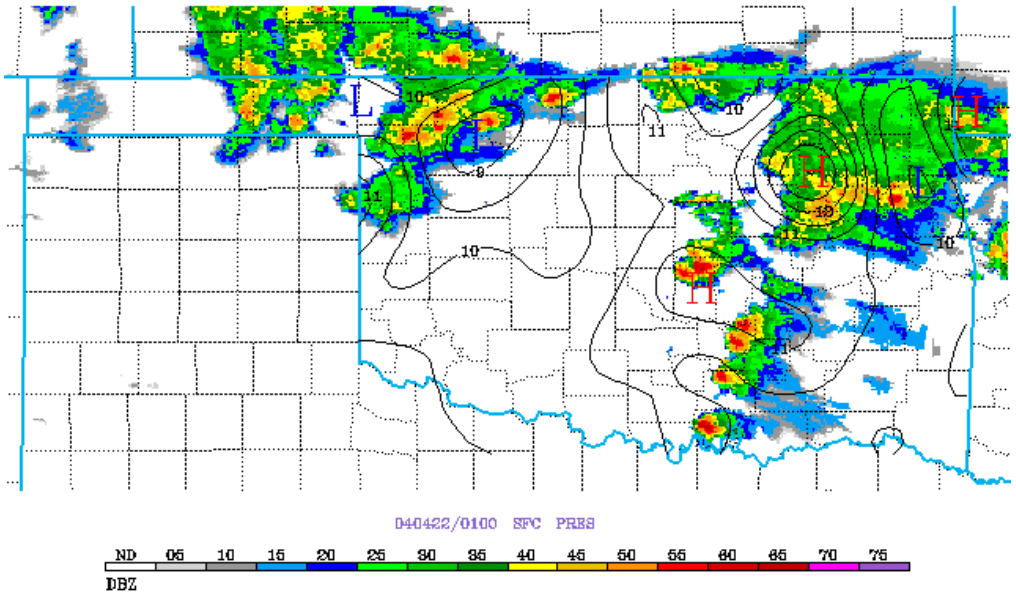

Figure 5.24: Same as Fig. 5.10 except at 0100 UTC 22 April 2004.

There was one exception to this average pattern in case 17a. As shown in Fig. 5.25, this case had an area of stratiform leading ahead of the MCR. There is a mesohigh just behind the MCR, but there is also a mesohigh on the leading edge of the stratiform region. This stratiform region was moving at a separate speed from the rest of the system and eventually caused the system to dissipate. Most of the LS cases moved from roughly west to east, but this case actually moved towards the northeast and had a different surface wind profile than most other cases (it formed on the same day as case 17b, which ended up being a parallel stratiform case).

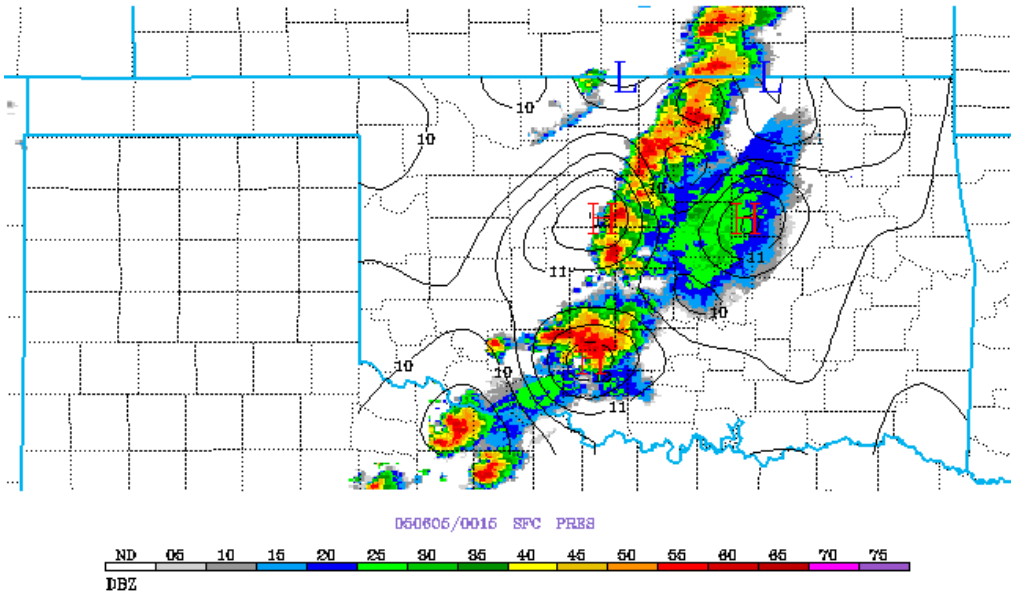

Figure 5.25: Same as Fig 5.10 except at 0015 UTC 5 June 2005.

5.2 Parallel stratiform systems

Unlike LS systems, where the stratiform is typically due east of the MCR, PS systems have a stratiform region to the northeast of the MCR. This unfortunately makes it

difficult for the stratiform to be inside of the state of Oklahoma at all times for various cases. This was a major issue with the cases presented here. Because of this, some patterns were more difficult to detect than they were for LS systems. In this study, PS systems also tended to evolve into TS systems more quickly than LS systems did, so there were fewer time steps available to examine their form.

The first case being examined is case number 17b, which occurred from 0130-0415 UTC on June 5 2005. Unlike most of the other cases, this case had its stratiform region completely contained inside of the state of Oklahoma. Although there weren't enough other cases to draw conclusions from what occurs in the stratiform region of PS systems in general, this case is an excellent example of a typical PS system that can be more thoroughly analyzed.

The case begins in PS form with two MCRs, one directly in line with the large stratiform region and a smaller cluster of cells about 50 km to the rear of the system (Fig. 5.26). Easterly flow has confluence just ahead of the system, near the eastern border of the MCR. Just to the southwest of this area of confluence is an area of diffluence also ahead of the advancing MCR, which is heading ENE. There is also an area of strong confluence just ahead of the advancing stratiform region, with prevalent westerly and northwesterly winds.

As the system reaches maturity by 0230 UTC (Fig. 5.27), several patterns of confluence and diffluence appear throughout the entire system. An area of confluence from southeasterly and southwesterly flow occurs inside the MCR. A second area of confluence exists on the northern edge of the MCR of southeasterly flow. In between the two areas of confluence is an area of strong diffluence, with a second area of strong

diffluence inside the core of the stratiform region. It is of note that all four regions exist solely in areas of precipitation, not on the borders of either the MCR or stratiform region.

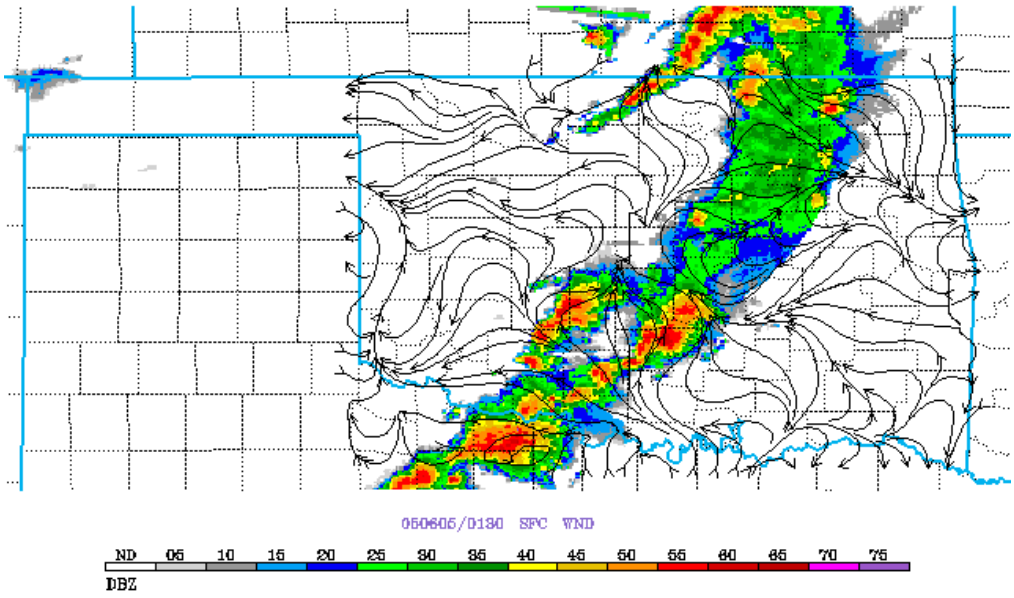

Figure 5.26: Same as Fig. 5.1 except at 0130 UTC 5 June 2005.

By 0330 UTC, the system is in an intermediate stage of transition between a PS system and a TS system. In Fig. 5.28, it is evident that the regions of strong confluence have shifted to areas ahead of the system, with the strongest confluence consisting of southerly flow ahead of the system's advance. Very strong diffluence exists throughout the entire MCR and even the stratiform region, though there is one region of confluence in the wake of the stratiform region at the northwest corner of the system.

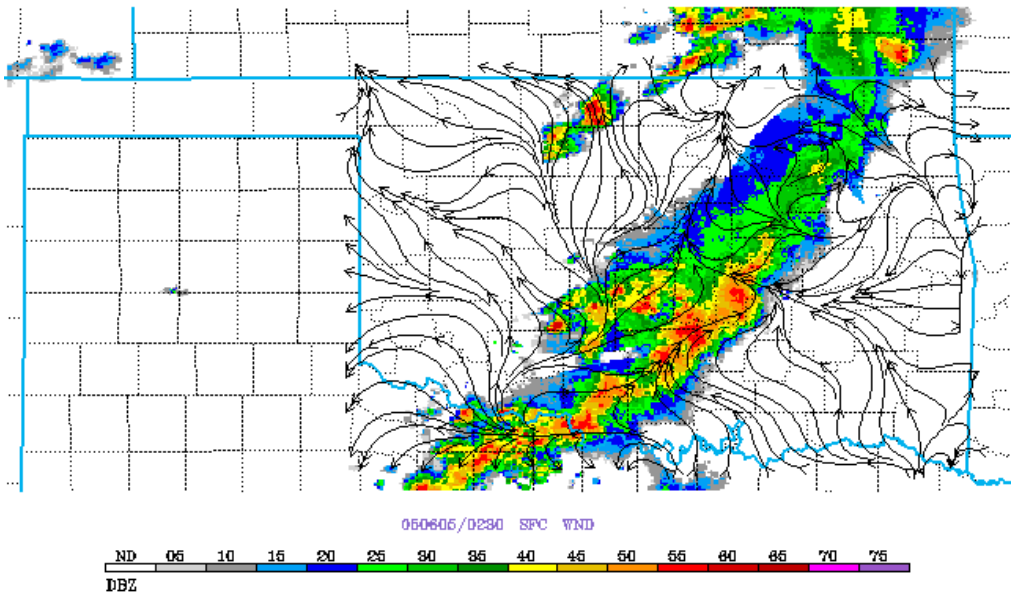

Figure 5.27: Same as Fig. 5.1 except at 0230 UTC 5 June 2005.

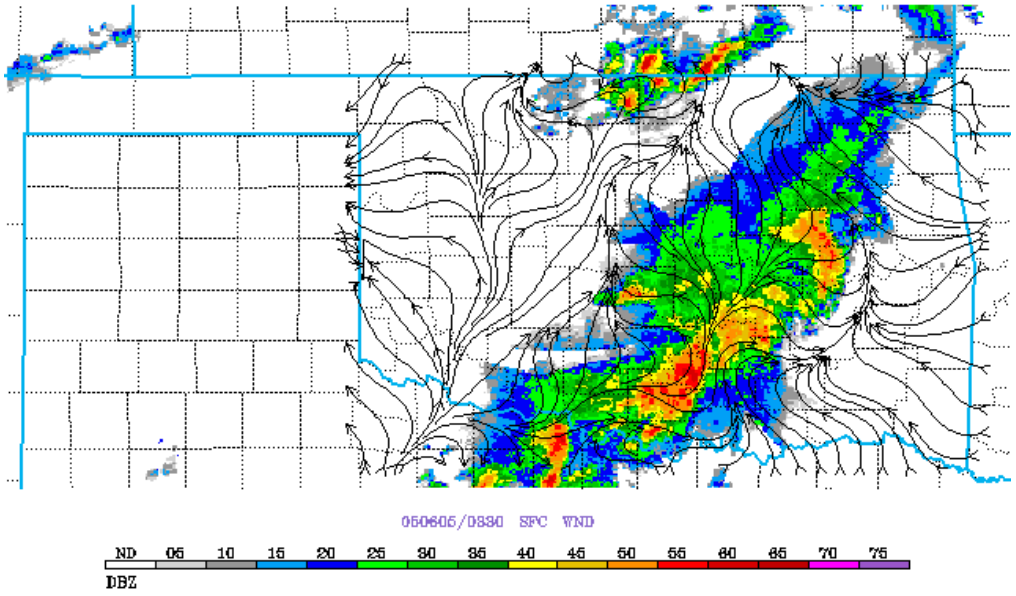

Figure 5.28: Same as Fig. 5.1 except at 0330 UTC 5 June 2005.

It is clear as the system evolved that diffluence became much more prevalent in the transitioning stages that it was in LS systems. Another major difference was that southerly flow only became existent ahead of the system until the transition period; LS systems tended to have southerly flow ahead of the system's advance much more consistently.

The θ pattern of this case is observed next. As seen in Fig. 5.29, the coldest air exists just behind the MCR. The warmest air exists due east, just ahead of the advancing MCR. There is a secondary area of warmth inside the stratiform region.

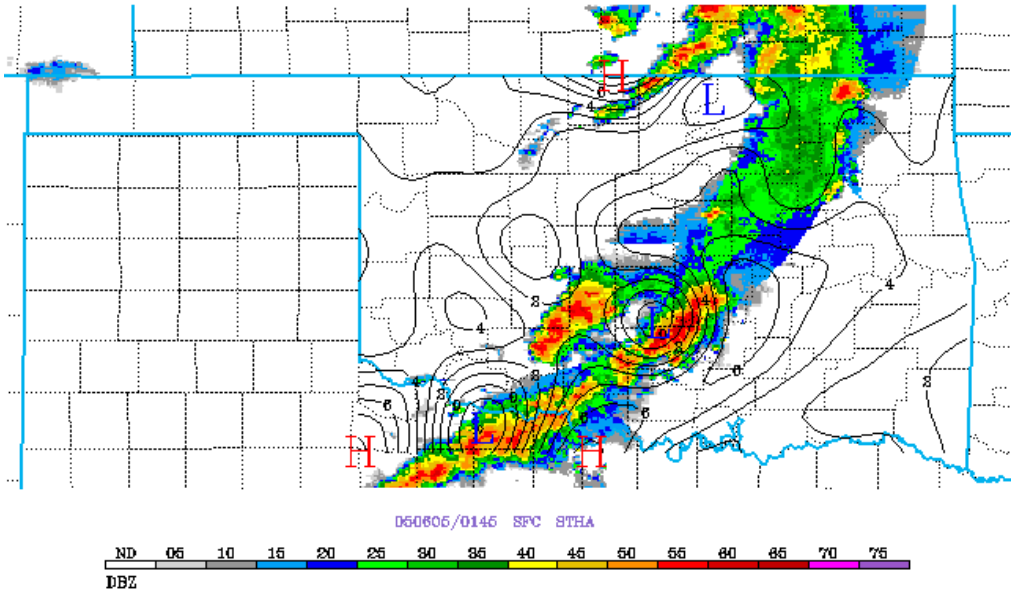

Figure 5.29: Same as Fig. 5.4 except at 0145 UTC 5 June 2005.

As the system advances to the ENE, the cold pool strengthens slightly (Fig. 5.30). There is also a second area of cold air at the very southwestern end of the system. The warmest

air is still ahead of the system but is now positioned southeast of the MCR instead of due east as before. It has now increased in temperature.

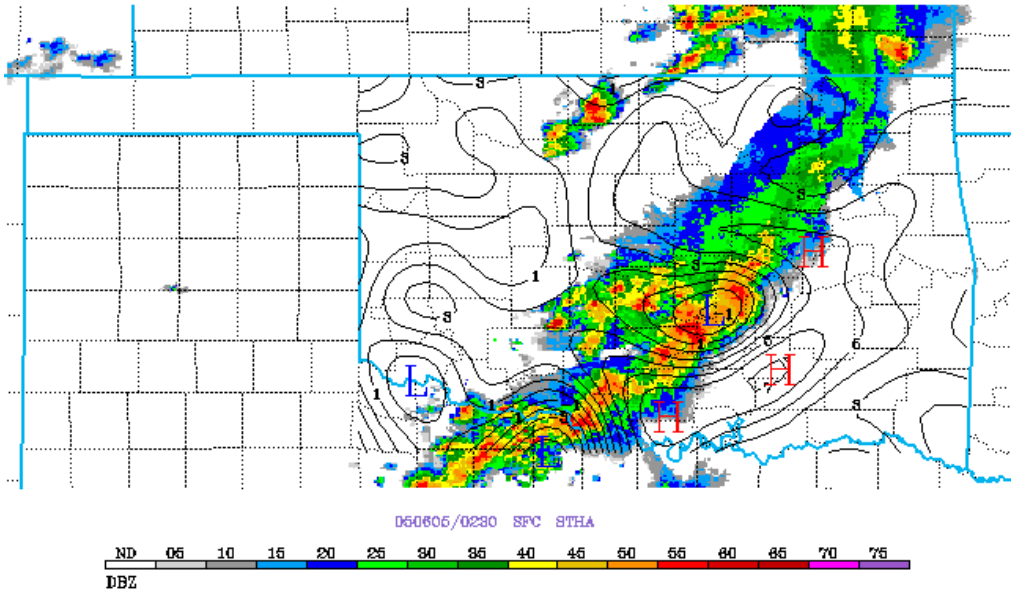

Figure 5.30: Same as Fig. 5.4 except at 0230 UTC 5 June 2005.

During the system's transition period, the temperature differential is slightly reduced. As shown in Fig. 5.31, there are two areas of cold air, with both being inside the MCR. Air is still warmest ahead of the system's advance. The stratiform region has warmer air than the MCR with a small pocket in the western edge of the stratiform area.

PS and LS systems have a somewhat similar structure in terms of the coldest temperatures occurring in or just behind the MCR. However, they differ when it comes to the warmest temperatures. Although the stratiform region does have higher potential temperatures than the MCR does in PS cases, the maximum areas of potential temperature are actually ahead of the system's advance. Thus, the warmest potential

temperatures don't necessarily follow the stratiform region and may simply be a function of the southerly flow advecting warm air ahead of the system's advance.

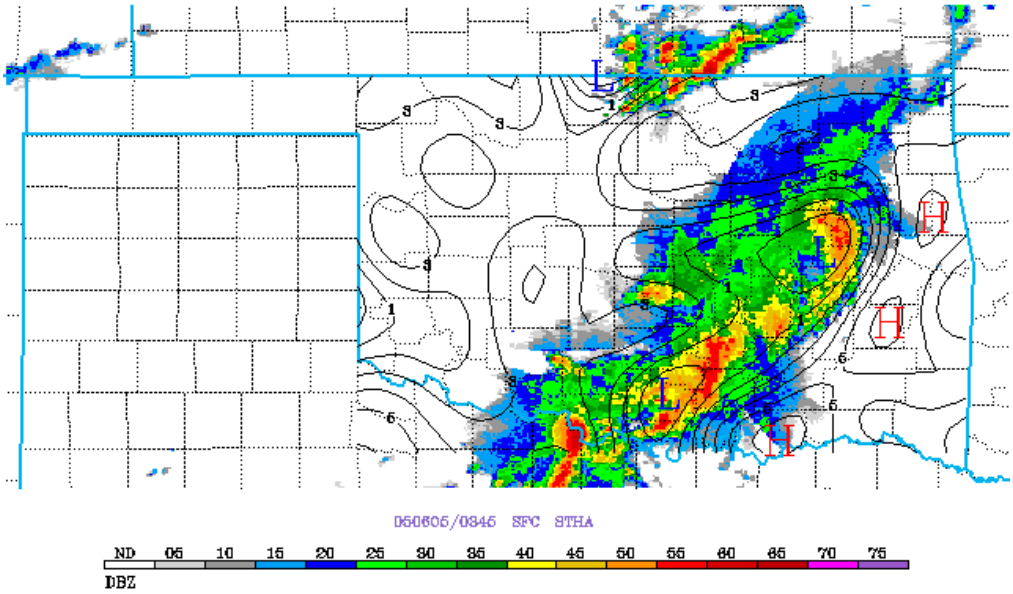

Figure 5.31: Same as Fig. 5.4 except at 0345 UTC 5 June 2005.

Equivalent potential temperatures are evaluated next. Figure 5.32 shows a very strong northwest-to-southeast differential of θ_e values, with greater values ahead of the system's advance and in the transition zone. Two areas of negatively buoyant air also exist; one is in the wake of the MCR and a second one in the wake of the stratiform region.

Advancing 45 minutes to 0230 UTC reveals a similar pattern, except now the differential has increased (Fig. 5.33). Low θ_e values exist on the western edge of the MCR. Two areas of high θ_e values exist as well; one is located in the transition zone and a second to the southeast of the most negatively buoyant region ahead of the system's

advance. More negatively buoyant air exists to the northeast near the northwestern corner of the stratiform region.

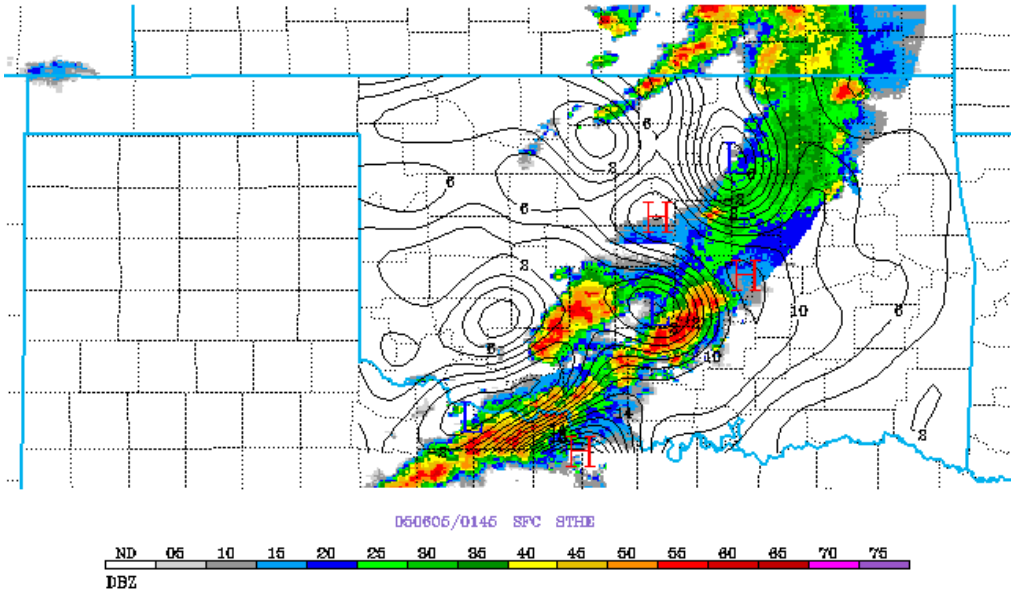

Figure 5.32: Same as Fig. 5.7 except at 0145 UTC 5 June 2005.

The θ_e differential is about the same magnitude at 0345 UTC (Fig. 5.34). The lowest temperature is present throughout the MCR. The most positively buoyant areas have moved slightly, with the positively buoyant air typically located in the southern edge of the stratiform area, moving north into the core of the stratiform region. The positively buoyant air ahead of the system has also moved north and is now almost due east of the leading edge of the MCR.

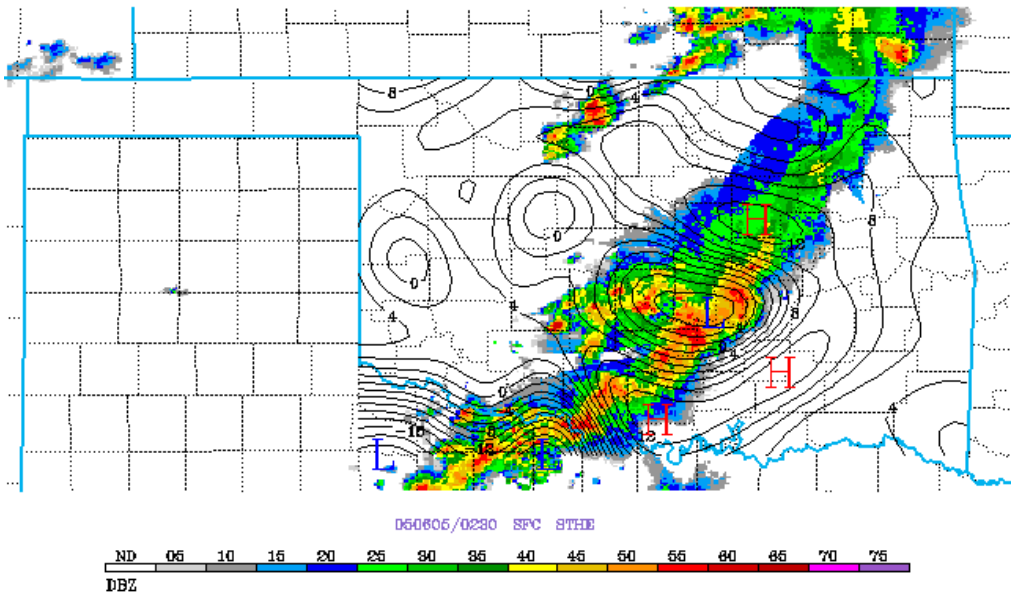

Figure 5.33: Same as Fig. 5.7 except at 0230 UTC 5 June 2005.

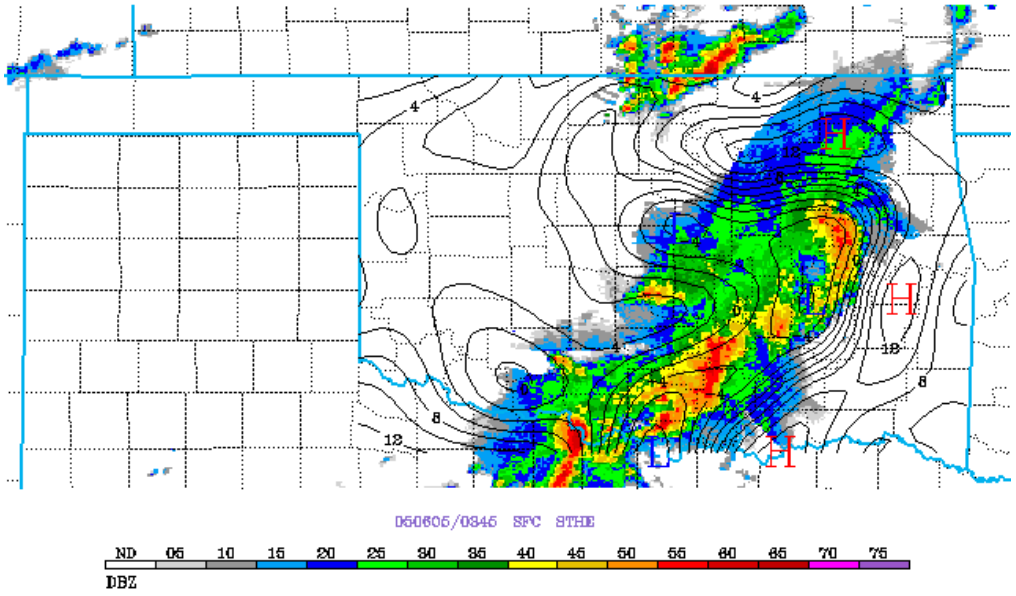

Figure 5.34: Same as Fig. 5.7 except at 0345 UTC 5 June 2005.

There were many similarities here between LS and PS systems. Like LS systems, PS systems tend to have their largest θ_e values either just ahead of the system's progression or in the transition zone. The smallest θ_e value regions also exist in the MCR or along its back edge. Even though the stratiform was directed towards the northeast in PS cases, the highest values still occurred in the transition zone (with the exception of Fig. 5.32 where the area had moved further north). This exception can possibly be explained by the system's transition into a TS state.

Finally, the pressure features of case 17b are examined. As shown in Fig. 5.35, mesohighs are observed; one inside the group of cells behind the MCR and a second inside the core of the stratiform region along the leading edge. A mesolow also exists ahead of the system just to the east of the MCR.

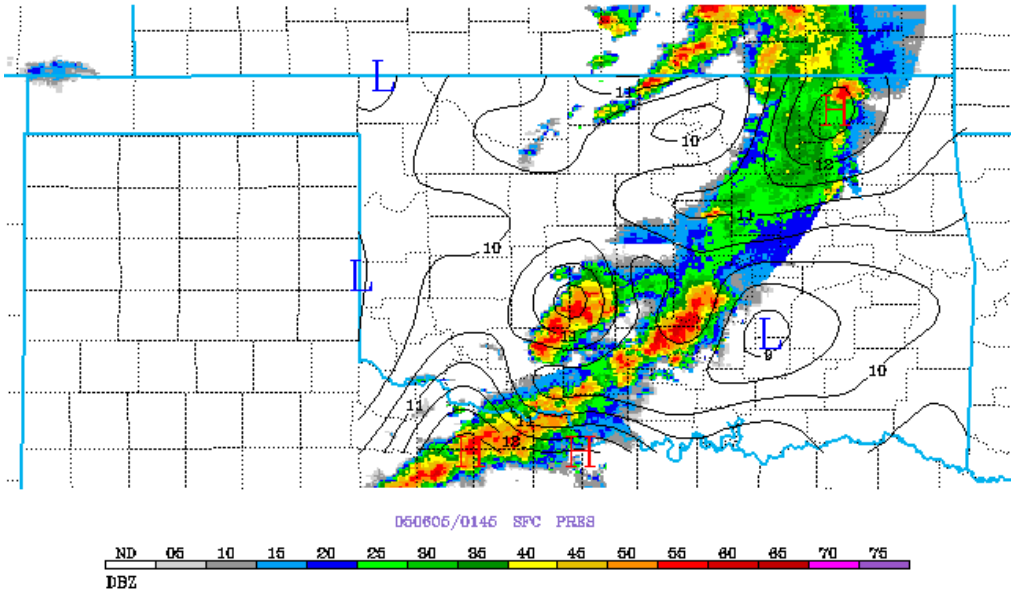

Figure 5.35: Same as Fig. 5.10 except at 0145 UTC 5 June 2005.

The system at 0245 UTC reveals a slightly different pattern (Fig. 5.36). Two mesohighs exist inside the MCR. A pair of mesolows also exist; the first is ahead of the system due south of the stronger mesohigh. The second mesolow is actually located along the western rear edge of the stratiform region.

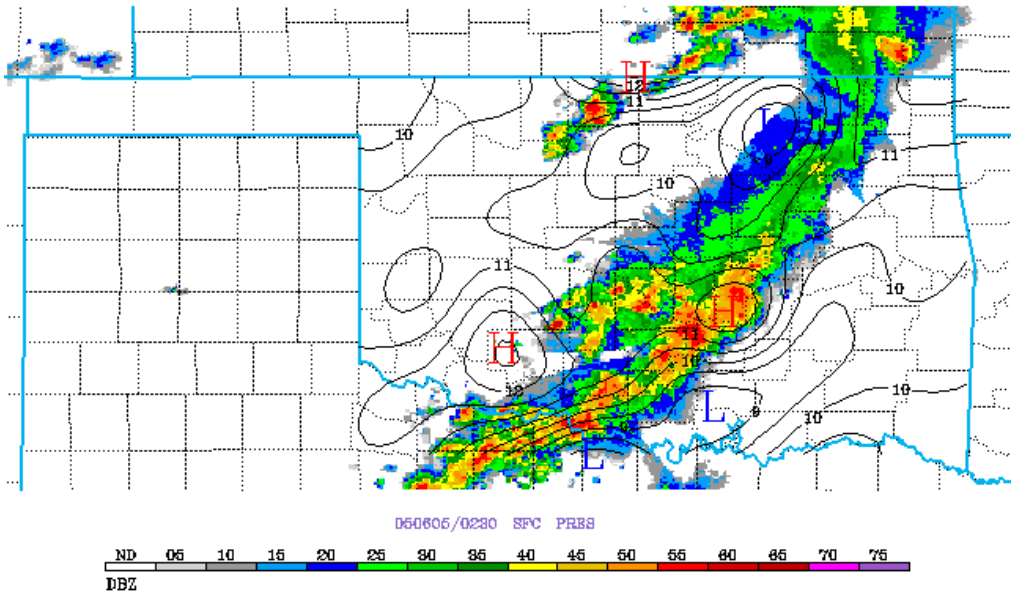

Figure 5.36: Same as Fig. 5.10 except at 0230 UTC 5 June 2005.

At 0345 UTC, shown in Fig. 5.37, this pattern has largely remained unchanged. A mesohigh inside the MCR and a mesolow ahead of the system's advance still exist. There is another mesolow still occurring on the very northern edge of the stratiform region towards the rear.

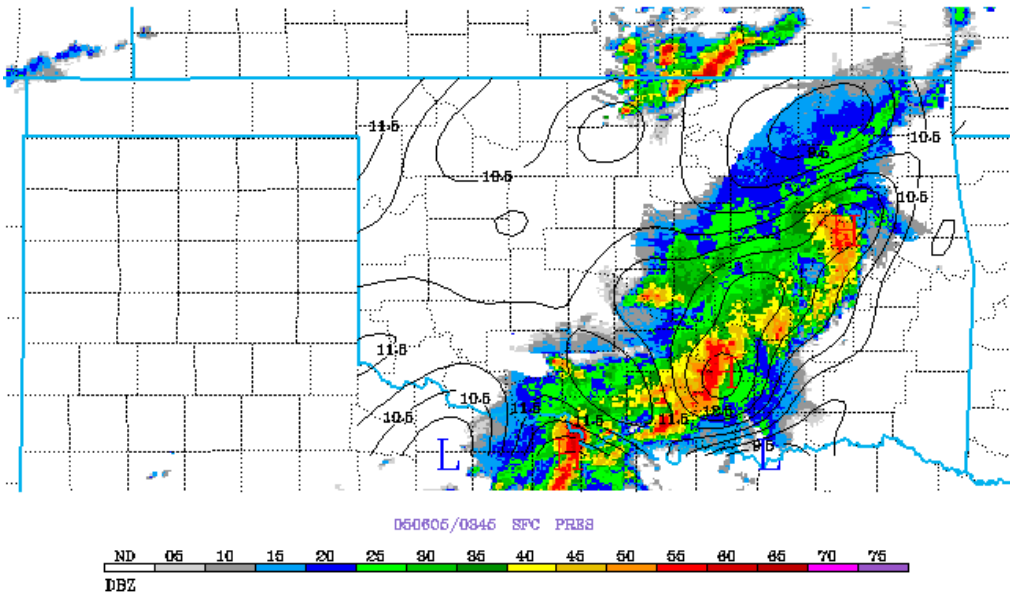

Figure 5.37: Same as Fig. 5.10 except at 0345 UTC 5 June 2005.

Similar to LS systems, PS systems have a mesohigh situated close to the MCR and a mesolow situated in advance of the system. It is less evident if the mesolow follows the stratiform region. It only appears starting at 0230 UTC, and might simply be due to the transition from parallel to trailing stratiform. It is difficult to discern this, as most of the cases had a stratiform region outside of the state's boundaries. This result will be compared with the second PS case to see if a similar pattern becomes evident.

The second case, which went from 1545-2200 UTC on April 24, 2007, unfortunately had its stratiform region located outside of the state after 1900 UTC, which makes determining the conditions inside the stratiform region impossible after this time. However, this case also developed fully inside the state's boundaries which allows a view of its entire life cycle.

At 1715 UTC, shown in Fig. 5.38, the case has just begun to develop a small region of lower dBZ values on the north side of the system. The strongest confluence is occurring just to the east of the most intense portion of the MCR ahead of the system, primarily from westerly and southerly flow. An area of strong diffluence exists about 50 km behind the northern edge of the system to the west.

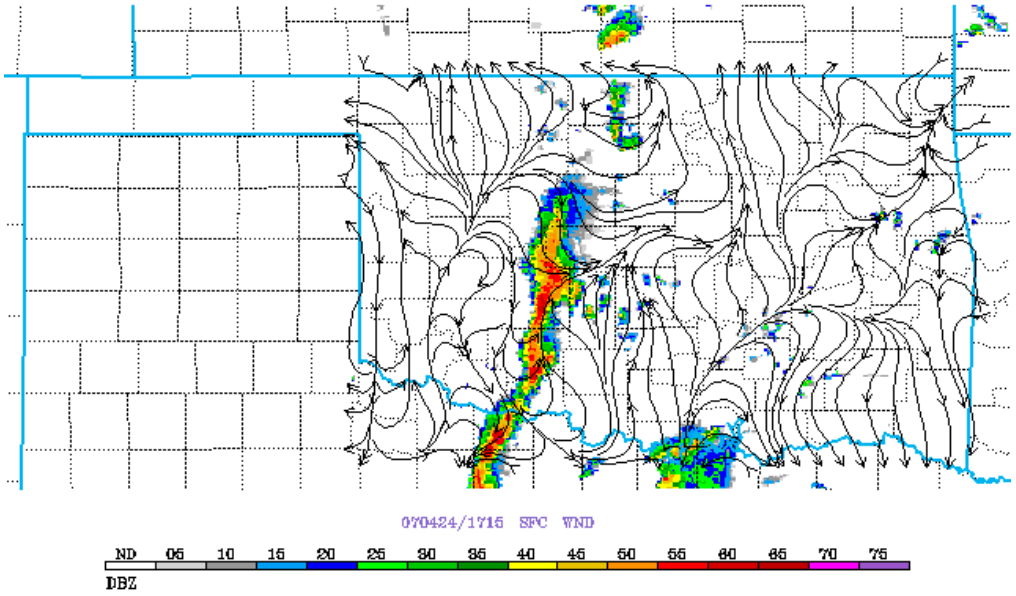

Figure 5.38: Same as Fig. 5.1 except at 1715 UTC 24 April 2007.

At 1815 UTC, the system has progressed further eastward with the stratiform region growing in size (Fig. 5.39). Confluence exists towards the center of the system with westerly flow; the flow is causing convection to stretch to the east. An area of diffluence exists in the wake of the stratiform region, about 30 km to the west. A second area of diffluence also exists just behind the southern edge of the system, also roughly 30 km to the west.

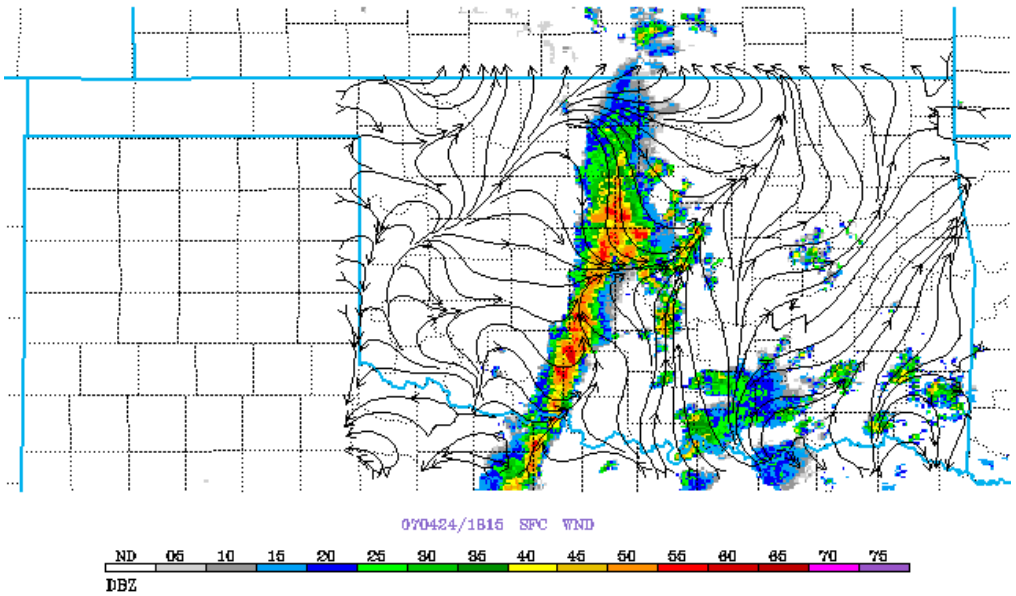

Figure 5.39: Same as Fig. 5.1 except at 1815 UTC 24 April 2007.

By 2000 UTC, the system has fully matured with the stratiform region now entirely out of the state. In Fig. 5.40, two main areas of confluence exist. The first is one of southerly and westerly flow just ahead of the system due east of the strongest area of convection. The second is in the southern part of the system, with confluent westerly flow throughout the MCR. The strongest area of diffluence is on the very western edge of the system, behind the strongest portion of the MCR.

This system consistently had diffluence in its wake, with confluence ahead of the system. This was less common in case 17b, but both cases had southerly flow ahead of the system near maturity. It was also common for both systems to have diffluence either in the MCR or just to the rear of the MCR.

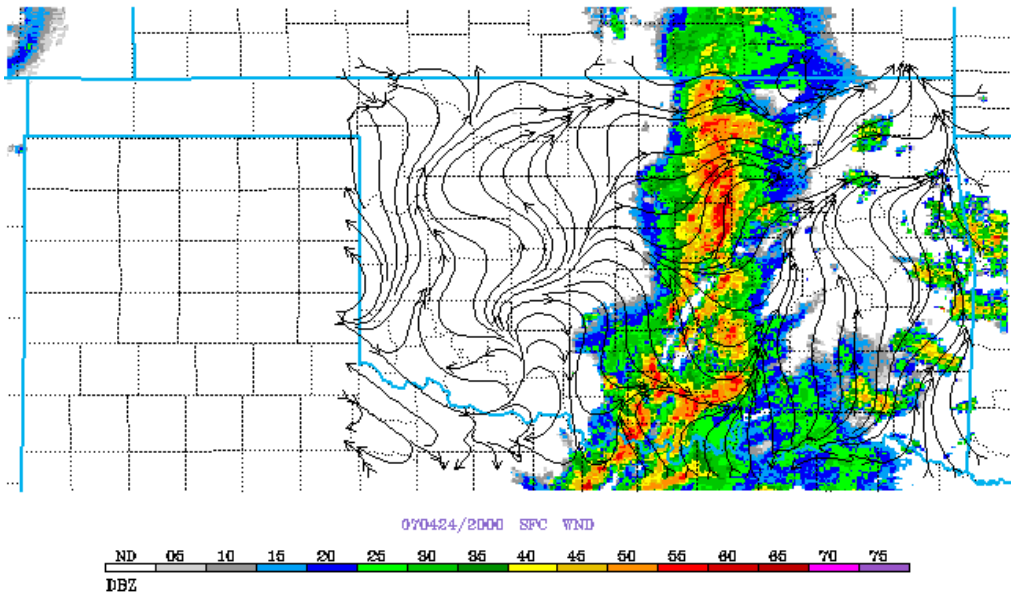

Figure 5.40: Same as Fig. 5.1 except at 2000 UTC 24 April 2007.

The θ pattern of case 19 showed similar results to case 17b. As seen in Fig. 5.41, the coldest air exists in the wake of the MCR, with the warmest air to the due east. The stratiform region is about the same temperature as the MCR, but it also is very small at this time and hasn't developed much yet.

By 1815 UTC, the same basic pattern remains (Fig. 5.42). Cold air exists along the western edge of the MCR near the most intense convection. Warm air is ahead of the system to the due east of the convection. The stratiform is now a little warmer than the MCR.

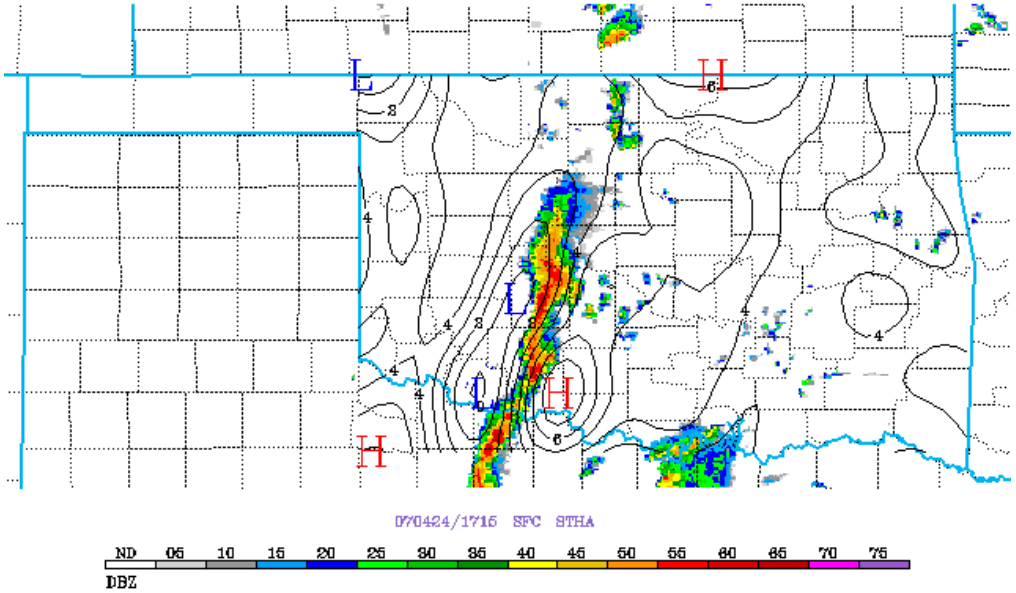

Figure 5.41: Same as Fig 5.4 except at 1715 UTC 24 April 2007.

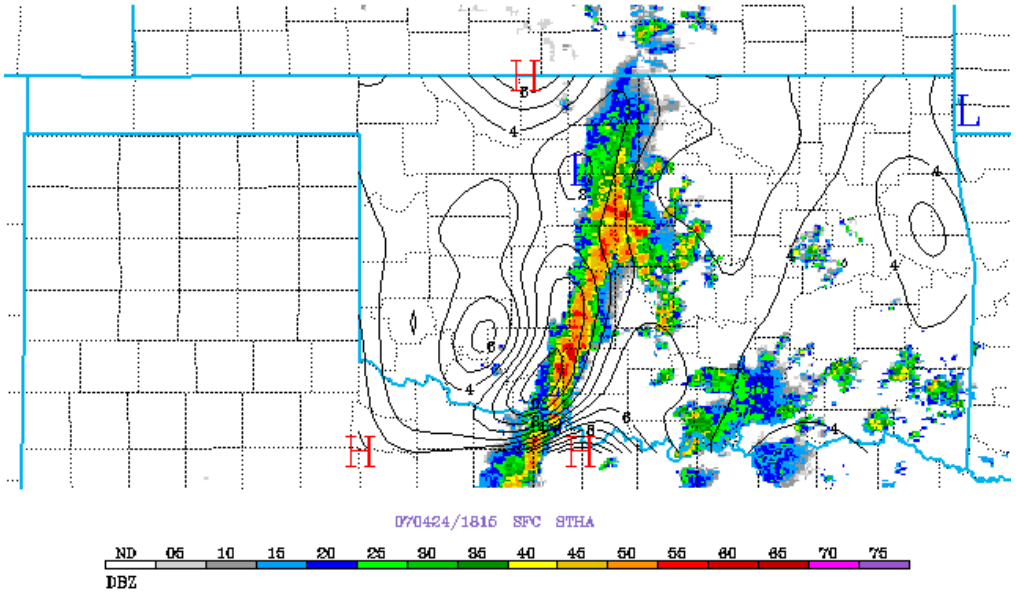

Figure 5.42: Same as Fig. 5.4 except at 1815 UTC 24 April 2007.

At 2000 UTC, the temperature differential has reduced significantly. The coldest temperature is still located just behind the MCR along its western border (Fig. 5.43). The temperature of the stratiform region can't be identified, but the warmest air is just ahead of the system's progression.

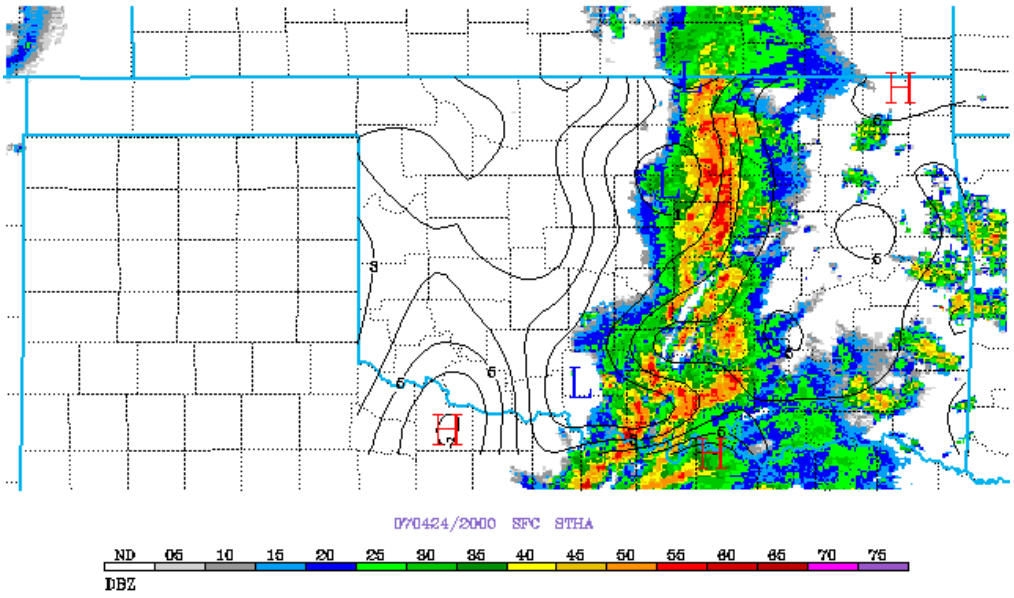

Figure 5.43: Same as Fig. 5.4 except at 2000 UTC 24 April 2007.

Both the LS and PS systems consistently had the coldest locations behind the strongest portion of the MCR and the warmest locations to the east of the system. This was the same average trend of the other cases not discussed here. It is more difficult to determine with confidence what the temperatures are in the stratiform region of PS systems due to a lack of data.

The locations of the highest θ_e air also remain similar between the two cases. In Fig. 5.44, the same patterns are again repeated. The highest θ_e air exists in two areas ahead of

the MCR; one is due east of the strongest convection and the other is east of the southern edge of the system. A third area of high θ_e air also exists to the northwest of the MCR. There is also a slight maximum in the transition region. The lowest θ_e air is just behind the MCR on its western edge.

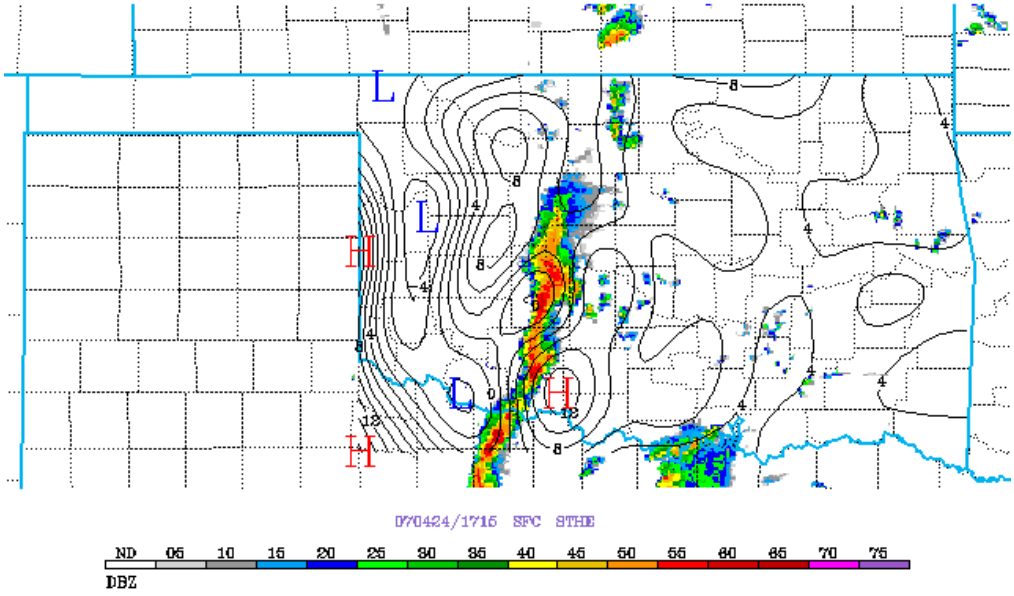

Figure 5.44: Same as Fig. 5.7 except at 1715 UTC 24 April 2007.

At 1815 UTC, the air has significantly become more negatively buoyant behind the MCR (Fig. 5.45). Temperatures have decreased here, with the most positively buoyant air still occurring ahead of the system, with the exception of the maximum found behind the northern part of the system. A range of moderate θ_e values also exists in the transition zone, which has significantly higher θ_e values than the MCR.

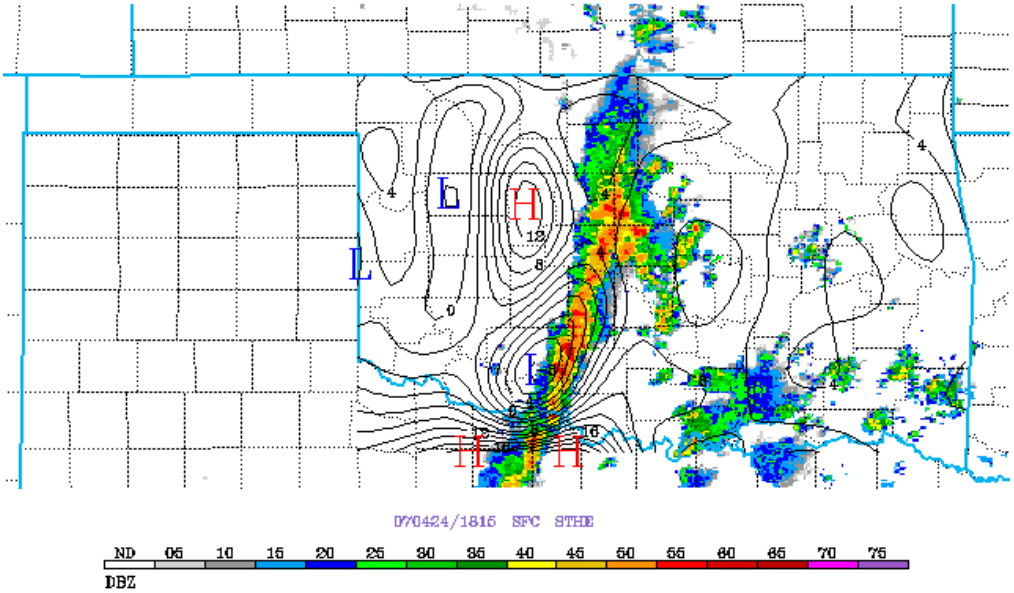

Figure 5.45: Same as Fig. 5.7 except at 1815 UTC 24 April 2007.

Near the system's maturity at 2000 UTC (Fig. 5.46), a strong west-to-east differential exists, with lower θ_e values bordering the rear of the strongest convection and higher θ_e values due east of the convective region. Stratiform temperatures are unavailable since the stratiform region is now to the north of Oklahoma's border.

Once again, both cases were very similar to each other and the LS cases. The most positively buoyant areas were ahead of the system's advance, with a secondary maximum of θ_e values in the transition zone. The lowest temperatures were always behind the area of strongest convection. Even though the potential temperatures don't follow the stratiform region, the equivalent potential temperatures seem to do so, at least partially. There was a secondary maximum in equivalent potential temperature along the transition

zone between stratiform and convection in all four cases, which also meets the average pattern found in other cases.

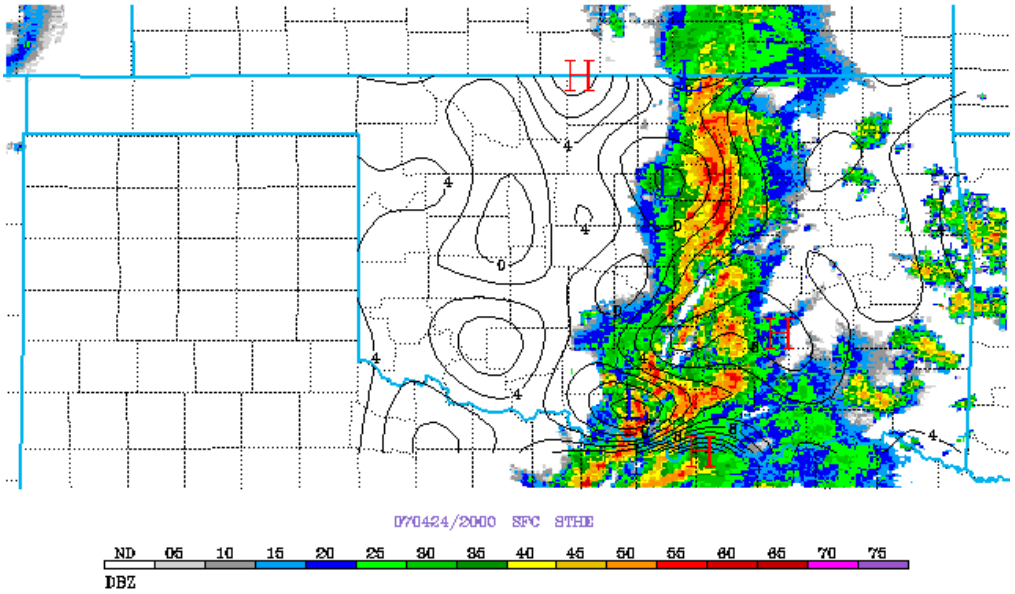

Figure 5.46: Same as Fig 5.7 except at 2000 UTC 24 April 2007.

Last, the surface pressure features were more difficult to discern in case 19 and ended up being largely inconclusive. As seen in Fig. 5.47, the pressure differentials were very small. The lowest area of pressure is ahead of the system, but the area behind the system is only 1 hPa greater. No contours were drawn inside of the stratiform region.

By 1815 UTC, slightly higher pressure exists over the MCR (Fig. 5.48). The stratiform region has an area of slightly lower pressure. It is difficult to identify, however, whether these features are of a magnitude great enough to indicate a mesohigh or mesolow.

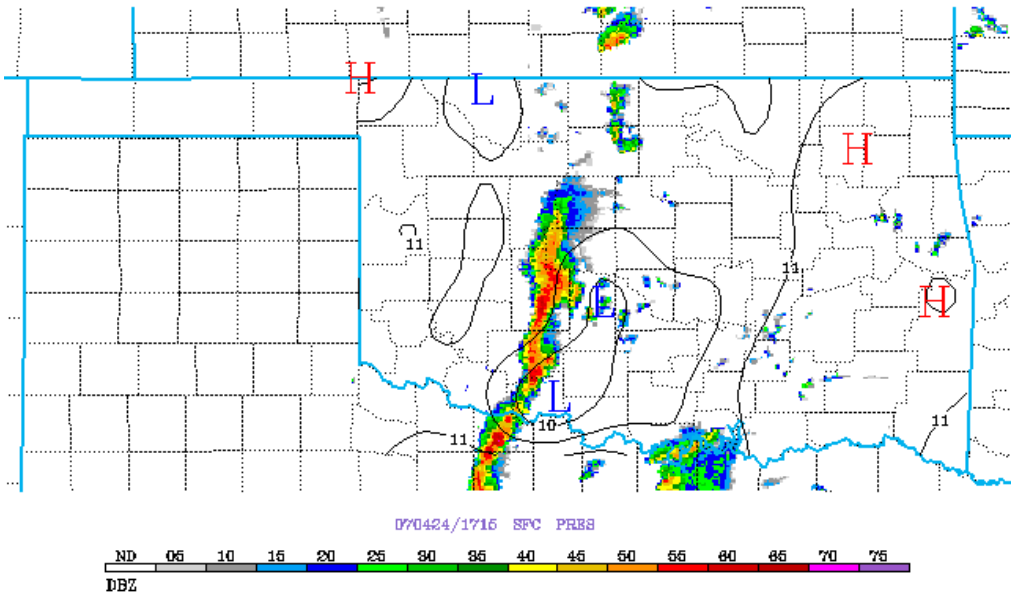

Figure 5.47: Same as Fig. 5.10 except at 1715 UTC 24 April 2007.

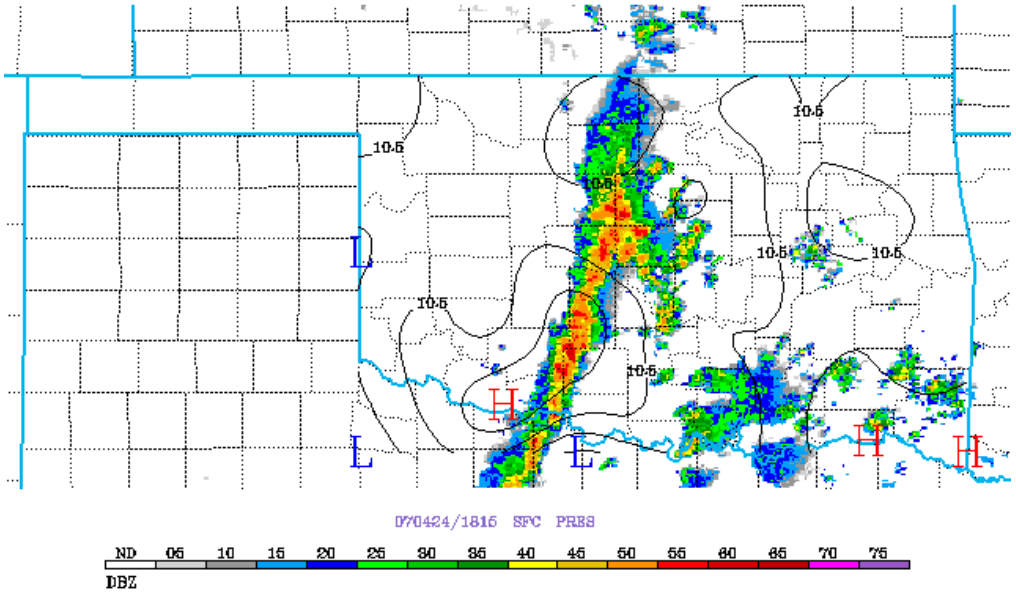

Fig. 5.48: Same as Fig. 5.10 except at 1815 UTC 24 April 2007.

Figure 5.49 shows a small area of low pressure ahead of the MCR and an area of slightly higher pressure behind the MCR. These magnitudes are, unfortunately, too small to allow any meaningful identification of the surface pressure features.

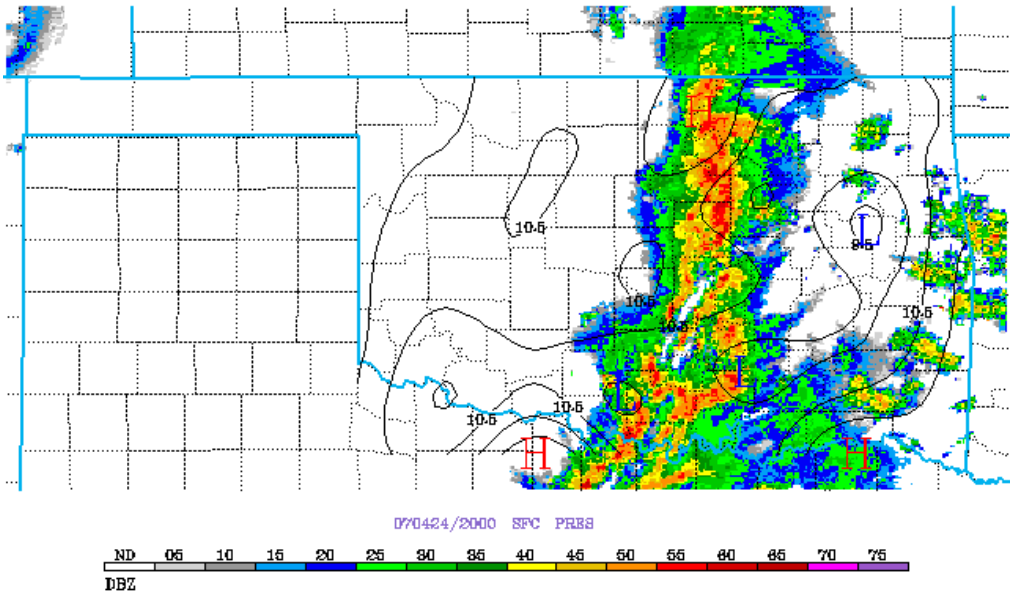

Figure 5.49: Same as Fig. 5.10 except at 2000 UTC 24 April 2007.

The pressure fields in this case were not particularly distinct due to small pressure differentials. There were slightly higher pressure readings behind the MCR, and slightly lower readings ahead of the system, which meets the pattern of previous cases. The vast majority of other PS cases, not shown here, had higher pressure readings near the MCR and lower pressure readings ahead of the system's advancement. What still remains uncertain is the behavior of the surface pressure fields inside the stratiform region; of the 10 PS cases analyzed, four were inconclusive, four showed somewhat higher pressure in the stratiform region, and two showed lower pressure in the stratiform region.

A complete summary of the surface features of both types, as well as a discussion of the original questions posed in the proposal of this thesis, will be discussed in the next chapter. It will also include conceptual models displaying the overall average surface features for each system type.

Chapter 6

DISCUSSION OF RESULTS

Based upon the results from the previous chapters, this chapter will highlight how questions initially raised in the proposal of the thesis have been answered. It will also provide a conceptual model that can be used for both LS and PS archetypes regarding their pressure, surface flow, and buoyancy parameters. This information can be used in further studies and to allow a greater understanding of how these systems evolve.

6.1 Proposal answers

As previously discussed in Chapter 2, Haertel and Johnson (2000) investigated the cause of surface pressure features in linear MCSs. Based upon a theory they developed, all moving stratiform regions associated with either PS or LS archetypes should exhibit mesohigh/wake low couplets. Therefore, the couplets are directly linked to and accompany the motion of the stratiform region, regardless of how the stratiform region is oriented in relation to the MCR.

If the pressure features of these systems are examined, it can be concluded that there is ample evidence to verify this hypothesis is true. Figures 5.10, 5.22, and 5.24 show this to be the case. In both LS cases analyzed from Chapter 5, the mesohigh/wake low couplet did stay with the stratiform region. This slightly differs from HJ 2000's conclusion, however, because the mesohigh was located behind the stratiform region instead of

preceding it, suggesting other mechanisms are at play. The one exception to the couplet staying with the stratiform region's motion was when the stratiform region separated from the MCR as in case 4, shown in Fig. 5.12.

It can't be concluded for certain what is causing the mesolow to form ahead of LS systems. These mesolows differ from the pre-squall lows found in TS systems; LS system mesolows are further away from the convective line. Therefore, the mechanism creating the mesolows in LS systems must be different. The most likely cause is a leading inflow jet which warms the lower troposphere and causes a decrease in surface pressure. This phenomenon has been observed in Pettet and Johnson (2003) (see Fig. 2.4). However, data on the storm-relative flow is needed to confirm this hypothesis.

The hypothesis of HJ 2000 has yet to be concluded for PS systems. The PS cases investigated in this study had issues with the stratiform region being outside of the state in many instances. Even when the stratiform region was inside the entire state, only a small number of cases could be analyzed properly. These cases also typically didn't have very clear centers of high or low pressure, as discussed with the example of case 19 in Chapter 5. Although there is evidence for a mesohigh either inside of or just behind the MCR and a pre-squall low ahead of the system's movement, evidence of the pressure fields inside the stratiform region remains lacking (with the exception of case 17b). That case showed a transition from PS to TS, and the mesohigh/wake low couplet observed in the northeastern section of the system (see Fig. 5.37) may be attributed to this transition instead of PS system dynamics.

The paper by Haertel and Johnson (2000) also studied the surface pressure response to cooling associated with a stratiform precipitation region of a squall line that was moving at 10 m s^{-1}. Shown in Fig. 6.1, the wake low intensifies after the stratiform region has ended (the stratiform only lasted four hours in their study). Because of this result, they conclude the wake low intensifies after the stratiform region has dissipated.

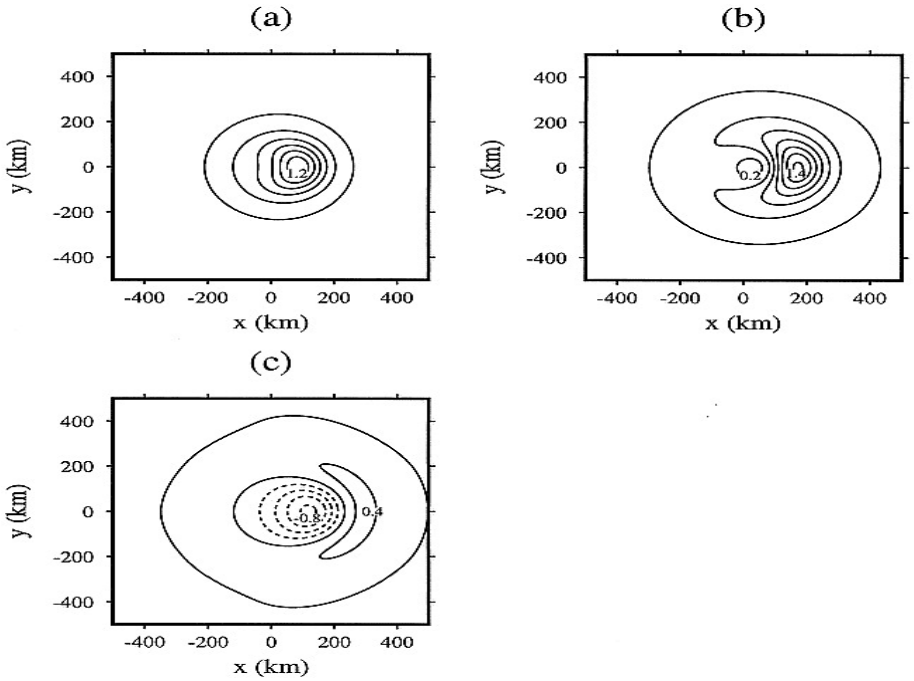

Figure 6.1: The surface pressure response to the moving, asymmetric cooling at (a) 2, (b) 4, and (c) 6 h. The contour interval is 0.2 hPa. From Haertel and Johnson (2000).

In LS systems, the exact opposite of this response is often observed, with the lowest pressures occurring to the east of the stratiform instead of the west. This process is most likely explained by a descending inflow jet on the leading edge of the system, as previously discussed by Parker and Johnson (2000) and Pettet and Johnson (2003). It is not clear, however, whether LS or PS systems experienced an amplification of the pressure couplet after the stratiform region collapsed. The main reason for this uncertainty is a lack of observations available when the stratiform region had collapsed. Usually, the cases studied in this paper ended up with a transition into a TS system. All of

the cases observed in this study either transferred into a TS system or into a system with no MCR left. Because of this reality, this study can't confirm or deny the pressure amplification pattern after the stratiform region terminated found in HJ 2000.

The thesis proposal also theorized that PS systems had a different pressure field on one end of the line as compared to another. This theory is based on the PS system's similar arrangement of stratiform to asymmetric TS systems, with a pressure pattern that should look similar to the one shown in Fig. 2.16 from Loehrer and Johnson (1995). Only one case, case 17b, had a discernible pressure pattern that seems to confirm this theory.

As shown below in Fig. 6.2, case 17b was just beginning its transition into an asymmetric TS system. At this stage, the stratiform region is still predominantly parallel to the MCR, so it still qualifies as a PS system. There is indeed a mesohigh/wake low couplet, with a low in the rear of the stratiform region and an area of higher pressure on the other side of the stratiform region. A pre-squall low is shown to the southeast of the system, and a mesohigh inside the MCR exists along the system's front edge. This pair of couplets looks very similar to Fig. 2.15, with the exception of the mesohigh found in the MCR. Case 17b showed well-defined behavior, but it can't be considered as confirming this theory until additional PS cases can be observed.

As discussed in Chapter 2, the strong pressure gradients observed in some TS systems can cause damaging easterly winds. Coleman and Knupp (2009) concluded that, in order for a pressure gradient to cause severe winds greater than 25 m s^{-1}, there needs to be a slow propagation speed and an ambient wind in a similar direction to the direction of the pressure gradient force. It needs to be determined if a similar event could occur for LS and PS systems.

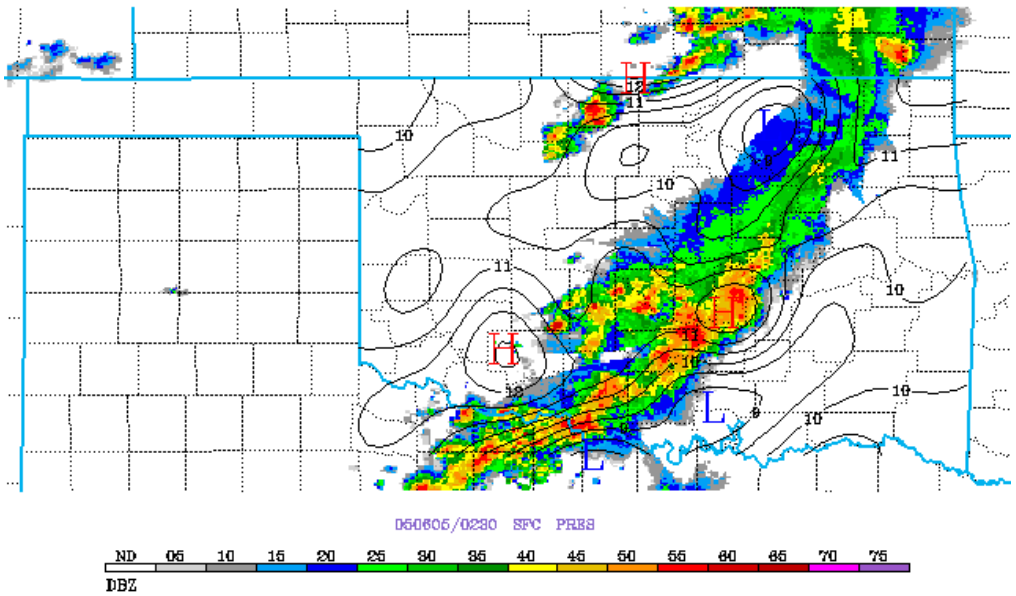

Figure 6.2: Same as Fig. 5.10 except at 0230 UTC 5 June 2005.

Based upon these results, LS systems tend to have stronger pressure gradients than PS systems, so these are more likely to have similar strong surface winds. The difference between the Coleman and Knupp study and this study is that LS systems have a pressure gradient force directed towards the front of the system instead of the rear due to the stratiform region's orientation.

An example of the strongest pressure gradient observed in any of the systems in this study is in Fig. 5.10, with a pressure difference of 5.5 hPa. Unlike the pressure gradients observed in TS systems, this gradient is oriented northwest to southeast instead of east to west. In addition, since the direction of the system's propagation is the same horizontal direction as the pressure gradient force, it isn't clear whether this contributes to stronger or weaker surface winds. The CK 2009 cases had a pressure gradient force pointed in the

opposite horizontal direction of the system's propagation. Furthermore, the pressure values in this study do not include any synoptic influence, which means the differential in case 4 could actually be greater than 5.5 hPa if the synoptic influence were included.

It would be difficult to determine, even if severe surface winds were observed, whether these winds were due to the pressure gradient or were simply part of the system's propagation. This study of LS and PS systems can't reach a conclusion regarding this phenomenon, but perhaps further study could.

6.2 Conceptual models of leading and parallel stratiform systems

Based on the information from Chapter 5, conceptual models of both systems can be developed (although not fully in the case of PS systems). These conceptual models represent an overall average of the structure found in all of the cases observed.

Shown below in Fig. 6.3, the LS system is presented during its mature stage. Notice that unlike Fig. 2.17 from Loehrer and Johnson (1995), LS systems have a low pressure center in the eastern portion of the stratiform region instead of the system's wake. This finding was similar to the cases observed in Pettet and Johnson (2003) where that study also found a mesolow ahead of the stratiform region.

The figure also shows the pattern of confluence and diffluence around the system, with confluence occurring on the eastern edge of the MCR with southerly flow and diffluence in the system's wake with flow towards the northwest and northeast. These flows help indicate a response to the mesohigh found in the system's rear and the mesolow found in the system's front.

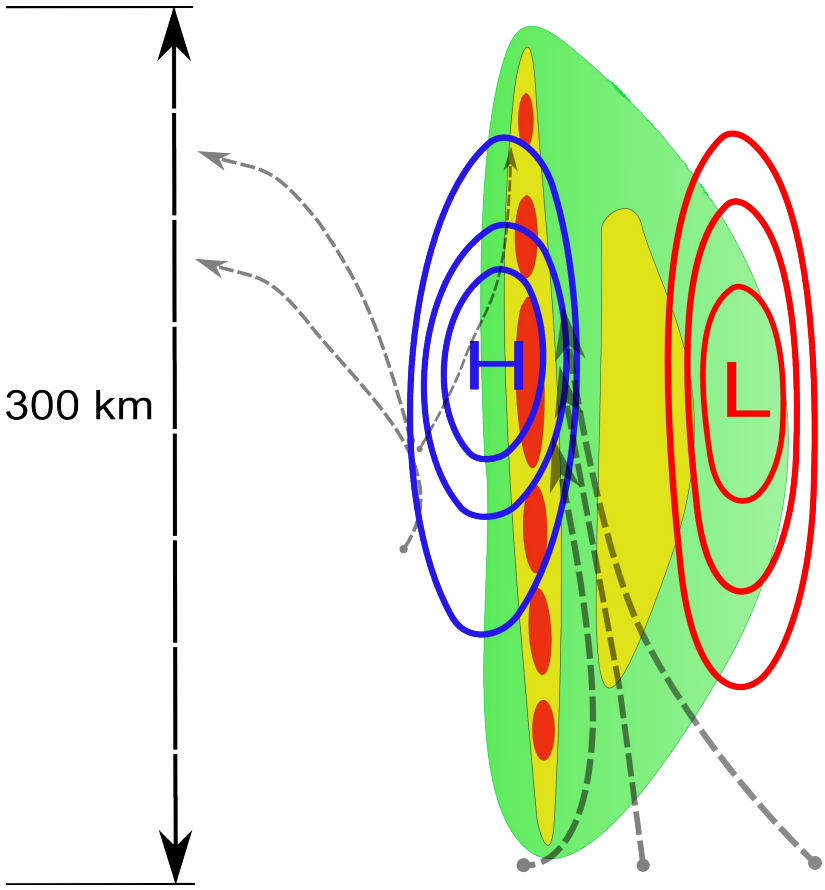

Figure 6.3: Conceptual model of a leading stratiform system at maturity. The color contours stand for red = 50 dBZ, yellow = 40 dBZ, and green = 20 dBZ. Pressure systems are marked with a blue H representing the mesohigh and the red L representing the mesolow. Contours are 1-hPa increments. Areas of confluence or diffluence and wind direction are represented by the arrows.

The next conceptual model, Fig. 6.4, shows the location of maximum and minimum θ_e values. These values tend to overlap well with the locations of the mesohigh and mesolow, with the lowest values occurring near the mesohigh and the highest values occurring near the mesolow. There is also a secondary maximum in the transition zone between the MCR and stratiform regions.

Compared to Fig. 2.14 from Correia and Arritt (2008), which observed a TS system, there are some similarities in terms of where the greatest values of equivalent potential

temperature are found. Similar to the LS system shown below, the TS systems they studied had maximum θ_e values located along the front of the system. The lowest θ_e values were found on the stratiform back-edge of the TS system, which is a similar location to the back-edge of the MCR in the LS system shown below. Therefore, the θ_e values are more dependent on their orientation to the front or rear of the system and not the placement of the stratiform region, at least for the surface values. The reason for the area of low values is downdrafts in the wake of the system, which transport lower θ_e values towards the surface as detailed by Newton and Newton (1959). The maxima observed are primarily from the transport of high θ_e values from the south.

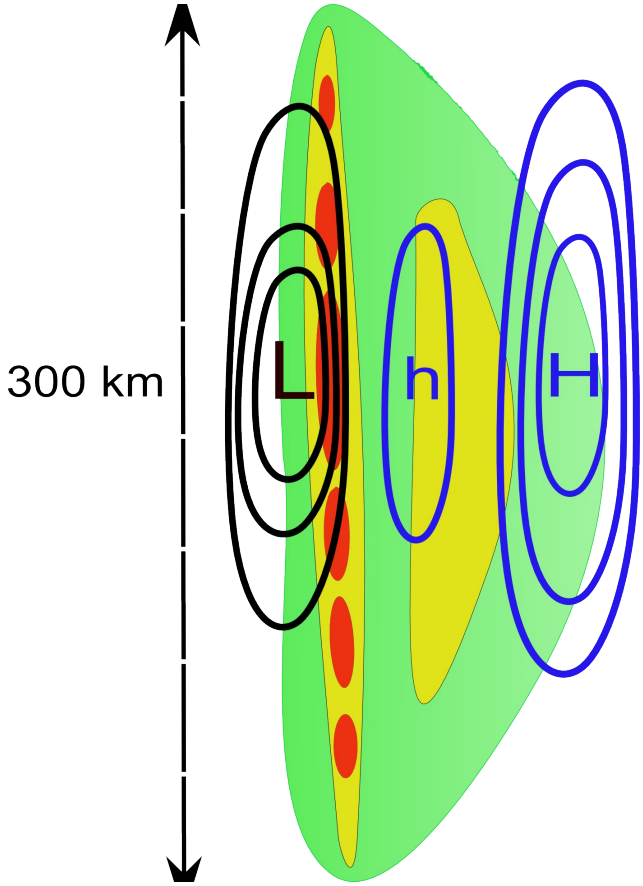

Figure 6.4: Same as Fig. 6.3 except the blue H and black L represent areas of high and low theta-e values. Contours are in 2°C increments. A secondary maximum, found in the transition region, is signified with a small h.

Next, the conceptual models for PS systems are shown. The first, in Fig. 6.5, is shown based on case 17b previously discussed in Chapter 5. The caveat for this conceptual model is that there weren't any other cases available to confirm the same pattern due to the stratiform region often being located outside of the state. Thus, this conceptual model is more theoretical than the LS model, which can be confirmed with many other cases showing the same pattern such as case 4 and 6 previously discussed in Chapter 5. However, this model is the most likely based upon the information available in this study.

Notice that there are two mesohigh/mesolow couplets. The first couplet, located along the southern end of the system, shows a mesohigh inside the MCR and a pre-squall low ahead of the system's advance, similar to TS systems. On the northern end of the system, near the stratiform region, there is a wake low behind the stratiform and a mesohigh on the eastern edge of the stratiform. This pattern held in case 17b until the system transformed into a TS system, after which the mesohigh on the edge of the system moved into the MCR that had formed there. This is very similar to the results previously discussed from Loehrer and Johnson (1995) regarding asymmetric TS systems.

The streamline flow is a little different from TS systems, with confluence occurring from the south more ahead of the system instead of along the convective line. Diffluence tends to occur more on the back edge of the MCR instead of in the wake as observed in LS systems. In case 17b, diffluence also occurred in the stratiform region, branching out towards the northwest and northeast. This can't be verified with other systems, however, due to the lack of cases with stratiform regions inside the state.

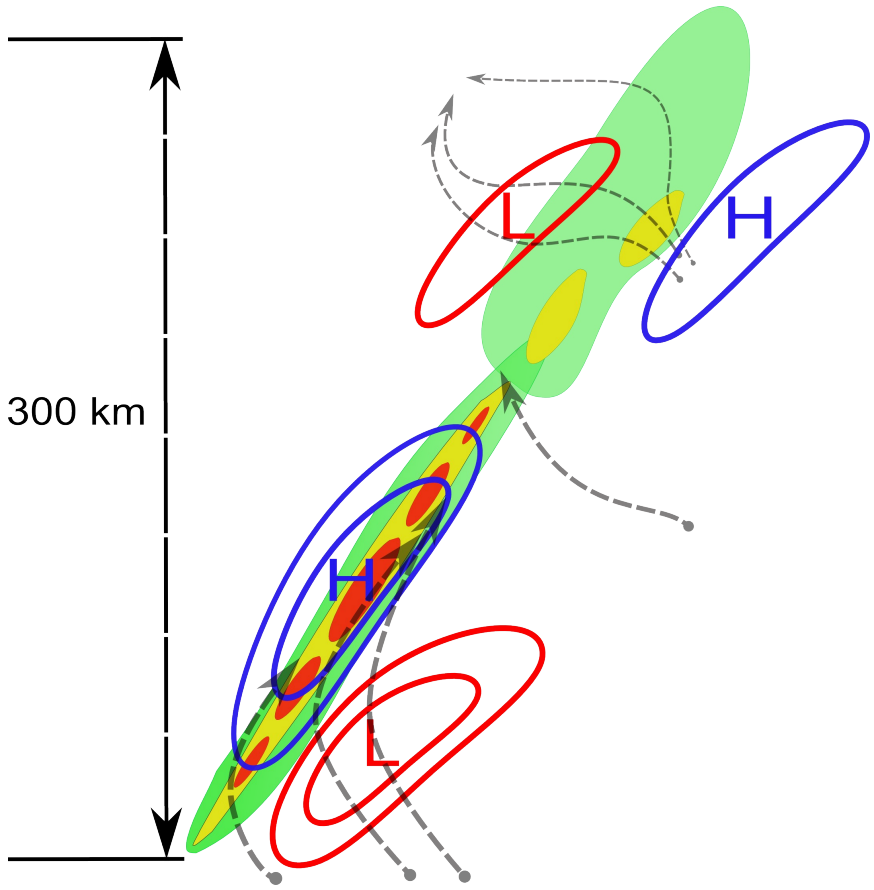

Figure 6.5: Same as Fig. 6.3 except that this is for a parallel stratiform system at maturity.

The final model, Fig. 6.6, shows the locations of high and low θ_e values. This pattern can be confirmed for the MCR, but the stratiform region needs more cases to be finalized. Similar to the LS model, the highest values are found ahead of the system's advance and the lowest values behind the MCR. Again, a secondary maximum occurs in the transition zone, even though the transition zone is located to the north of the convection instead of to the east like in LS systems. In addition, a secondary minimum occurs along the back edge of the stratiform region. These results are also similar to the findings of Correia and Arritt (2008) for TS systems as previously discussed, including especially the minimum found in the wake of the stratiform region.

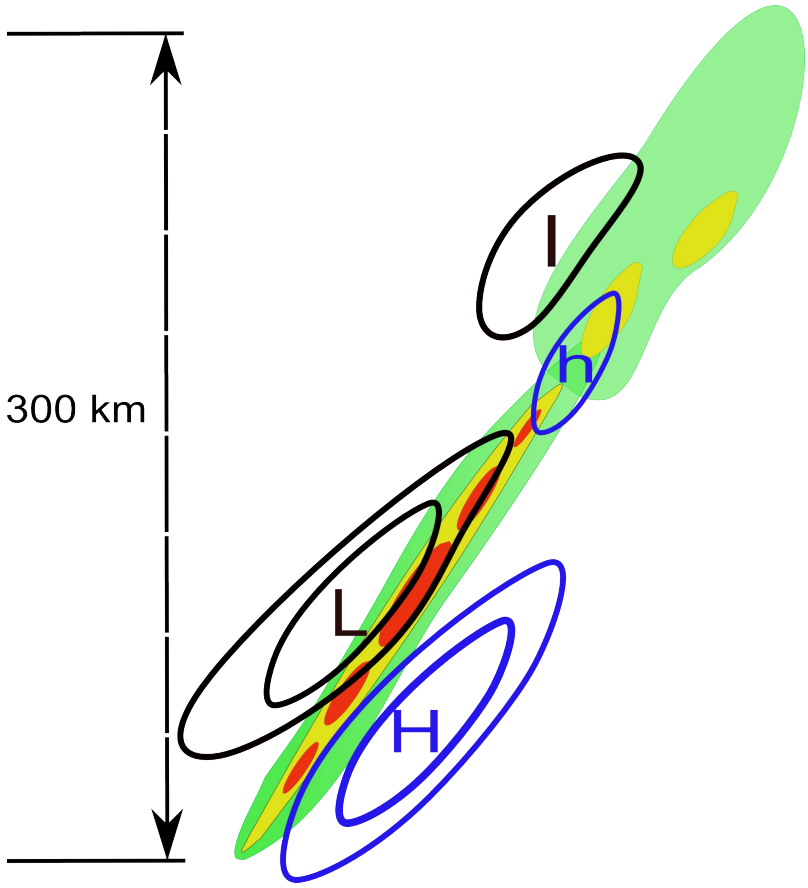

Figure 6.6: Same as Fig 6.4 except that this is for a parallel stratiform system at maturity. In addition, a secondary minimum, found along the back edge of the stratiform region, is indicated with a small l, and a secondary maximum with a small h.

In conclusion, there is now a verifiable conceptual model for the location of mesohighs and mesolows in LS systems, but the model for PS systems requires further study to be verified. Equivalent potential temperature values seem to correlate well with pressure values in both systems, with low equivalent potential temperatures in areas of high pressure and high equivalent potential temperatures in areas of low pressure. There is a slight exception to this rule in the wake of the stratiform region of PS systems, where a wake low is located at the same location as low θ_e values. The surface wind patterns match the pattern indicated in Figure 2.2, showing line parallel flow at the surface for

both LS and PS systems from Parker and Johnson (2000). The preliminary information found in this study can be used as a starting point for future work in this area, which will be discussed in the final chapter.

Chapter 7

FINAL CONCLUSIONS

7.1 Summary of results

In order to investigate surface wind, pressure, and temperature fields associated with leading stratiform (LS) and parallel stratiform (PS) systems, which have heretofore received little study, data from the Oklahoma Mesonet were utilized. These observations were particularly valuable to document LS and PS system surface fields due to the mesonet's uniquely high resolution consisting of over 160 stations during the years 2002-2007. Thirteen LS cases and ten PS cases were identified throughout these six years (see appendix A for more specific information) and were chosen due to their geographic location inside of the state of Oklahoma.

The synoptic conditions these systems tend to develop in were investigated. Similar to the findings of Parker and Johnson (2000), frontal boundaries were very important to the initiation and maintenance of both types of systems. Both system types usually formed in the warm sector of an approaching frontal system. LS systems typically had a surface low pressure center located in northeast New Mexico and moisture advection from a low-level jet (LLJ). A trough existed with an axis through western Oklahoma of moderate strength at 500 hPa, and the system was located in the right entrance region of a jet

streak. PS systems had a surface low pressure center that was more variably located, with an average location in southwest Kansas. PS systems didn't require LLJ influence most of the time and had a trough of moderate strength with an axis through the western panhandle of Oklahoma at 500 hPa. These systems were also located in the right entrance region of a jet streak.

Both system types were then analyzed for their surface features. LS systems tended to have a mesolow occurring ahead of the stratiform region which tended to overlap with the pre-squall low's location usually observed in TS systems. A mesohigh was located on the rear edge of the main convective region (MCR), and the mesohigh/mesolow pressure couplet tended to straddle the stratiform region ahead of this MCR. Streamlines indicated confluence of southerly flow along the eastern edge of the MCR, with diffluence towards the northwest and northeast in the system's wake. Potential and equivalent potential temperatures tended to overlap with pressure centers, with higher temperatures observed in mesolows and lower temperatures observed in mesohighs.

PS systems had few good cases that could be used due to their tendency to have stratiform located outside of the state. Based upon the best case along with the theory that PS systems have a similar structure to asymmetric TS systems, a preliminary theory has been developed about PS system structure that needs to be confirmed with further study. Namely, two pressure couplets were observed, with one pair that followed the MCR and a second following the stratiform region. The stratiform region pair consisted of a wake low behind the stratiform region and a mesohigh along the eastern edge of the stratiform region. The MCR pair consisted of a mesohigh along the back edge of the MCR and a pre-squall low ahead of the system's advance. Streamlines showed confluence of

southerly flow farther ahead of the system's advance than in the case of LS systems. Diffluence occurred both in the stratiform region and in the system's wake, with flow towards the northwest and northeast. Both potential and equivalent potential temperatures followed the same pattern present in LS systems, with low temperatures near mesohighs and high temperatures near mesolows.

The largest pressure difference observed in any of the systems was found in case 4, with a pressure differential of 5.5 hPa between the mesohigh and mesolow. A pressure gradient force in this case was directed from northwest to southeast, which is the opposite horizontal direction of the force found in wake low/mesohigh couplets of TS systems. Weaker pressure gradients were observed on average in PS systems, meaning the possibility of a strong, pressure gradient influenced wind gust is more likely in LS systems than PS systems.

7.2 Future work

The primary goal of this study was to discover the surface pressure features of LS and PS systems and to determine if these pressure features were similar at all to the far more observed TS systems. The theory that a mesohigh/wake low couplet straddles the stratiform region of a system, regardless of the system's stratiform orientation, was tested. The theory is based on Haertel and Johnson (2000) and their conclusion that a pressure couplet exists as long as a linear MCS has a moving stratiform region. This theory was proven to not be true for LS systems. These systems have a mesohigh following the mesolow instead of leading it. The likely cause of the leading mesolow is a descending inflow jet near the mesolow's location that lowers the surface pressure. The

lack of a mesolow in the wake of the system is likely due to precipitation downdrafts, which raise the surface pressure. More work is required for PS systems, however, to test HJ 2000's theory.

In order to confirm the conceptual model developed in Chapter 6, more PS cases need to be studied. Surface pressure features in the stratiform region are lacking especially. It was confirmed in this study that there is a mesohigh on the rear edge of the MCR and a pre-squall low ahead of the system's advance, but the surface pressure field in the stratiform region has only been observed in detail with a single case. It would also be beneficial to find additional LS and PS cases in other regions besides Oklahoma to validate the conceptual models developed in the previous chapter. This will prove difficult, however, until other states and regions develop networks with similar resolution to Oklahoma's Mesonet.

While surface winds were observed in this study, there wasn't enough time to observe the vertical wind structure of these cases. Study of the vertical wind profile will help to further confirm the work of Parker and Johnson (2000). It may also serve as an indicator to what exactly is causing the surface pressure patterns observed in this study. This could help confirm the theory regarding the mesolow's cause of a leading inflow jet in LS systems and can provide additional information as to what vertical wind profiles produce either the longest-lived systems or those with the highest amounts of precipitation.

It would also be productive to utilize the study done by Coleman and Knupp (2009) and apply their study to LS and PS systems. It needs to be determined if strong surface pressure gradients in these two system types produce surface wind gusts over 25 m s^{-1} as well. LS systems have a pressure gradient force directed towards the front of the system

instead of the rear like trailing stratiform (TS) systems do. Different parameters will need to be established for LS and PS systems from the ones used in CK 2009 to predict which scenarios are most likely to cause these severe surface wind gusts.

Due to the possibility of both systems causing flash flooding (LS systems for their slow movement as noted by Parker and Johnson 2000 and PS systems for their back-building tendencies as noted by Schumacher and Johnson 2005), improved forecasting of these systems will prove beneficial to warn of this threat. The data from this and other further studies should be used to model the systems. This modeling can be used as a forecast tool to improve predictions of each system's development and evolution so that timelier flash flood warnings can be issued to save lives.

It would also be helpful to study the vertical thermodynamic properties of these systems in more detail. A study similar to Correia and Arritt (2008) could be performed to find the patterns of moisture transport inside both system types. This needs to be done in order to help further explain the surface pressure features found in both system types and to help confirm previous studies on system structure (such as Parker 2007b with the profile of PS systems and Parker and Johnson 2004 for LS systems).

PS and LS systems both need to be further studied in these areas so that ultimately the severe weather they frequently cause can be forecasted more quickly. Further study of surface features will remain difficult until more dense observation networks are built in other locations, and studies of the vertical wind and thermodynamic structure will require soundings at a higher temporal resolution than the current one of every 6-12 hours. If these steps are taken, however, and more is discovered regarding the internal dynamics of

these systems, more accurate and timely warnings can be issued to help save property and lives.

REFERENCES

Adams-Selin, R. and R. Johnson, 2010: Mesoscale surface pressure and temperature features associated with bow echoes. *Monthly Weather Review*, **138,** 212-227.

Cohen, A., M. Coniglio, S.F. Corfidi, and S.J. Corfidi, 2007: Discrimination of mesoscale convective system environments using sounding observations. *Weather and Forecasting*, **22,** 1045-1062.

Coleman, T. and K. Knupp, 2009: Factors affecting surface wind speeds in gravity waves and wake lows. *Weather and Forecasting*, **24,** 1664-1679.

Coniglio, M., D. Stensrud, and L. Wicker, 2006: Effects of upper-level shear on the structure and maintenance of strong quasi-linear mesoscale convective systems. *Journal of the Atmospheric Sciences*, **63**, 1231-1252.

Coniglio, M., H. Brooks, S. Weiss, and S. Corfidi, 2007: Forecasting the maintenance of quasi-linear mesoscale convective systems. *Weather and Forecasting*, **22,** 556-570**.**

Correia, J., Jr. and R. Arritt, 2008: Thermodynamic properties of mesoscale convective systems observed during BAMEX. *Monthly Weather Review*, **136**, 4242-4271.

Dial, G., J. Racy, and R. Thompson, 2010: Short-term convective mode evolution along synoptic boundaries. *Weather and Forecasting*, in press.

Duchon, C., 1979: Lanczos filtering in one and two dimensions. *Journal of Applied Meteorology*, **18**, 1016-1022.

Fankhauser, J., G. Barnes, and M. LeMone, 1992: Structure of a midlatitude squall line formed in strong unidirectional shear. *Monthly Weather Review*, **120**, 237-260.

Fovell, R., G. Mullendore, and S. Kim, 2006: Discrete propagation in numerically simulated nocturnal squall lines. *Monthly Weather Review*, **134**, 3735-2752.

French, A. and M. Parker, 2008: The initiation of multiple modes of convection within a meso-alpha-scale region. *Weather and Forecasting*, **23**, 1221-1252.

—— 2010: The response of simulated nocturnal convective systems to a developing low-level jet. *Journal of the Atmospheric Sciences*, in press.

Fujita, T., 1955: Results of detailed synoptic studies of squall lines. *Tellus*, **7**, 405-436.

Gaffin, D., 1999: Wake low severe wind events in the Mississippi River Valley: A case study of two contrasting events. *Weather and Forecasting*, **14**, 581-603.

Gale, J., W. Gallus Jr., and K. Jungbluth: Toward improved prediction of mesoscale convective system dissipation. *Weather and Forecasting*, **17**, 856-872.

Gallus, W., Jr., N. Snook, and E. Johnson: Spring and summer severe weather reports over the Midwest as a function of convective mode: A preliminary study. *Weather and Forecasting*, **23**, 101-113.

Haertel, P. and R. Johnson, 2000: The linear dynamics of squall line mesohighs and wake lows. *Journal of the Atmospheric Sciences*, **57**, 93-107.

Hilgendorf, E. and R. Johnson, 1998: A study of the evolution of mesoscale convective systems using WSR-88D data. *Weather and Forecasting*, **13**, 437-452.

Houze, R., Jr., B. Smull, and P. Dodge, 1990: Mesoscale organization of springtime rainstorms in Oklahoma. *Monthly Weather Review*, **118**, 613-654.

James, R., J. Fritsch, and P. Markowski, 2005: Environmental differences between cellular and slabular convective lines. *Monthly Weather Review*, **133**, 2669-2691.

Jewett, B. and R. Wilhelmson, 2006: The role of forcing in cell morphology and evolution within midlatitude squall lines. *Monthly Weather Review*, **134**, 3714-3734.

Johnson, R., 2001: Surface mesohighs and mesolows. *Bulletin of the American Meteorological Society*, **82**, 13-31.

Johnson, R. and P. Hamilton, 1988: The relationship of surface pressure features to the precipitation and air flow structure of an intense midlatitude squall line. *Monthly Weather Review*, **116**, 1444-1472.

Knievel, J. and R. Johnson, 1998: Pressure transients within MCS mesohighs and wake lows. *Monthly Weather Review*, **126**, 1907-1930.

—— 2002: The kinematics of a midlatitude, continental mesoscale convective system and its mesoscale vortex. *Monthly Weather Review*, **130**, 1749-1770.

Loehrer, S. and R. Johnson, 1995: Surface pressure and precipitation life cycle characteristics of pre-storm mesoscale convective systems. *Monthly Weather Review*, **123**, 600-621.

Mahoney, K., G. Lackmann, and M. Parker, 2009: The role of momentum transport in the motion of a quasi-idealized mesoscale convective system. *Monthly Weather Review*, **137**, 3316-3338.

Newton, C. and H. Newton, 1959: Dynamical interactions between large convective clouds and environment with vertical shear. *Journal of Meteorology*, **16**, 483-496.

Nuss, W. and D. Titley, 1994: Use of multiquadric interpolation for meteorological objective analysis. *Monthly Weather Review*, **122**, 1611-1631.

Parker, M., 2007a: Simulated convective lines with parallel stratiform precipitation. Part I: An archetype for convection in along-line shear. *Journal of the Atmospheric Sciences*, **64**, 267-288.

—— 2007b: Simulated convective lines with parallel stratiform precipitation. Part II: Governing dynamics and associated sensitivities. *Journal of the Atmospheric Sciences*, **64**, 289-313.

Parker, M. and R. Johnson, 2000: Organizational modes of midlatitude convective systems. *Monthly Weather Review*, **128**, 3413-3436.

—— 2004: Structures and dynamics of quasi-2D mesoscale convective systems. *Journal of the Atmospheric Sciences*, **61**, 545-567.

—— 2004a: Simulated convective lines with leading precipitation. Part I: Governing dynamics. *Journal of the Atmospheric Sciences*, **61**, 1637-1655.

—— 2004b: Simulated convective lines with leading precipitation. Part II: Evolution and Maintenance. *Journal of the Atmospheric Sciences*, **61**, 1656-1673.

Pedgley, D., 1962: A meso-synoptic analysis of the thunderstorms on 28 August 1958. Memo No. 106, British Meteorological Office, Geophysics, 74 pp.

Pettet, C. and R. Johnson, 2003: Airflow and precipitation structure of two leading stratiform mesoscale convective systems determined from operational datasets. *Weather and Forecasting*, **18**, 685-699.

Rasmussen, E. and S. Rutledge, 1993: Evolution of quasi-two-dimensional squall lines. Part I: Kinematic and reflectivity structure. *Journal of the Atmospheric Sciences*, **50**, 2584-2606.

Schumacher, R. and R. Johnson, 2005: Organization and environmental properties of extreme-rain-producing mesoscale convective systems. *Monthly Weather Review*, **133**, 961-976.

Skamarock, W., M. Weisman, and J. Klemp, 1994: Three-dimensional evolution of simulated long-lived squall lines. *Journal of the Atmospheric Sciences*, **51**, 2563-2584.

Smith, A., G. McFarquhar, R. Rauber, J. Grim, M. Timlin, B. Jewett, and D. Jorgensen, 2009: Microphysical and thermodynamic structure and evolution of the trailing stratiform regions of mesoscale convective systems during BAMEX. Part I: Observations. *Monthly Weather Review*, **137**, 1165-1185.

Stoelinga, M., J. Locatelli, R. Schwartz, and P. Hobbs, 2003: Is a cold pool necessary for the maintenance of a squall line produced by a cold front aloft? *Monthly Weather Review*, **131**, 95-115.

Storm, B., M. Parker, and D. Jorgensen, 2007: A convective line with leading stratiform precipitation from BAMEX. *Monthly Weather Review*, **135**, 1769-1785.

Szeto, K. and H. Cho, 1994: A numerical investigation of squall lines. Part II: The mechanics of evolution. Journal of the Atmospheric Sciences, **51**, 425-433.

Vescio, M. and R. Johnson, 1992: The surface-wind response to transient mesoscale pressure fields associated with squall lines. *Monthly Weather Review*, **120**, 1837-1850.

Appendix A

LIST OF INCLUDED CASES

Table A.1: The dates and times of all cases, along with each case's archetype. The first column lists the number of each case as described in the text. The second column lists the date of each case used for this study. The third column lists the starting time of each case used for this study. The fourth column lists the ending time of each case used for this study. The last column lists which archetype the system was categorized as with the ranking given to that case included in parentheses as discussed in Chapter 3. Both starting and ending times are based upon the case system being in its archetype form, not necessarily its initiation or dissipation. Cases 5 and 11 could not be used for the analysis described in this paper due to their passage solely through the panhandle region. All cases occurred within the state of Oklahoma.

Case Number	Date	Start (UTC)	End (UTC)	Stratiform Pattern
1	18 Apr 2002	0045	0700	Leading(7)
2	24-25 May 2002	2045	0130	Leading(9)
3	27 May 2002	0000	0400	Leading(7)
4	16 Apr 2003	0000	0400	Leading(9)
5	18 Apr 2003	0745	0945	Leading(7)
6	21-22 Apr 2004	2045	0145	Leading(10)
7	22-23 Apr 2004	2115	0100	Leading(8)
8	05-06 Apr 2005	1915	0100	Leading(7)
9	19 May 2005	0515	1200	Leading(8)
10	24 Apr 2006	1945	2345	Leading(7)
11	22 Apr 2007	0000	0430	Leading(10)
12b	12 Apr 2002	1400	1900	Leading(9)
17a	04-05 Jun 2005	2145	0130	Leading(9)
12a	12 Apr 2002	0945	1400	Parallel(7)
13a	20 Apr 2003	0000	0245	Parallel(7)
13b	20 Apr 2003	0245	0530	Parallel(8)
14	21 Apr 2004	0000	0500	Parallel(9)
15a	30 May 2004	1645	1915	Parallel(8)
15b	30 May 2004	1915	2245	Parallel(9)
16	26 Apr 2005	0000	0430	Parallel(7)
17b	05 Jun 2005	0130	0415	Parallel(10)
18	24 Apr 2006	1315	1800	Parallel(8)
19	24 Apr 2007	1545	2200	Parallel(9)